AD-A118 038 AIR FORCE INST OF TECH WRIGHT-PATTERSON AFB OH SCHOO--ETC F/G 17/7
APPLICATION OF OUTPUT PREDICTIVE ALGORITHMIC CONTROL TO A TERRA--ETC(U)
MAR 82 M E BISE
UNCLASSIFIED AFIT/GE/EE/82M-1 NL

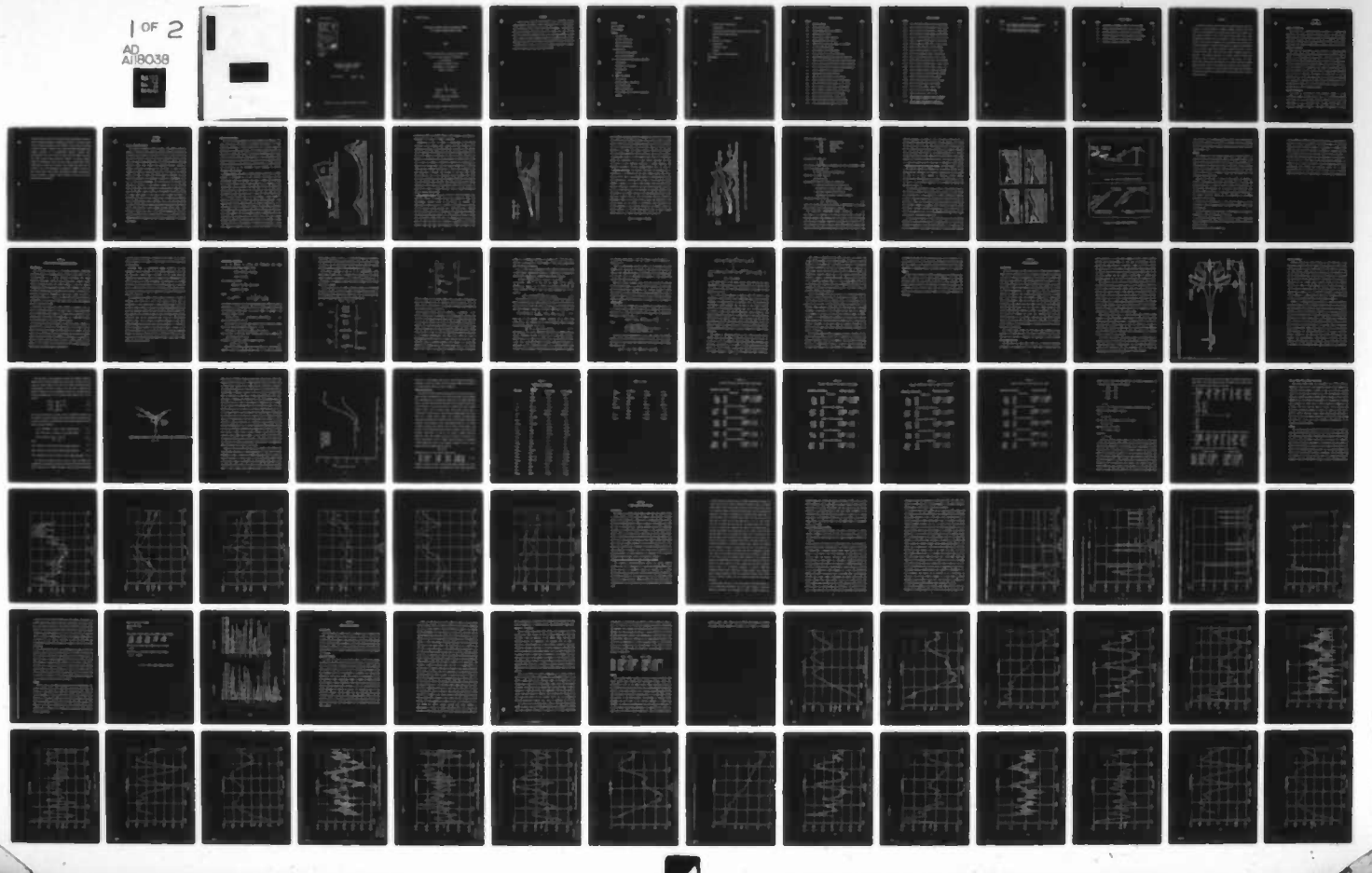

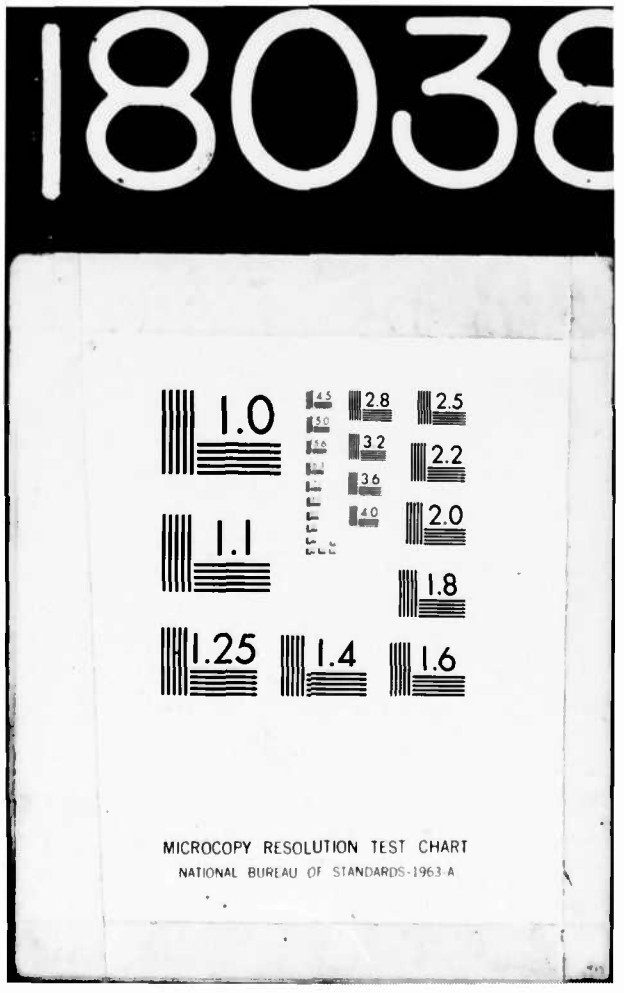
18038
1.0
1.1
1.25
1.4
1.6
1.8
2.0
2.2
2.5
2.8
3.2
3.6
4.0
4.5
5.0
MICROCOPY RESOLUTION TEST CHART
NATIONAL BUREAU OF STANDARDS-1963-A

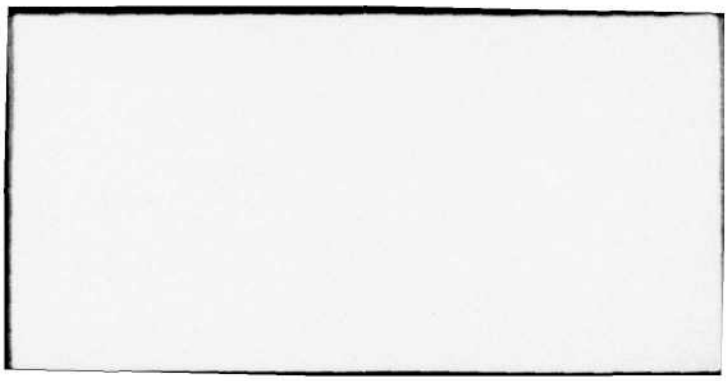

AFIT/GE/EE/82M-1

APPLICATION OF OUTPUT PREDICTIVE ALGORITHMIC CONTROL TO A TERRAIN FOLLOWING AIRCRAFT SYSTEM

THESIS

AFIT/GE/EE/82M-1 Michael E. Bise
GS-12 USAF

AFIT/GE/EE/82M-1

APPLICATION OF OUTPUT PREDICTIVE ALGORITHMIC CONTROL TO A TERRAIN FOLLOWING AIRCRAFT SYSTEM

THESIS

Presented to the Faculty of the School of Engineering
of the Air Force Institute of Technology
Air University
in Partial Fulfillment of the
Requirements for the Degree of
Master of Science

by

Michael E. Bise, B.S.A.E.
GS-12 USAF
Graduate Electrical Engineering

March 1982

Preface

I would like to thank my thesis advisor, Dr. J. Gary Reid, and my thesis committee consisting of Capt. James Silverthorn, Dr. John D'Azzo, and Ron Anderson for all of their help and encouragement. I would like to thank Larry Gearhart and Joel Levy of Lear Siegler Inc. for the many hours they sacrificed teaching me how to run and debug TCODAS. I would like to thank the Flight Dynamics Laboratory for sponsoring this thesis, especially Stan Lash for his help on the F-111/MAW. Finally, I would like to thank my wife, Carol, for her love and support these past 15 months, and for giving birth to our first child, Matthew.

Contents

Contents

List of Figures

List of Figures

List of Figures

List of Tables

Abstract

An effective automatic terrain following command generation system is required to safely maintain a desired clearance altitude above the terrain. For survivability, the aircraft must penetrate at transonic or high subsonic speeds at very low altitudes above ground level. This introduces new problems such as wind gusts, a faster radar update of the terrain, faster aircraft response time, and increased pilot workload. To insure survivability, a control algorithm must be capable of interpreting all of the above input data and perform flawlessly during a terrain following mission. This report uses the terrain following scenario to evaluate a new digital controller, the Output Predictive Algorithmic Controller. This controller was able to track, during low level penetration, actual terrain data using as an aircraft model the F-111/MAW (Mission Adaptive Wing). The F-111/MAW was chosen for this study due to its direct lift capability. Two wing sweeps (35 degrees and 58 degrees) were chosen to evaluate the effectiveness of direct lift during a terrain following mission.

CHAPTER 1

Introduction

General Introduction

This thesis is a follow-on effort to AFIT M. S. Thesis "The Application of Output Predictive Digital Control to Wing Flutter Suppression and Terrain Following Problems" by David Chaffin. The Output Predictive Controller will be used to follow an actual terrain profile using a multiple-input F-111/MAW (Mission Adaptive Wing) aircraft model.

Problem Formulation

Past work with the Output Predictive Controller has been with simple linear, single-input, single-output systems following function type of inputs (i.e., sine waves, unit step, etc.). This effort will see how effectively the Output Predictive Controller follows actual terrain data from the Fulda Gap region of Germany using a seventh-order linear model of the F-111/MAW. The F-111/MAW has two inputs, flap and elevator, and has been optimized to fly a terrain following mission. Two wing sweeps will be used to determine the effect of direct lift on aircraft performance. All of the aircraft states will be monitored to determine which states are important in low level flight. Recommendations will be formulated to further study the optimization and integrated controls problem during a terrain following mission.

Thesis Organization

The thesis is organized into seven chapters. Chapter 1 is the introductory chapter discussing how the work is to be performed. Chapter 2 discusses the terrain following problem in general and the history and development of four algorithms over the past several years. The algorithms discussed in Chapter 2 led into a new approach to terrain

following which is known as the Output Predictive Algorithmic Controller (OPAC). The OPAC development is documented in Chapter 3. The model chosen to use the OPAC controller is the F-111/MAW. A brief history of the MAW is given in Chapter 4. Chapter 4 also includes the model development from transfer functions to a seventh-order physical variable state representation. The terrain model is also briefly discussed. The model must follow random terrain patterns; therefore, a digital computer program was developed to read the terrain data, calculate cubic spline coefficients, and then fit a smooth curve through that data for the aircraft to fly. This development is discussed in Chapter 5 along with other flight control system design considerations. Chapter 6 presents the results and Chapter 7 suggests further research in the area of terrain following/terrain avoidance.

CHAPTER 2

Background

Terrain Following Problem

An effective automatic terrain following (ATF) command generation system is required to safely maintain a desired clearance altitude above the terrain. The question of why fly at very low altitudes can be best answered by looking at missile and radar detection systems currently being used. These weapon systems have an increased altitude and downrange capability which, when coupled with increased accuracy, results in steadily decreasing survivability for the pilot. In order to more effectively combat the increased accuracy of this type of air defense system, the idea of flying under enemy radar was proposed. As radar technology advanced it was necessary to define new requirements in the area of ATF system development. For survivability, the aircraft must penetrate at transonic or high subsonic speeds at very low altitudes above ground level. This introduces new problems such as wind gusts at very low altitudes, flying "blind" over the backside of mountains, a need for faster radar update of the terrain which increases the chance of detection, much faster aircraft response time, increased pilot workload, and more sophisticated control algorithms. While the total ATF problem includes aircraft dynamics, command generation techniques, flight control system characteristics, terrain sensors (forward looking radar, radar altimeters, LASER radar, etc.), pilot safety considerations, and pilot interface with the system, the next section will concern itself with four command generation techniques that are currently operational or are under development.

Algorithm Development

Two of the methods (Template and Angle Command) are empirical. The other two (Optimal and ADLAT) are optimized controllers, i.e., they essentially calculate an optimum flight path over a period of time and performance is achieved due largely to an optimal trade-off between the clearance altitude and vertical acceleration parameters. The current terrain following systems are defined below. A brief discussion of the theory of operation of each system will provide means of evaluating each system's capabilities and limitations. The discussion will also provide an understanding of the subsequent "fixes" necessary to provide acceptable ATF performance.

1. Template System. This type of system employs a range gate, R, whose position is determined by the set clearance altitude, H_o, and the instantaneous radar scan angle, β,. The range is chosen after reviewing the aircraft's dynamic response characteristics and the roughness of the terrain most often encountered. The range gate divides the radar scan into two sectors, a climb sector and a dive sector. This range gate and the upper and lower scan angles form a "template" and is shown in Fig. 2.1. If terrain intrudes within the climb sector a climb command is generated, and terrain intruding into the dive sector generates a dive command. The generated command signal is directly proportional to the nearest terrain obstacle within the template. In other words, an obstacle that intrudes within the maximum range of the dive sector will generate a large dive command. This dive command decreases in magnitude until that point where the obstacle enters the climb sector. The climb command steadily increases as the obstacle grows closer to the aircraft. If after crossing the peak a second obstacle is detected far downrange, a large dive command is generated in order to return the aircraft to it's set

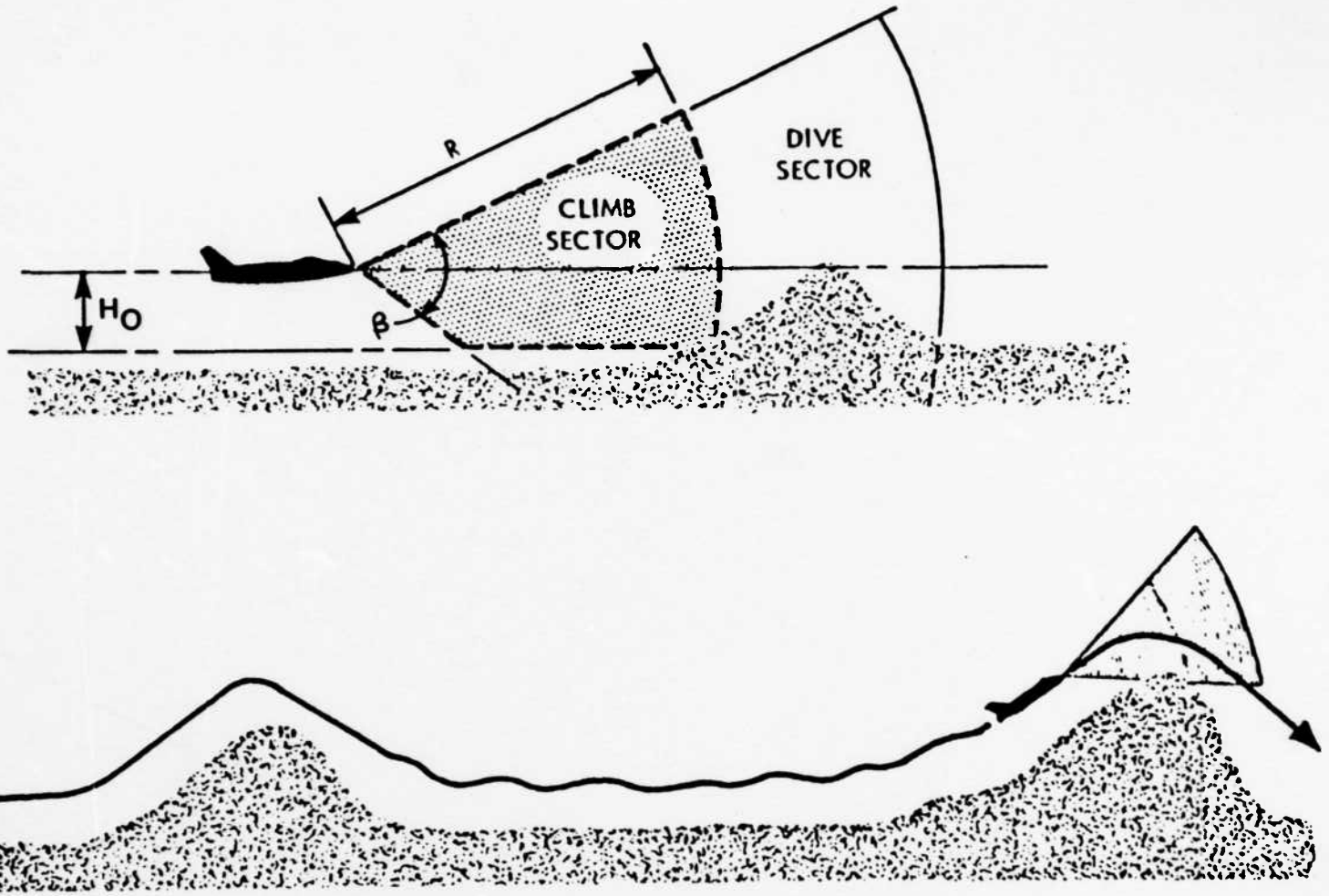

Fig 2.1 TEMPLATE AUTOMATIC TERRAIN FOLLOWING SYSTEM

altitude clearance in a minimum amount of time. However, if no terrain is detected during a scan, no command is generated.

Examination of Fig. 2.1 shows an undercutting of the desired clearance, called clipping, after crossing the first obstacle and an associated oscillatory flight along the set clearance altitude between the two obstacles. The clipping occurs when the minimum radar range is set too far ahead of the aircraft and thus the reverse slope of the mountain is not detected. Only the far obstacle is detected by the radar and a large dive command is generated resulting in a narrow miss or impact on the reverse slope. Since the Template system can only generate climb and dive commands, oscillations in flight path trajectory occur when descending a mountain and continue to the next peak. These oscillations are due to the alternating control commands that first detect the upcoming ground and then the obstacle downrange. The inclusion of a low altitude radar altimeter into the ATF system would prevent clipping and would eliminate the oscillatory flight over the terrain. It would also be useful in flight over water where no signal is generated from the forward looking radar.

2. Angle Command System. Referring to Fig.2.2, during the radar scan, each time terrain is detected within some preselected range, the instantaneous sighting angle to the terrain is measured. The instantaneous sighting angle is a function of the antenna look angle, β, and the aircraft's pitch attitude, Θ ,. This angle plus a selected clearance offset angle over the detected terrain determines the commanded instantaneous flight path angle, γ_c, for the aircraft to follow to safely clear the terrain. During each scan, the maximum required flight path angle to clear the peak of an obstacle is compared to the present aircraft flight path angle. The difference in these two angles is the

COMMAND EQUATION

$$\gamma_c = \left(\frac{H_o}{R} + \theta + \beta\right) - \gamma$$

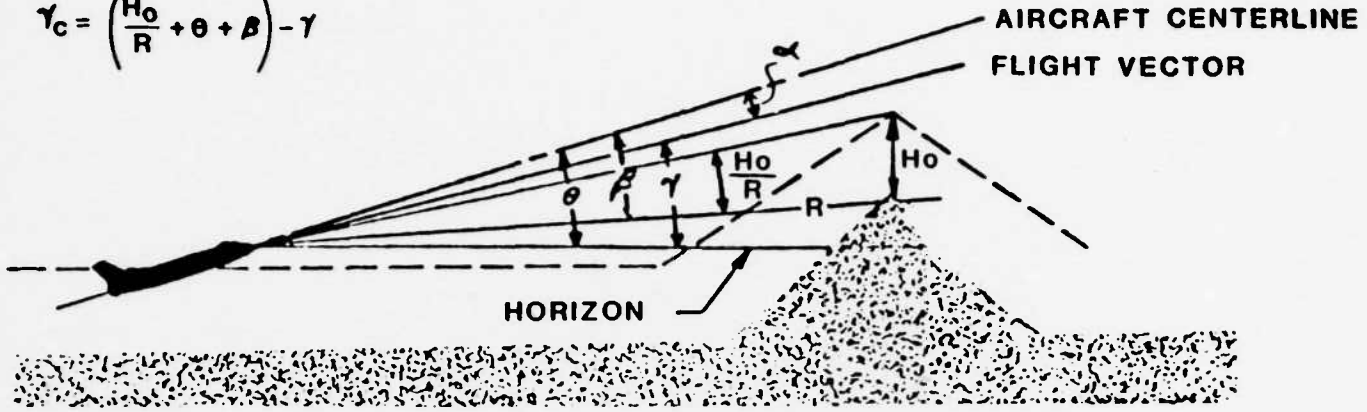

Fig 2.2 ANGLE COMMAND AUTOMATIC TERRAIN FOLLOWING SYSTEM

pitch command. The system constantly commands the aircraft to fly towards the highest point of offset clearance, that is, the aircraft is flying "peak to peak" with no dive commands generated to return the aircraft to the set altitude clearance over the terrain (Fig. 2.3 curve a). The addition of an offset (e.g. radar altimeter) improves the aircraft's terrain following capability (Fig. 2.3 curve b), yet it still results in a nose-up peak overshoot of the highest terrain point. In an attempt to reduce the sensitivity of far range terrain detection and thus concentrate on more immediate obstacles, a shaped offset, F_s, was developed and added to the pitch command equation (Fig. 2.3 curve c).

3. Optimal Controller. The Optimal Controller was developed due to inadequecies of the Template and the Angle Command systems. The use of optimal control theory was proposed because it minimizes deviation from the flight path on a continual basis instead of flying from one terrain obstacle to another (i.e., peak to peak flying). Since the scope of this chapter is background information into the control algorithms and not a derivation, the derivation is not described. An excellent discussion and derivation of the optimal controller and path generation using a cubic spline fit is given in Ref 2.1. Use of the optimal controller requires an performance index to be written which describes the importance of the various states of the system. A mathematical model describing the aircraft dynamics is also required. Therefore, the optimal system, by design, controls the vertical flight path as well as speed (through engine control). The system state equation can be written as

$$\dot{\underline{x}}(t) = A\underline{x}(t) + B\underline{u}(t) \qquad (2.1)$$

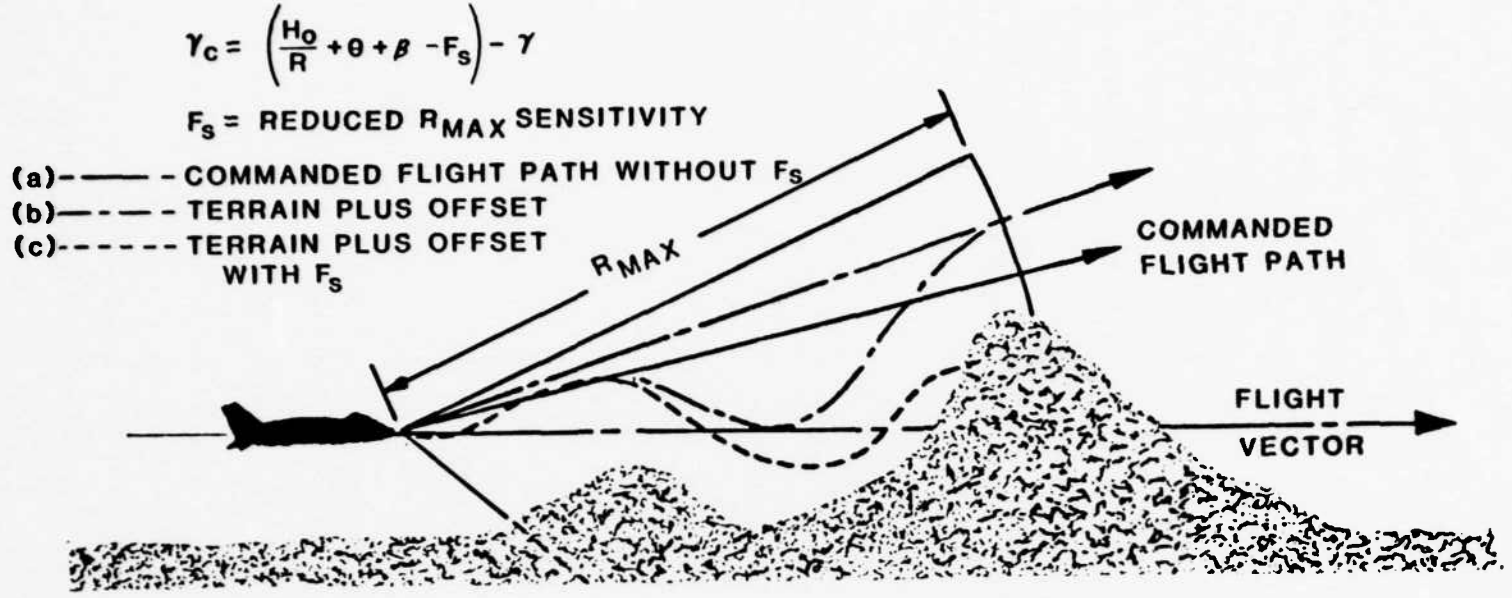

Fig 2.3 SHAPED OFFSET FOR ANGLE COMMAND

where the state vector is,

$$\underline{X} = \begin{bmatrix} u \\ w \\ q \\ \theta \\ \delta \\ T \\ h \end{bmatrix} \quad \begin{matrix} \text{forward velocity} \\ \text{vertical velocity} \\ \text{pitch rate} \\ \text{pitch angle} \\ \text{control surface} \\ \text{thrust} \\ \text{altitude} \end{matrix} \tag{2.2}$$

and the control vector is,

$$\underline{u} = \begin{bmatrix} \delta_C \\ \Delta T \end{bmatrix} \tag{2.3}$$

The control is determined by minimizing the error or performance index (PI) of the optimal regulator

$$J = \tfrac{1}{2} \int_0^{t_f} (\underline{y}^T Q \underline{y} + \underline{U}^T R \underline{U}) \, dt \tag{2.4}$$

where y is the output vector of

$$\underline{y}(t) = C \underline{x}(t) \tag{2.5}$$

The weighting matrices, Q and R, are defined as

Q - A positive semi-definite diagonal matrix representing the output weighting constants

R - A positive definite diagonal matrix representing the control weighting constants

The optimal control vector is

$$\underline{u} = -R^{-1} B^T P \underline{x} \tag{2.6}$$

where the optimal gain matrix, $G = -R^{-1}B^TP$, is approximated by the steady state solution of the following Riccati equation

$$\dot{P} = -PA - A^TP + PBR^{-1}B^TP - C^TQC \, , \quad P(t_f) = 0 \tag{2.7}$$

The matrix P is obtained by solving the matrix Riccati equation by numerical methods. These equations must be solved in reverse time because only the final (boundary) conditions are known. The solutions for P(t) are generally time varying. However, they rapidly approach steady state values as the integration proceeds toward present time. Generation of the

desired trajectory is given in Fig. 2.4. The terrain profile is determined by measuring the vertical distance between each scanned terrain point and the aircraft. The scanned altitude is subtracted from the aircraft's inertial altitude, referenced to an inertial reference line (sea level), and stored in the onboard computer as a discrete horizontal altitude increment. When there are disjointed or abrupt path changes, the controller trades altitude error for vertical acceleration in a ratio determined by the PI. Thus they are smoothed in a safe manner.

4. Advanced Low Altitude Techniques (ADLAT). The ADLAT system is another of the advanced systems and demonmstrates performance superior to the older empirical techniques. One essential characteristic of this system is that it is easily adapted to changing aircraft dynamic characteristics. The theoretical development of the ADLAT system is given in Ref 2.2. An all digital simulation of this system was created and documented in Ref. 2.3.

The ADLAT command scheme is shown in Fig 2.5. The general trajectory for clearing an obstacle with altitude T is a pull-up to an angle equal to the maximum rate of climb (within set g-limits) followed by a pushover in time to clear the obstacle at the desired set altitude clearance and with zero climb or sink rate. Both the pull-up and pushover accelerations are constant, leading to parabolic arcs. The pull-up parabola passes through the aircraft's position predicted one time constant into the future. The angle Γ_p in Fig. 2.5 is the commanded climb angle and is equal to the slope of the desired flight path.

If the predicted position is below the climb limit line, the pull-up parabola is reflected about the line as shown in Fig. 2.6. The recovery trajectory, asymptotic to the desired flight path, is the reflection of the pull-up parabola the aircraft would have if it were an equal distance

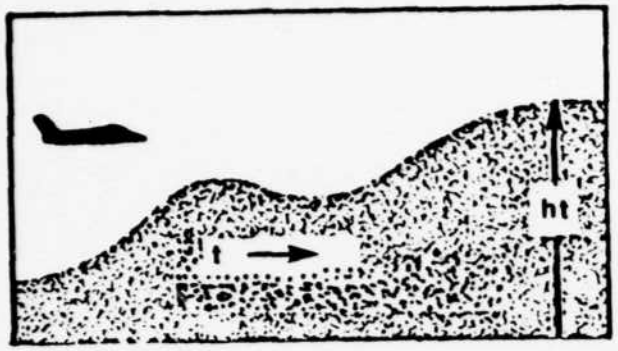

(1) STORE TERRAIN

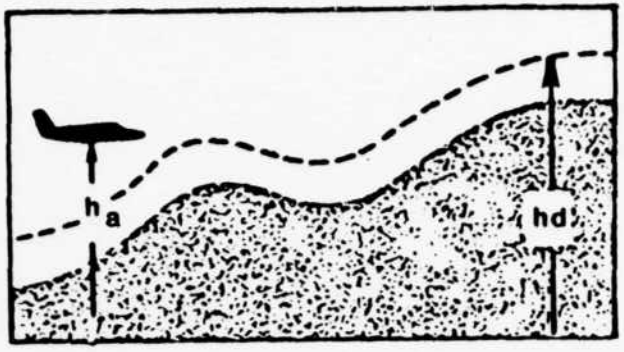

(2) GENERATE DESIRED CLEARANCE PATH

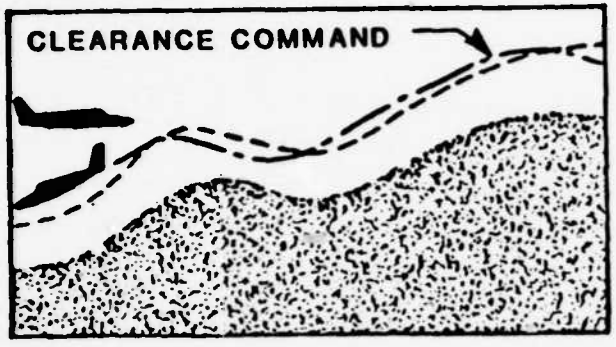

(3) FAST TIME REVERSE FLIGHT

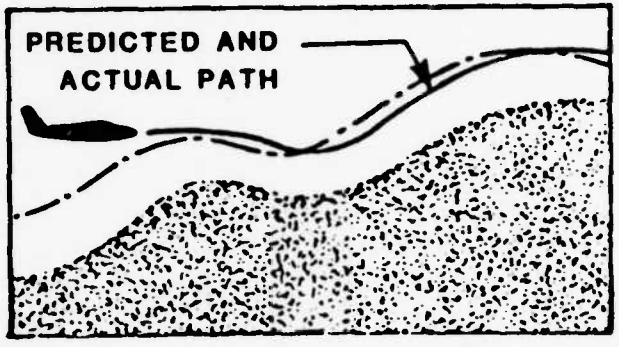

(4) REAL TIME FORWARD FLIGHT

Fig 2.4 FOUR PARTS OF OPTIMAL CONTROLLER

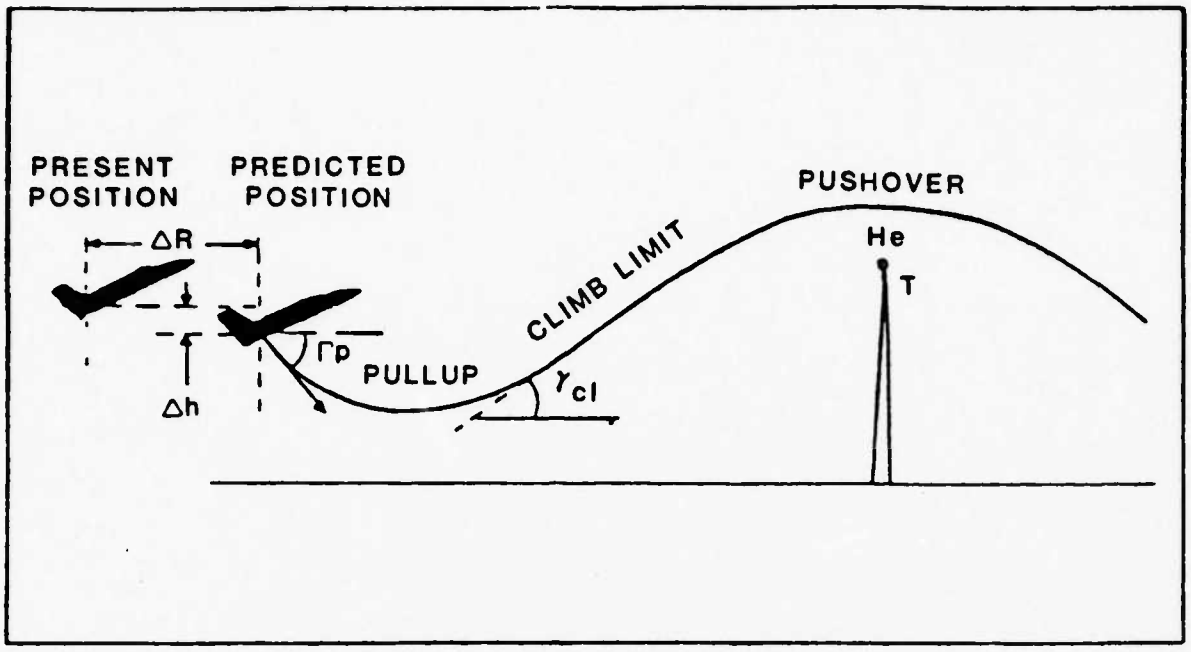

Figure 2.5 ADLAT COMMAND SCHEME

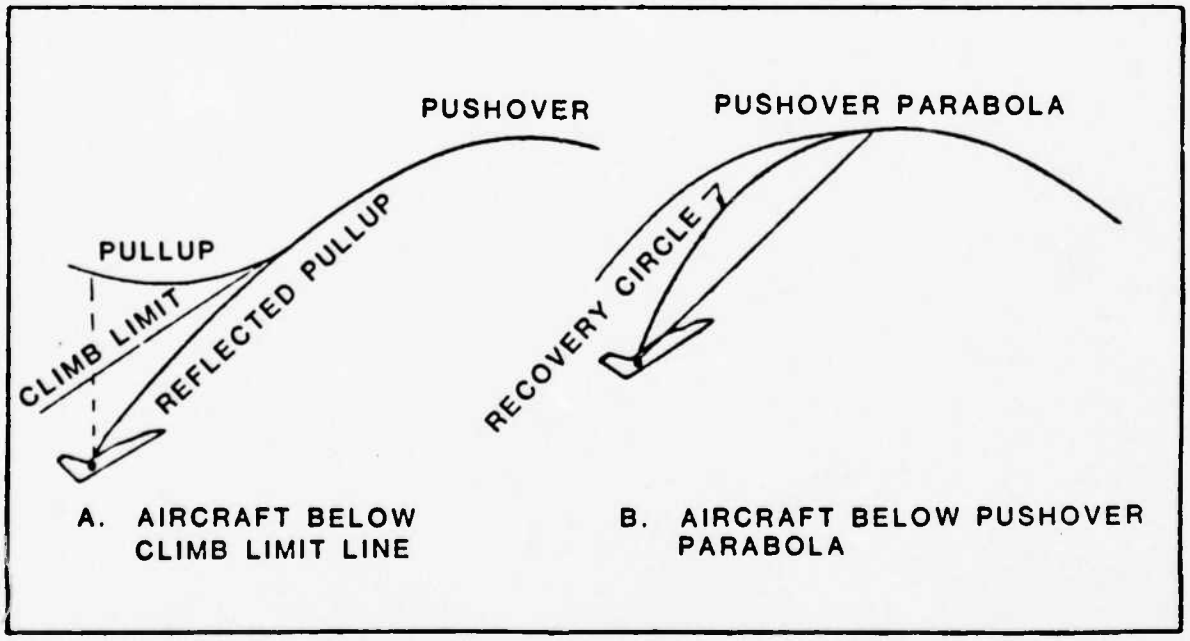

Figure 2.6 PUSHOVER GEOMETRY

above the path. If the predicted position is below the pushover parabola, the recovery trajectory is a circular arc passing through the predicted position and horizontally through the desired clearance point above the obstacle (Ref. 2.4).

Summary

The Template and Angle Command systems require numerous "fixes" as discussed above. Several parameters must be pre-selected based on the type of terrain most encountered. This leads to unknown performance if it becomes necessary to alter the aircraft's flight path, causing different terrain to be encountered. Direct coupling of the radar with the flight control system results in reduced safety and reliability since the algorithms operate open-loop.

The Optimal Controller terrain following system is capable of directly incorporating operational constraints such as maximum and minimum speed limits, a selectable terrain clearance limit, and way-point arrival time. The objective is to include these constraints while minimizing engine cycling and set clearance altitude. The advantages of the Optimal Controller (which are also applicable to the ADLAT controller) are as follows.

1. Reliability is increased due to the continual update of terrain information, thus eliminating many of the adverse forward looking radar characteristics.

2. Predicted trajectory plus the radar altimeter makes the aircraft fly closed-loop on the reverse slopes of mountains.

3. The prediction equations include the aircraft's dynamic constraints and the generated desired flight path includes both vertical velocity and negative g-limits.

The disadvantages of such a system are,

1. The prediction equations predict a flight path over a long distance to which the aircraft is committed to fly. Rapid changes in the desired flight path cause the whole trajectory to be updated in computer memory which may cause time delay problems in applying an "optimal control".
2. The complete aircraft state equations must be known along with the weighting and optimal gain matrices. The calculation of the coefficients of the matrices is very complex and is configuration dependent. For instance, if an aircraft drops bombs, both the aerodynamic and inertia coefficients have changed. The equations solved are a linear representation of the aircraft. If the aircraft enters a non-linear regime the results from an optimal control solution may be questionable.

CHAPTER 3

Output Predictive Algorithmic Controller

Introduction

The following discussion of the Output Predictive Algorithmic Controller (OPAC) is a condensed version of Ref. 3.5 with emphasis on the tracking problem in a terrain following environment. The Output Predictive Algorithmic Controller was derived from a digital control concept developed by Rault and Richalet (Refs. 3.1 and 3.2). OPAC is fundamentally and philisophically different from "feedback" controllers such as the linear quadratic regulator and its variants in which there is an explicit notion of "feedback" of the current "state" to derive a closed-loop control law. Instead, the closed-loop control is achieved by accomplishing, at every cycle of the digital control loop, three separate and very distinct functions:

1. Prediction. The system zero input response is predicted into the future an appropriate number of time steps. This prediction calculation may be accomplished in any number of different ways or methods but it is essential that the prediction be closed-loop, i.e., based upon the most current measurements of the actual output variables.

2. Desired Future Reference Trajectory. The desired output response is calculated into the future for the same number of time steps. This is what gives the control scheme its great power in the dynamic tracking task, for it is generally quite easy to specify how one wants the future output trajectory to behave. For example, in this study it is desired to have the future trajectory follow the future terrain profile. If the system is not currently on the desired path, then a simple exponential decay path to the desired path is constructed.

3. Future Control Calculation. Calculation of the "best" set of future control inputs that will make the system follow the desired future path is accomplished.

Obviously there is considerable design flexibility in this "predictive" control strategy, but this control flexibility is at the same time both a benefit and a detriment. For one thing, there are inherently many design parameters to be chosen in the implementation, and these can present an enigma. Fortunately, some guidelines are provided which will give good performance over the systems tested. Also, since the control technique does not involve a closed-loop state variable model, the closed-loop stability cannot be determined by means of evaluating the eigenvalue locations.

To accomplish task 3 above - future control calculation - it must be formulated and solved as a linear least squares problem. This is accomplished by the introduction of "output smoothing points"; that is, the future output reference trajectory includes output sample points at a much finer sampling interval than the interval at which the controls are being updated. This technique avoids the large oscillations and resulting instability that can be encountered when using only one-step-ahead prediction (Ref. 3.6) by having an explicit weighting on the output response between control switch times. By this technique, it is seen that there is an implicit control of the internal energy or "state" of the system even though there is no explicit control of anything resembling "state". The off-line calculations of this method are substantial, but the on-line calculations become as simple as taking a single vector inner product at each control cycle.

Mathematical Formulation

It is desired to control the continuous, nth order, single-input/single-output linear system

$$\dot{x}(t) = A x(t) + B u(t) \tag{3.1}$$

$$y(t) = C x(t) \tag{3.2}$$

with discrete time model

$$x(k+1) = F x(k) + G u_d(k) \tag{3.3}$$

$$y(k*T_c) = C x(k) \tag{3.4}$$

where

$$F = e^{A*T_c} \qquad G = \left[\int_0^{T_c} e^{A\tau} d\tau \right] B \tag{3.5}$$

The system is assumed to be single-input/single-output (SISO) for ease of presentation, but the subsequent results are easily generalized to the multi-input/multi-output case. The control input is assumed to be piecewise constant, that is,

$$u(t) = u_d(k) \qquad t \in (k*T_c, (k+1)*T_c) \tag{3.6}$$

for the control switch time, T_c.

Letting zero be the current time, future output is related to present state x(0), and future inputs $\{u_d(0), u_d(1), \ldots\}$ via

$$y(k*T_c) = y_{zi}(k*T_c) + \sum_{i=0}^{k-1} h_d(k-i)\, u_d(i) \tag{3.7}$$

The $y_{zi}(k*T_c)$ is the zero input response which may be computed by

$$y_{zi}(k*T_c) = C F^k x(0) \tag{3.8}$$

and $h_d(k)$ is the discrete impulse response function

$$h_d(k) = C F^{k-1} G \tag{3.9}$$

The control problem is formulated by setting up a linear equation problem to force the predicted output in Eq. 3.7 to match the desired

future path, $y_d(k*T_c)$, k=1,2,3,.... If the control task is a regulator, then the desired path brings the system down to rest; if the control task is tracking, then the desired path is made to follow the desired tracking trajectory. OPAC uses perfect state measurements to compute y_{zi}.

The control problem is set up as an overdetermined linear least-squares problem. This is accomplished by examination of the future output trajectory intermediate to the control switch interval, T_c. By this approach, the undesired output oscillations between control switch times can be avoided.

To this end let L be the number of discrete controls to be predicted into the future and let NSM be the number of output "smoothing points" to be calculated between each control switch time. Then it may be shown that the linear equation problem of OPAC can be formulated as

$$\bar{H}U = Y_D - Y_{zi} \tag{3.10}$$

where

$$U = \begin{bmatrix} u_d(0) \\ \Delta u_d(1) \\ \Delta u_d(2) \\ \vdots \\ \Delta u_d(L-1) \end{bmatrix}_{L\times 1} \tag{3.11}$$

$$Y_D = \begin{bmatrix} y_d(1) \\ y_d(2) \\ \vdots \\ y_d(NSM*L) \end{bmatrix}_{(NSM*L)\times 1} \tag{3.12}$$

$$Y_{zi} = \begin{bmatrix} y_{zi}(1) \\ y_{zi}(2) \\ \vdots \\ y_{zi}(NSM*L) \end{bmatrix}_{(NSM*L)\times 1} \tag{3.13}$$

$$\bar{H} = \begin{bmatrix} h_1 & 0 & \cdot & \cdot & \cdot & 0 \\ h_2 & h_1 & \cdot & \cdot & \cdot & 0 \\ \cdot & \cdot & & & & \cdot \\ \cdot & \cdot & & & & \cdot \\ \cdot & \cdot & & & & \cdot \\ h_L & h_{L-1} & \cdot & \cdot & \cdot & h_1 \end{bmatrix}_{(NSM*L)\times L} \tag{3.14}$$

$$h_k = \begin{bmatrix} \sum_{i=1}^{NSM*(k-1)+1} h_d(i) \\ \vdots \\ \sum_{i=1}^{NSM*k} h_d(i) \end{bmatrix}_{NSM\times 1} \tag{3.15}$$

and now, because of the shorter sample time, $T_D=T_C/NSM$, the appropriate $h_d(i)$ are found from Eqs. 3.3 through 3.5 and 3.9 using T_D in Eq. 3.5 rather than T_C. Note from Eq. 3.11 that the calculated future control at time $t\in(k*T_C,(k+1)*T_C]$ is given by

$$u(t) = u_d(k) = u_d(0) + \Delta u(1) + \Delta u(2) + \ldots + \Delta u(k) \tag{3.16}$$

that is, the $\Delta u(i)$ are the changes to the previous control applied. This turns out to be physically meaningful in that it is often more important to know and to minimize the amount of control change from sample to sample rather than the absolute control level itself. The control linear equation problem, Eq. 3.10, may be formulated either way, and it simply means that the H in Eq. 3.14 and the least-squares weighting would have to be modified appropriately. Also note that, while Eq. 3.10 is formulated and "solved" with all L future controls as in Eq. 3.11, only the first $u_d(0)$ is actually applied to the system; in a closed-loop operation the problem will be reformulated and solved at each control sample time. Thus it is really only necessary, on-line, to calculate

$u_d(0)$. It is necessary, however, to formulate Eq. 3.10 with all L controls, as the number of future inputs, L, has a very strong effect upon closed-loop performance.

Now, Eq. 3.10 is an overdetermined linear equation problem for which a least-squares, "approximate" solution is appropriate. To provide for control design flexibility, a weighted least squares criterion

$$J(U^*) = \sum_{i=1}^{NSM*L} q_i \left[H_i U - (y_D(i) - y_{zi}(i)) \right]^2 \qquad (3.17)$$

is utilized, where H is the ith row vector of $\bar{H}$. Letting $Q=\text{diag}[q_1,q_2,\ldots q_{NSM*L}]$ be the matrix of weighting parameters, the "normal equation" solution to Eq. 3.10, which minimizes Eq. 3.17, is given by

$$U^* = (\bar{H}^T Q \bar{H})^{-1} \bar{H}^T Q (Y_D - Y_{zi}) \qquad (3.18)$$

The solution to Eq. 3.18 turns out to be efficient with regard to memory storage because the large dimension H in Eq. 3.14 never has to be actually created and put into memory. Rather, it may be shown that the much lower dimension, symmetric, LxL matrix $(\bar{H}^T Q \bar{H})$ may be created from

$$\left[(\bar{H}^T Q \bar{H})_{ij} \right] = \left[\sum_{k=\max(i,j)}^{L} h_{k-i+1}^T Q_k h_{k-j+1} \right] \qquad (3.19)$$

where Q_k is the NSMxNSM diagonal submatrix of Q such that $Q=\text{diag}[Q_1,Q_2,\ldots Q_L]$. Likewise the Lx1 vector $\bar{H}^T Q(Y_D-Y_{zi})$ may be created from the scalar elements, i=1,2,...,L,

$$\sum_{k=1}^{L} h_{i-k+1}^T Q_k (Y_D - Y_{zi})_k \qquad (3.20)$$

where $(Y_D-Y_{zi})_k$ are the Lx1 dimension partitions of the NSM*L dimension (Y_D-Y_{zi}). Therefore, by Eqs. 3.19 and 3.20 it is seen that only the L vectors $\{h_1,h_2,\ldots h_L\}$ need to be created rather than the entire $\bar{H}$ matrix in Eq. 3.14. This reduces memory storage requirements necessary to compute Eq. 3.18 by a considerable amount. It is remarked, though, that if memory is not a problem it would definitely be preferrable for reasons

of numerical conditioning to use the singular value decomposition to solve Eq. 3.17.

Once the least-squares solution of Eq. 3.18 is obtained, the first element of U^*, the $u_d^*(0)$, is applied to the system over the next T_c units of time. Then the problem is reformulated at the next sample time, and the next $u_d^*(0)$ is calculated and applied. In this fashion the control law is made "closed loop."

The only remaining variables in Eq. 3.18 which are not fully defined are the predicted output, Y_{zi}, and the desired trajectory, Y_D. The former would normally involve an estimator (e.g., a Kalman filter) to insure that prediction is made "closed loop". Detailed consideration of this is beyond the scope of this study. The future desired trajectory is control objective dependent. The tracking case is discussed in the next section.

Tracking Case

The solution of the OPAC, Eq.3.18, involves the Y_D vector of Eq. 3.12 of the future desired trajectory $y_D(k)$, k=1,2,...,NSM*L. If the control objective is to reach some constant value, y_{set}, then an exponential decay path to reach this y_{set} is

$$y_D(k) = y_{set} - \beta^k \left[y_{set} - y(0) \right] \tag{3.21}$$

where

$$\begin{aligned} \beta &= \exp(-T_c/(NSM*\tau)) \\ T_c &= \text{Control Switch Time} \\ NSM &= \text{Number of Output Samples per Control} \\ \tau &= \text{Desired Time Constant} \\ y(0) &= \text{Output Value at Current Time} \end{aligned} \tag{3.22}$$

The tracking task implementation of the OPAC control law involves formation of the future desired trajectory in Y_D, Eq. 3.12. Let $y_{tr}(t)$, t>0, where 0 is the current time, denote the "true" desired future output path. Then we let

$$y_D(1) = y_{tr}(T_D) + \beta \left[y(0) - y_{tr}(0) \right] \tag{3.23}$$

$$Y_D(2) = Y_{tr}(2T_D) + \beta^2 \left[Y(0) - Y_{tr}(0) \right] \tag{3.24}$$

$$\vdots$$

$$Y_D(L*NSM) = Y_{tr}(L*NSM*T_D) + \beta^{L*NSM} \left[Y(0) - Y_{tr}(0) \right] \tag{3.25}$$

where

$$T_D = T_c / NSM$$

is the sample time of the output points. Thus, the discrete $y_D(k)$ approaches the true continuous $y_{tr}(t)$ exponentially as k incrreases. With Y_D defined as such, the tracking implementation of the OPAC is again defined by Eq. 3.18.

If a very rapid response is desired, then the absolute time constant, τ, is made very small with accompanying large values of control necessary. If a slower response is acceptable, then may be made larger with smaller inputs required. The influence on the control problem, according to the least-squares weighting (Eq. 3.17), is that the system is forced to follow this desired exponential decay trajectory. The desired system time constant is thus selectable by the system designer according to the desired control levels available and the desired performance criterion. With proper control levels available, almost any speed of response could be achieved with virtually no overshoot. However, previous studies have shown that a very fast response will result in poor robustness.

The number of "smoothing points" on the output between control changes, NSM, and the number of prediction steps into the future, L, turned out to be key parameters affecting closed-loop performance and stability - particularly L, the number of control predictions into the future. As a rule of thumb, it seems that L should be selected between the bounds $n \lesssim L \lesssim (2n-1)$, where n is the underlying state dimension.

The number of smoothing points, NSM, also had a key effect upon closed-loop performance. It was known that NSM>2 was required or else the linear equation problem, Eq. 3.10, would be reduced to one-step-ahead prediction regardless of the value of L selected (Refs. 3.4 and 3.6). It also seemed logical that the greater the value of NSM the tighter the closed-loop trajectory should stay to the desired exponential decay trajectory. However, increasing NSM beyond n produced more oscillations in the closed-loop response. Thus, as a rule of thumb, NSM=n seems to be a reasonable value. However, the actual closed-loop performance is also strongly influenced by two other factors as well - the sample time T_c and the least-squares cost function Q.

Unlike the deadbeat control law of Ref. 3.3, the absolute speed of response is controlled here more by the desired time constant than it is by control switch time T_c. However, just like the deadbeat case of Ref. 3.3, T_c can have a strong influence upon the conditioning of the inherent linear equation problem (Eq. 3.10) and hence upon closed-loop robustness. It was shown in Ref. 3.5 that the best value of T_c appeared to correspond to the peak of the reciprocal condition number of $(\bar{H}^T Q \bar{H})$. Therefore, it is hypothesized that choosing T_c to minimize the condition number (maximize the reciprocal condition number) will be a robust design strategy regardless of the basic speed of response demanded of the system. This and many more issues regarding closed-loop robustness are left to be explored.

The previous control design parameters mentioned (τ,L,NSM, and T_c) offer considerable design flexibility in themselves, but certainly the greatest flexibility exists in the symmetric, positive definite weighting matrix Q. For computational reasons it is best to keep this diagonal or at least block diagonal. But even diagonal it has NSM*L free parameters.

A number of possibilities were explored in Ref. 3.7 for selection of Q, but as a general rule it can be said that weighting Q more heavily during the latter portion of the predicted trajectory did much better than equal weighting or weighting heavily the early portion of the trajectory.

Summary

A generalized discussion of OPAC as pertaining to tracking has been given. The influence of the various design parameters has also been discussed along with some useful guidelines for their selection. The control switch time may be very important to closed-loop robustness, and a method to find the best switch time by picking the value which maximizes the reciprocal condition number of the normal equations is discussed.

CHAPTER 4

Model Development

Introduction

The aircraft chosen for this study is the F-111/MAW (Mission Adaptive Wing). Unlike a conventional wing, the MAW can automatically reconfigure in flight for efficient performance at any altitude, at any speed, and under any flight condition. The variable-camber MAW can always be in the best camber configuration for whatever flight mode is chosen. For terrain following, the MAW is ideal because the direct lift permits the aircraft to maneuver responsively to avoid obstacles, and gust alleviation improves ride quality, thus reducing crew fatigue. The F-111 is chosen due to the variable swept wing geometry. Flying 100 ft. above ground level (AGL) requires, among other things, fuel efficiency and obstacle avoidance. A highly swept wing will reduce the drag and at the same time increase fuel efficiency, but will mask the inboard portion of the trailing edge flap thus, reducing the direct lift capability. A wing with less sweep will increase the direct lift capability but will also increase the drag on the aircraft, thus limiting the overall mission range on the aircraft. The two models chosen have sweeps of 35 degrees and 58 degrees. The aircraft dynamics associated with each of the wing sweeps will be discussed.

The terrain model chosen for this study was a moderately rough profile in the Fulda Gap region of Germany. A discussion of the terrain and how the aircraft's trajectory was generated is also included.

Mission Adaptive Wing

The MAW does what other wings cannot do. It maintains aerodynamic efficiency at all speeds and in all flight modes no matter what the

flight condition is or what pilot command is given. Smooth flexible leading and trailing edges are the key to performance. Unlike conventional wings, there are no spoilers, flaps, or fairings to break the smooth contour of it's upper and lower surfaces. The actuation system is confined within the airfoil shape. The flexible leading edge is one continuous segment, and the flexible trailing edge is divided into separate segments for roll control and shifting the aerodynamic load.

The concept is not new. Birds fly with variable camber wings and the Wright brothers first introduced lateral control by manually twisting the tips of their airplane wings. Today, wings have hinged ailerons and spoilers for lateral control. They also have trailing-edge flaps and leading-edge slats for high lift during takeoff and landing. However, these devices do not permit maximum aerodynamic efficiency over the entire range of flight conditions. These wings are designed for a primary mission, say, subsonic cruise, and will pay penalties during takeoffs, landings, and higher cruising speeds. The MAW has the capability of being automatically reconfigured for any flight regime.

When sensors detect gust or maneuver loads, the variable camber segments of the trailing-edge flaps deflect to change the wing load distribution. This moves the center of pressure forward as load factor increases. Thus, bending loads are kept low enough for the MAW to withstand high g-forces. To alleviate gusts, the trailing-edge segments deflect automatically as a function of gust accelerations, thus reducing the gust loads felt by the aircraft.

For direct lift control, the variable camber trailing-edge flaps in combination with the horizontal tail permit control of pitch attitude, flight path, and angle of attack. Direct lift will allow the aircraft to maneuver more responsively to avoid obstacles. Fig. 4.1 shows the leading-edge and trailing-edge flap layout on the F-111/MAW.

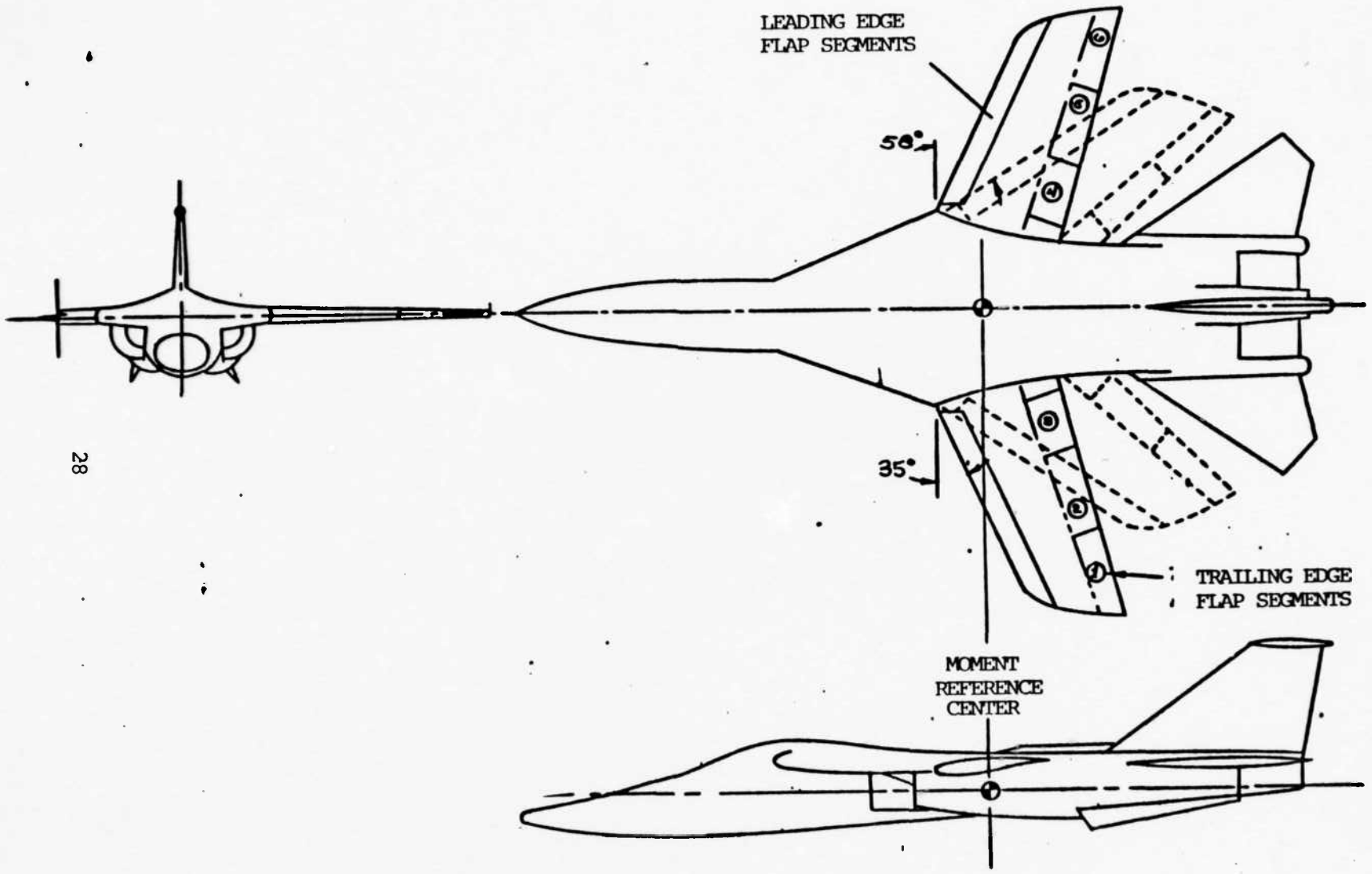

Fig. 4.1 Leading and Trailing Edge Flaps for F-111/MAW

Aircraft Dynamics

Classical methods of linear analysis are used extensively in the preliminary design of aircraft control systems since these methods offer tremendous insight into the dynamic behavior of the system at relatively low cost. However, before analysis techniques can be applied to the control system design task, a suitable dynamic model must be developed for the aircraft and the control system, and transfer functions must be generated for the various system elements. This can be a tedious procedure if a number of flight conditions and/or a number of aircraft or control system configurations must be examined. However, the digital computer can be effectively used to perform this analysis. The use of the digital computer to compute aircraft dynamics is discussed below while the control system design procedure is discussed in Chapter 5.

TTYLON is a teletype-interactive program for computing longitudinal aircraft transfer functions. Orginally called the Flight Vehicle Analysis Program and documented in Ref. 4.1, this program consists of thirty-three subroutines specifically designed to interface with a specially prepared main program. TTYLON consists of two major sections: the aerodynamic data section and the flight case section. Aircraft longitudinal aerodynamic data is entered as a function of Mach number in the first section. In the second section, the designer inputs the flight case which is defined by Mach, altitude (feet), weight (lbs), center of gravity, and flight path angle (degrees). The program determines the trim angle of attack, elevator deflection, and thrust at this flight condition and then computes the non-dimensional, stability-axis derivatives and the body-axis dimensional derivative parameters. A new flight case can then be requested or the complete data entry sequence can be repeated.

The derivation of the equations of motion for TTYLON is based on Newton's laws of motion referenced to an axis fixed in space. The force acting on a body is equal to the time rate of change of momentum and the torque applied to the body is equal to the time rate of change of the moment of momentum. For the longitudinal motion of an aircraft this can be stated mathematically for the reference system shown in Fig. 4.2 as follows:

$$\Sigma F_x = \frac{d}{dt}(m\bar{V})_x \tag{4.1}$$

$$\Sigma F_z = \frac{d}{dt}(m\bar{V})_z \tag{4.2}$$

$$\Sigma M = \frac{d}{dt}\bar{H}_y \tag{4.3}$$

This report will proceed no further with the fundamental derivation of the equations of motion. Numerous reports have treated this subject, such as Refs. 4.2 and 4.3. For convenience, the linearized equations of motion that are used by TTYLON are:

$$\Delta X + \Delta T \cos\epsilon_T = m(\dot{u} + W_o q + \theta q \cos\theta_o) \tag{4.4}$$

$$\Delta Z - \Delta T \sin\epsilon_T = m(U_o \alpha - U_o q + \theta q \sin\theta_o) \tag{4.5}$$

$$\Delta M + \Delta T Z_T \cos\epsilon_T = I_{yy}\dot{q} \tag{4.6}$$

$$\dot{\theta} = q \tag{4.7}$$

where

$$\Delta X = m(X_{\dot{u}}\dot{u} + X_u u + X_{\dot{\alpha}}\dot{\alpha} + X_\alpha \alpha + X_q q + X_{\delta e}\delta_e) \tag{4.8}$$

$$\Delta Z = m(Z_{\dot{u}}\dot{u} + Z_u u + Z_{\dot{\alpha}}\dot{\alpha} + Z_\alpha \alpha + Z_q q + Z_{\delta e}\delta_e) \tag{4.9}$$

$$\Delta M = I_{yy}(M_{\dot{u}}\dot{u} + M_u u + M_{\dot{\alpha}}\dot{\alpha} + M_\alpha \alpha + M_q q + M_{\delta e}\delta_e) \tag{4.10}$$

The stability derivatives that are used as input in TTYLON are a combination of wind tunnel and flight test data and are given in Ref 4.4. Ref 4.5 derives the F-111/MAW flap models. There are three trailing-edge

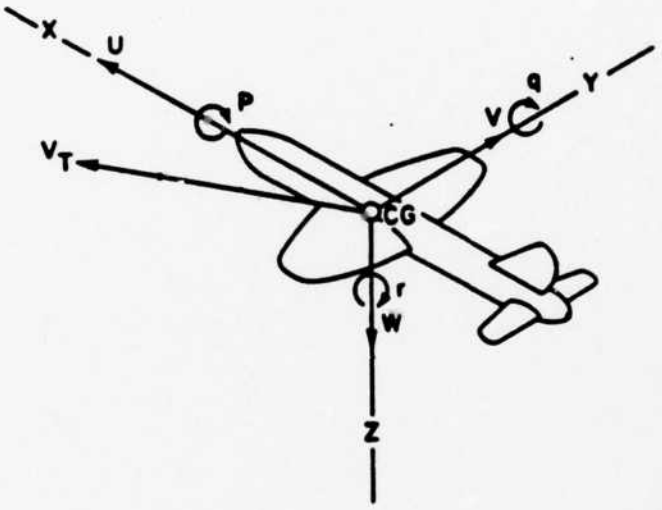

REFERENCE INERTIAL AXIS AND ASSOCIATED AIRFRAME MOTION

Fig. 4.2

flaps and one continuous flexible leading-edge flap per wing. Since this terrain following study is at a flight condition where only small angle of attack (AOA) excursions are required during longitudinal maneuvers, the leading-edge flap is not used. Deflection of the leading-edge flap at low AOA causes a negative increment in lift on the wing. The leading-edge flap is deflected at high AOA to prevent flow separation on the wing. Again due to longitudinal maneuvering only, the trailing-edge flaps are deflected as one unit. With a wing sweep of 35 degrees on the F-111/MAW, the full span of trailing-edge flaps can be utilized for direct lift. The design criteria for an aircraft on a low-level penetration mission is to fly at minimum drag as fast as possible. The maximum speed is determined by the shock wave on the wing. Any large increase in speed will cause shock induced separation of flow on the wing which will result in a large increase in drag as shown Fig. 4.3. Therefore, Fig 4.3 shows the best aircraft configuration to be at the 58 degree wing sweep. However, flying at very low altitudes introduces other design factors that must be taken into account. These factors include maximum maneuverability, gust response, ride quality (crew fatigue), and the amount of deviation from the desired trajectory. With a wing sweep of 58 degrees the inboard flap is covered by the overwing fairing thus reducing direct lift capability. Both wing sweeps will be used in this study.

Table 4.1 gives the data that was used in TTYLON. Both elevator and trailing-edge flap data are entered separately into the control surface parameter in order to compute the transfer functions. Table 4.2 shows the transfer functions to elevator input at the 35 degree wing sweep; Table 4.3 gives the transfer functions to the trailing-edge flap input at the 35 degree wing sweep; Table 4.4 gives the transfer functions to elevator input at the 58 degree wing sweep; and Table 4.5 gives the transfer

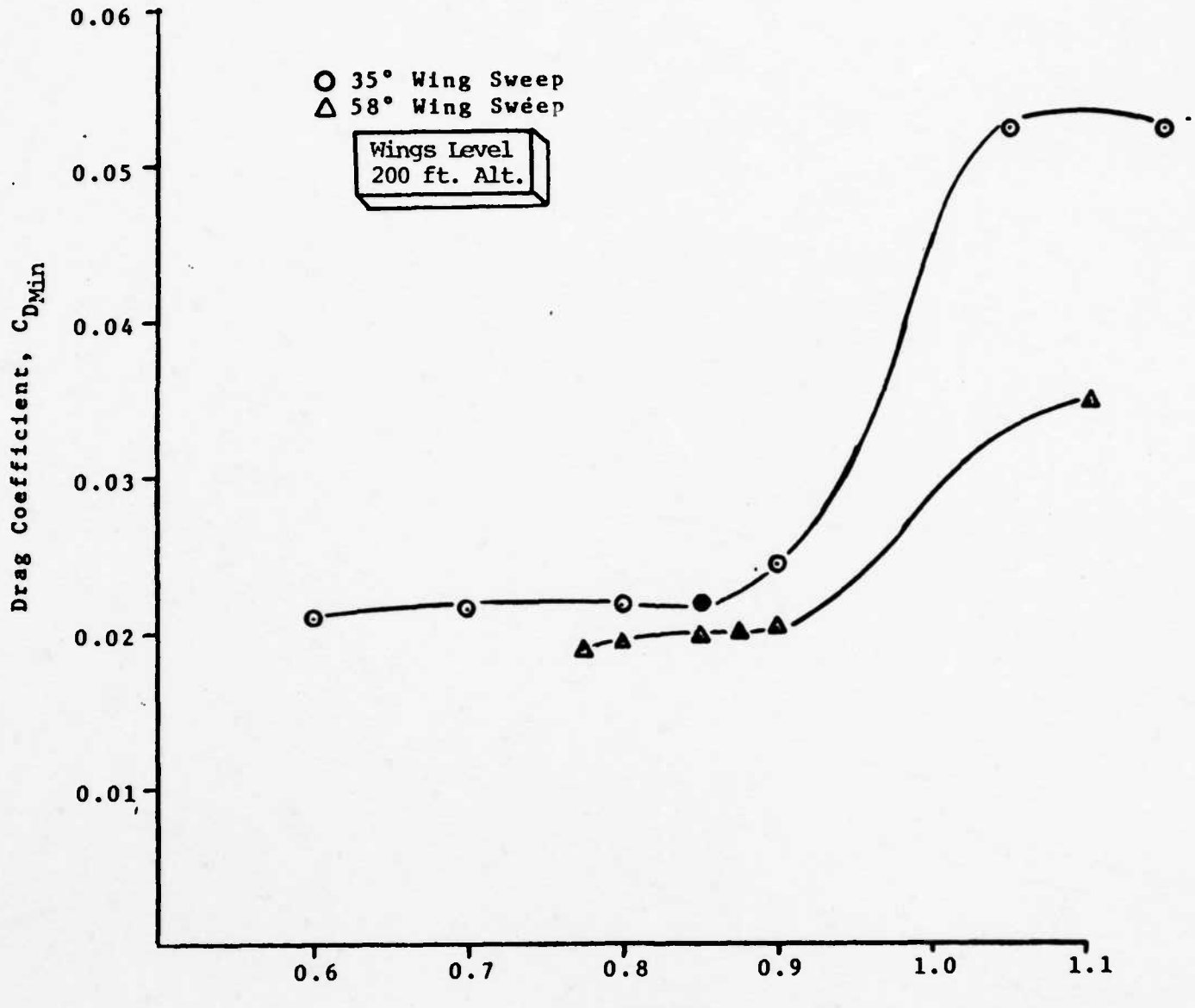
0.06
0.05
0.04
0.03
0.02
0.01
Drag Coefficient, $C_{D_{Min}}$
35° Wing Sweep
58° Wing Sweep
Wings Level
200 ft. Alt.
0.6
0.7
0.8
0.9
1.0
1.1
MACH NUMBER

Fig. 4.3

functions to trailing-edge flap input at the 58 degree wing sweep. A discussion of how the elevator and trailing-edge flaps were blended in the flight control system are given in Chapter 6.

Model Transformation

By using the transfer functions described in the previous section, a phase variable representation of the state space matrix was developed. This representation is inconvenient, however, for the reasons described below. A seventh-order model was developed from the original fourth-order model described in the previous section by adding two control surface actuator states and an altitude state. Each control input needs a seventh-order A matrix since a phase variable representation can only be used for a single output system. The resulting fourteenth-order representation proved to be inconvenient for on-line computer operations. Secondly, it was necessary to use a transformation matrix, P , to recover a physical variable that would be used to excite the gust mode in the aircraft. The transformation matrix that was chosen is a matrix of the numerator coefficients of each of the state's transfer functions. Therefore, given the transfer functions in Tables 4.2 through 4.5 a linear transformation from the phase variable system to the physical variable system can be made. A new "physical variable" state, Z, can be computed from the original state by setting

$$Z = P^{-1}X \tag{4.11}$$

expanding Eq. 4.11 for the elevator input yields,

$$\begin{bmatrix} U \\ \alpha \\ q \\ h \end{bmatrix} = \begin{bmatrix} 1077.4 & 62.488 & 1982.10 & 14.801 \\ -0.0062 & -0.789 & -34.07 & -0.255 \\ 0.0 & -0.842 & -34.21 & -33.866 \\ -778.3 & -33605 & 205.40 & 256.200 \end{bmatrix} \begin{bmatrix} x_1 \\ x_2 \\ x_3 \\ x_4 \end{bmatrix} \tag{4.11a}$$

Finally, in order to follow a low altitude terrain profile, all of the aircraft's states need to be initialized which cannot easily be done in

TABLE 4.1

Aerodynamic and Geometric
Data for the F-111/MAW

PARAMETER	COMPUTER SYMBOL	35 DEG SWEEP	58 DEG SWEEP
A	AREA	604.0	604.0
$\bar{c}$	CHORD	10.5	10.5
ε_T	EPSTH	0.0	0.0
Z_T	ZT	0.0	0.0
c.g.	REF CG	0.29	0.32
W	WEIGHT	67220.0	67220.0
I_{YY}	IYY	408900.0	408900.0
M	REF MACH	0.9	0.9
C_{L_M}	CLM	0.0	0.0
$C_{L_{\alpha=0}}$	CL(AOA=0)	-0.09	-0.09
C_{L_α}	CLA	0.105	0.056
$C_{L_{\delta e}}$	CLDE	0.013	0.013
$C_{L_{\delta_{TF}}}$	CLDF	0.0215	0.0087
C_{L_q}	CLQ	5.0	5.0
$C_{L_{\dot{\alpha}}}$	CLAD	2.5	2.5
$C_{L_{Max}}$	CLMAX	1.0	1.0
C_{m_M}	CMM	0.0	0.0
$C_{m_{C_{L=0}}}$	CM(CL=0)	-0.075	0.015
$C_{m_{C_L}}$	CMCL	-0.2495	-0.2679
$C_{m_{\delta e}}$	CMDE (CL)	-0.0255	-0.0285
$C_{m_{\delta_{TF}}}$	CMDF (CL)	-0.0045	-0.0046
C_{m_q}	CMQ	-27.0	-22.5
$C_{m_{\dot{\alpha}}}$	CMAD	-4.0	-4.0
C_{D_M}	CDM	0.1	0.035
$C_{D_{Min}}$	CDMIM	0.024	0.018

TABLE 4.1 cont.

$C_{L_{C_{D_{Min}}}}$	CL(CDMIN)	0.095	-0.02
KC_L^2	KCL2	0.00082	0.0014
$\delta e_{C_{D_{Min}}}$	DE(CDMIN)	0.0	0.0
$K\delta e^2$	KDE2	0.0	0.0
T_{max}	TMAX	25000.0	25000.0
Altitude	ALT	200.0	200.0
γ	GAMMA	0.0	0.0
$C_{D_{\delta e}}$	CDDE	0.0009	0.0002
$C_{D_{\delta TF}}$	CDDF	0.0036	0.0004

TABLE 4.2

Transfer Functions to Elevator Input (35 Deg Sweep)

Polynomial Coefficients		Polynomial Factors
	Denominator	
1.0	S**4	(-0.023662) + j(0.033897)
5.1072	S**3	(-0.023662) + j(-0.033897)
33.0860	S**2	(-2.53) + j(5.1424)
1.5630	S**1	(-2.53) + j(-5.1424)
0.05613	S**0	
	Forward Velocity Numerator	
9.8849	S**3	(-0.016764) + j(1.2322)
1186.7	S**2	(-0.016764) + j(-1.2322)
54.787	S**1	(-120.02) + j(0.0)
1801.7	S**0	
	Angle of Attack Numerator	
-0.2547	S**3	(-0.052112) + j(0.0)
-30.794	S**2	(0.004703) + j(0.0)
-1.4593	S**1	(-120.84) + j(0.0)
-0.0075	S**0	
	Pitch Rate Numerator	
-30.426	S**3	(-0.485250) + j(0.0)
-57.407	S**2	(-1.8383) + j(0.0)
-2.714	S**1	(0.0) + j(0.0)
	Altitude Rate Numerator	
256.18	S**3	(-0.047395) + j(0.0)
369.50	S**2	(14.141) + j(0.0)
-52627.00	S**1	(-15.536) + j(0.0)
-2667.60	S**0	

TABLE 4.3

Transfer Functions to Flap Input (35 Deg Sweep)

Polynomial Coefficients		Polynomial Factors
	Denominator	
1.0	S**4	(-0.023662) + j(0.033897)
5.1072	S**3	(-0.023662) + j(-0.033897)
33.0860	S**2	(-2.53) + j(5.1424)
1.5630	S**1	(-2.53) + j(-5.1424)
0.05613	S**0	
	Forward Velocity Numerator	
45.466	S**3	(-0.008504) + j(0.51117)
1223.2	S**2	(-0.008504) + j(-0.51117)
32.674	S**1	(-26.886) + J(0.0)
319.5	S**0	
	Angle of Attack Numerator	
-0.4213	S**3	(-0.065655) + j(0.0)
-11.457	S**2	(0.017867) + j(0.0)
-0.5449	S**1	(-27.148) + j(0.0)
-0.0135	S**0	
	Pitch Rate Numerator	
-103.12	S**3	(-0.04955) + j(0.0)
-10.407	S**2	(-0.9596) + j(0.0)
-0.4903	S**1	(0.0) + j(0.0)
	Altitude Rate Numerator	
423.68	S**3	(-0.047348) + j(0.0)
1149.8	S**2	(3.6986) + j(0.0)
-9920.9	S**1	(-6.3652) + j(0.0)
-427.27	S**0	

TABLE 4.4

Transfer Functions for Elevator Input (58 Deg Sweep)

Polynomial Coefficients		Polynomial Factors
	Denominator	
1.0	S**4	(-0.011560) + j(0.040469)
3.6855	S**3	(-0.011560) + j(-0.040469)
18.208	S**2	(-1.8312) + j(3.8429)
0.4255	S**1	(-1.8312) + j(-3.8429)
0.0321	S**0	
	Forward Velocity Numerator	
14.801	S**3	(-0.013735) + j(0.73722)
1982.1	S**2	(-0.013735) + j(-0.73722)
62.483	S**1	(-133.89) + j(0.0)
1077.4	S**0	
	Angle of Attack Numerator	
-0.2547	S**3	(-0.011585) + j(0.006959)
-34.07	S**2	(-0.011585) + j(-0.006959)
-0.7893	S**1	(-133.73) + j(0.0)
-0.0062	S**0	
	Pitch Rate Numerator	
-33.866	S**3	(-0.025257) + j(0.0)
-34.205	S**2	(-0.98476) + j(0.0)
-0.8423	S**1	(0.0) + j(0.0)
	Altitude Rate Numerator	
256.18	S**3	(-0.023157) + j(0.0)
205.43	S**2	(11.071) + j(0.0)
-33605.0	S**1	(-11.85) + j(0.0)
-778.3	S**0	

TABLE 4.5

Transfer Functions to Flap Input (58 Deg Sweep)

Polynomial Coefficients		Polynomial Factors
	Denominator	
1.0	S**4	(-0.011560) + j(0.040469)
3.6855	S**3	(-0.011560) + j(-0.040469)
18.208	S**2	(-1.8312) + j(3.8429)
0.4255	S**1	(-1.8312) + j(-3.8429)
0.0321	S**0	
	Forward Velocity Numerator	
10.639	S**3	(-0.001002) + j(0.60711)
473.47	S**2	(-0.001002) + j(-0.60711)
4.8706	S**1	(-44.501) + j(0.0)
174.51	S**0	
	Angle of Attack Numerator	
-0.1705	S**3	(-0.011618) + j(0.019758)
-7.637	S**2	(-0.011618) + j(-0.019758)
-0.1775	S**1	(-44.776) + j(0.0)
-0.0041	S**0	
	Pitch Rate Numerator	
-7.2942	S**3	(-0.025985) + j(0.0)
-5.5748	S**2	(-0.73829) + j(0.0)
-0.1399	S**1	(0.0) + j(0.0)
	Altitude Rate Numerator	
171.44	S**3	(-0.023147) + j(0.0)
344.45	S**2	(4.725) + j(0.0)
-5428.5	S**1	(-6.711) + j(0.0)
-125.83	S**0	

phase variable form. Since the equations are linearly independent, the following relationships are established

$$\underline{X} = \begin{bmatrix} x_1 \\ x_2 \\ x_3 \\ x_4 \end{bmatrix} \quad \underline{Z} = \begin{bmatrix} U \\ \alpha \\ q \\ \dot{h} \end{bmatrix} \tag{4.12}$$

$$X = PZ \tag{4.13}$$

The rows of the P^{-1} matrix are the numerator coefficients of each physical variable transfer function.

Since

$$\dot{X} = AX + BU \tag{4.14}$$

Eq. 4.13 can be substituted into 4.14 to yield

$$P\dot{Z} = APZ + BU \tag{4.15}$$

Rearranging Eq. 4.15 yields

$$\dot{Z} = [P^{-1}AP]Z + [P^{-1}B]U \tag{4.16}$$

Similarly

$$y = CX = CPZ \tag{4.17}$$

Since the aircraft's states remain the same regardless of which input is used, the $[P^{-1}AP]$ martrices calculated for both the elevator and flap inputs should be identical. Any differences can be attributed to roundoff error and lack of precision (five significant figures) in the transfer function coefficients. An average of the two matrices was chosen. The eigenvalues and transfer functions were then rechecked to determine any significant deviation from the original plant's eigenvalues. Once it was determined that the eigenvalues were similar, the interactive computer program TOTAL was used to calculate the transformation matrices. For this study the output state that needed to be monitored was altitude. This

state plus two actuator states on the inputs were added to complete the plant matrix. The transformed A,B, and C matrices and the state vector for the 58 degree sweep model are given below,

$$A = \begin{bmatrix} -0.0233 & 64.6 & -59.77 & -0.03194 & 0.0 & 14.8 & 10.64 \\ 0.0 & -1.103 & 0.9866 & 0.0 & 0.0 & -0.2547 & -0.1705 \\ 0.00095 & -15.45 & -2.559 & 0.0 & 0.0 & -33.87 & -7.294 \\ -0.0036 & 1109.5 & 13.47 & 0.0 & 0.0 & 256.18 & 171.4000 \\ 0.0 & 0.0 & 0.0 & 1.0 & 0.0 & 0.0 & 0.0 \\ 0.0 & 0.0 & 0.0 & 0.0 & 0.0 & -0.628 & 0.0 \\ 0.0 & 0.0 & 0.0 & 0.0 & 0.0 & 0.0 & -0.698 \end{bmatrix}$$

$$B = \begin{bmatrix} 0.0 & 0.0 \\ 0.0 & 0.0 \\ 0.0 & 0.0 \\ 0.0 & 0.0 \\ 0.0 & 0.0 \\ 0.628 & 0.0 \\ 0.0 & 0.698 \end{bmatrix}$$

$$C = \begin{bmatrix} 0.0 & 0.0 & 0.0 & 0.0 & 1.0 & 0.0 & 0.0 \end{bmatrix}$$

$$Z = \begin{bmatrix} U \\ \alpha \\ q \\ h \\ \dot{h} \\ \delta_e \\ \delta_f \end{bmatrix}$$

The transformed A matrix for the 35 degree sweep model is shown below,

$$A = \begin{bmatrix} -0.05602 & 146.54 & -72.39 & -0.0319 & 0.0 & 9.885 & 45.47 \\ 0.00009 & -2.057 & 0.9866 & 0.0 & 0.0 & -0.2547 & -0.4213 \\ 0.001997 & -26.84 & -2.994 & 0.0 & 0.0 & -30.43 & -10.31 \\ -0.08893 & 2068.5 & 13.47 & 0.0 & 0.0 & 256.2 & 423.7 \\ 0.0 & 0.0 & 0.0 & 1.0 & 0.0 & 0.0 & 0.0 \\ 0.0 & 0.0 & 0.0 & 0.0 & 0.0 & -0.628 & 0.0 \\ 0.0 & 0.0 & 0.0 & 0.0 & 0.0 & 0.0 & -0.698 \end{bmatrix}$$

The eigenvalues for each aircraft model are shown below,

	58 Degree Sweep	35 Degree Sweep
EV(1)=	(-0.01156) + j(0.04047)	(-0.02456) + j(0.03301)
EV(2)=	(-0.01156) + j(-0.04047)	(-0.02456) + j(-0.03301)
EV(3)=	(-1.831) + j(3.843)	(-2.529) + j(5.139)
EV(4)=	(-1.831) + j(-3.843)	(-2.529) + j(-5.139)
EV(5)=	(0.0) + j(0.0)	(0.0) + j(0.0)
EV(6)=	(-0.628) + j(0.0)	(-0.628) + j(0.0)
EV(7)=	(-0.698) + j(0.0)	(-0.698) + j(0.0)

Terrain Model and Trajectory Generation

The terrain model chosen for this study is a 42 mile stretch of moderately rough terrain in the Fulda Gap region of West Germany. The compressed terrain profile is shown in Fig. 4.8 while the expanded version of the Fulda Gap is shown in Fig. 4.9. The generated trajectory takes into account the control surface actuator dynamics and the g-limits imposed due to crew fatigue. The generation of a trajectory is a complete design problem in itself due to design constraints imposed by the aircraft, the crew, and the type of terrain to be followed. The trajectory generation problem is beyond the scope of this effort. However, several selected control system outputs were monitored to determine if any of the imposed constraints in the aircraft were exceeded and also gain insight into which parameters were important in the trajectory generation problem.

Summary

The aircraft transfer functions are derived for the F-111/MAW. The data for this model was extracted from wind tunnel and flight test data and linearized using standard linearization techniques as shown in Refs. 4.2 and 4.3. The F-111/MAW is chosen due to the direct lift capability and the gust alleviation improvement to ride quality. Two wing sweeps, 35 degrees and 58 degrees, are chosen. At the 35 degree wing sweep the full span of trailing-edge flaps can be used. For the low-level penetration mission the wing sweep that is used is 58 degrees, but the inboard flap is covered by the overwing fairing. Both wing sweeps are studied to determine aircraft performance during a terrain following mission.

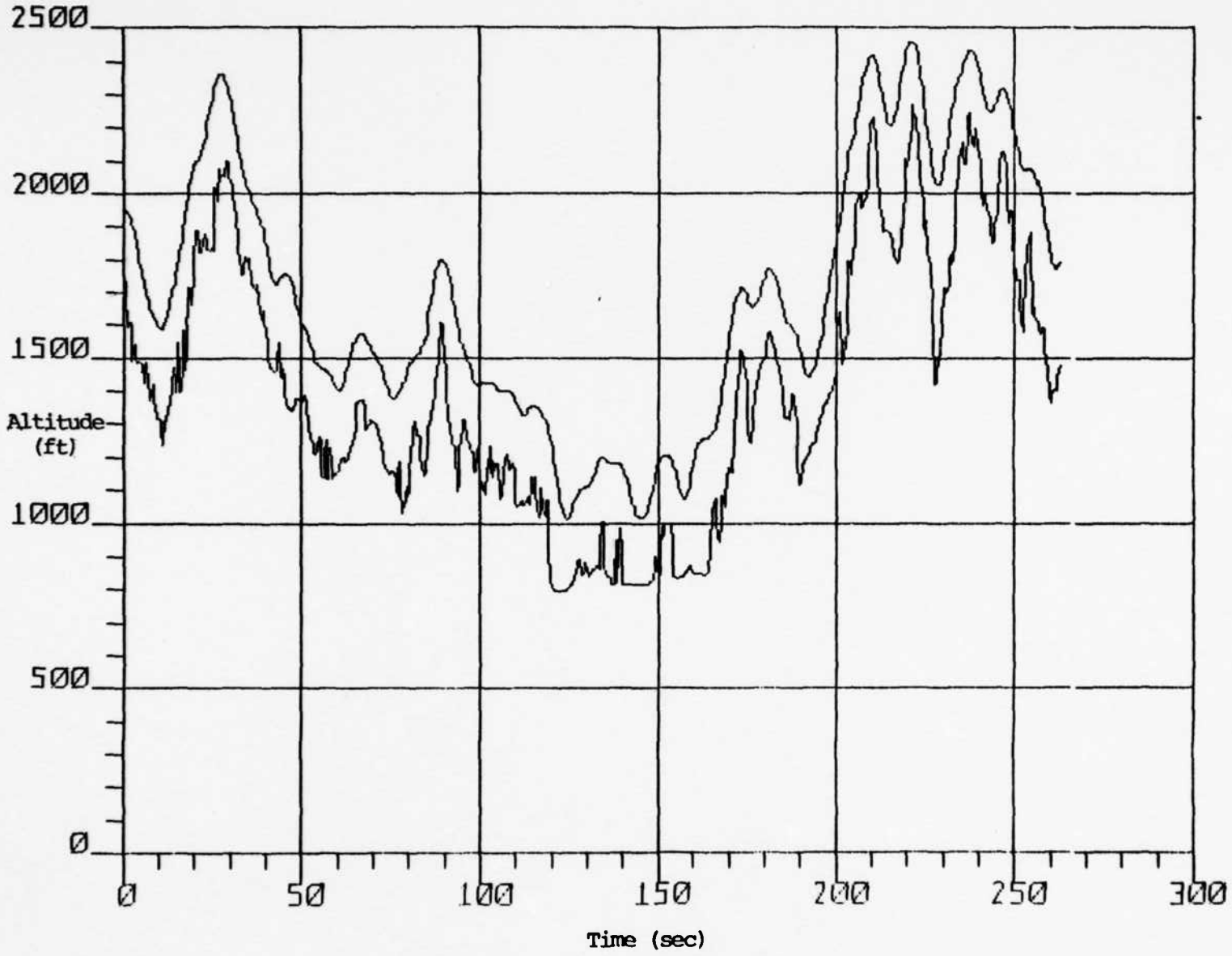

Fig. 4.6 Terrain Profile with Desired Trajectory

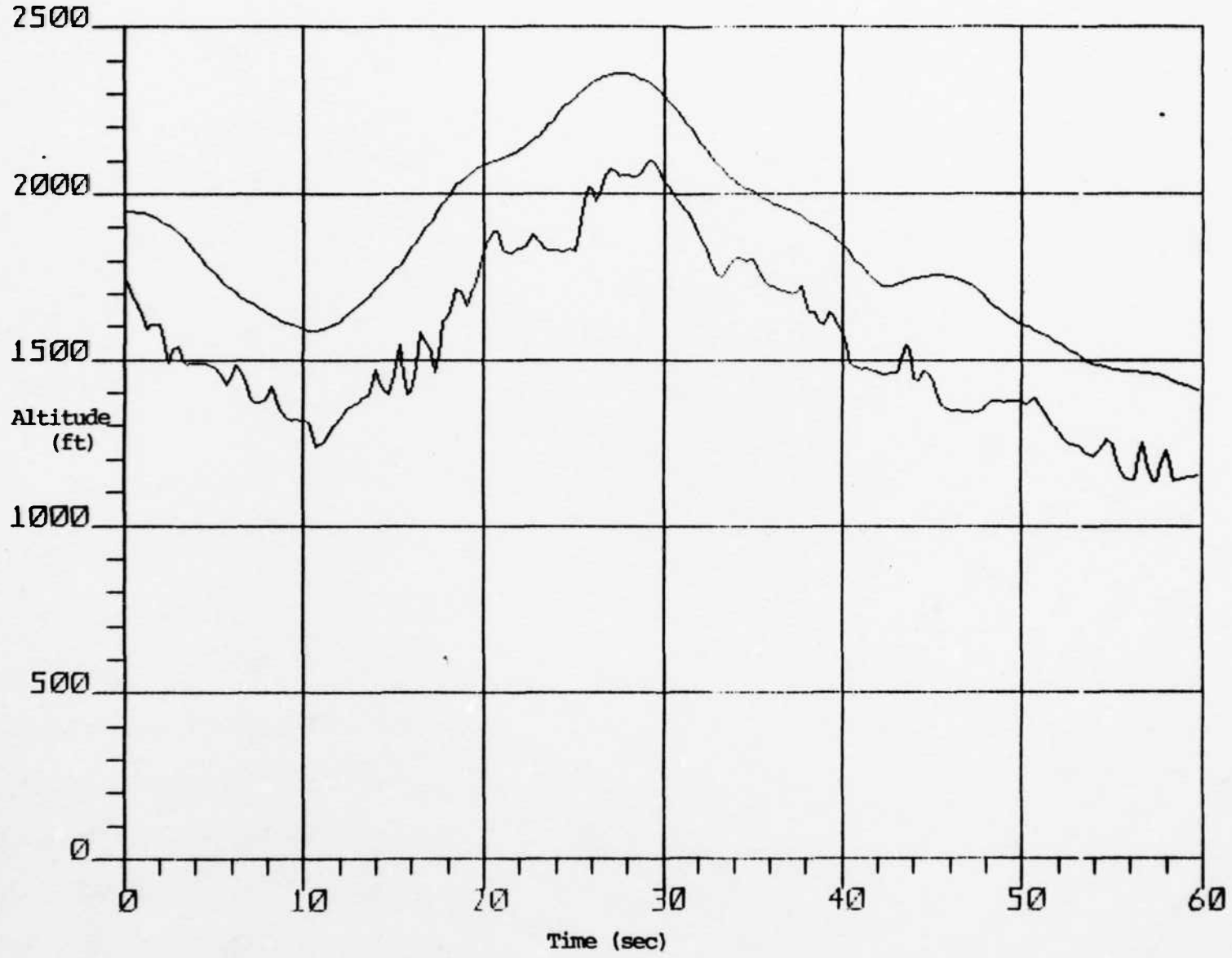

Fig. 4.7 Expanded Terrain Profile with Desired Trajectory

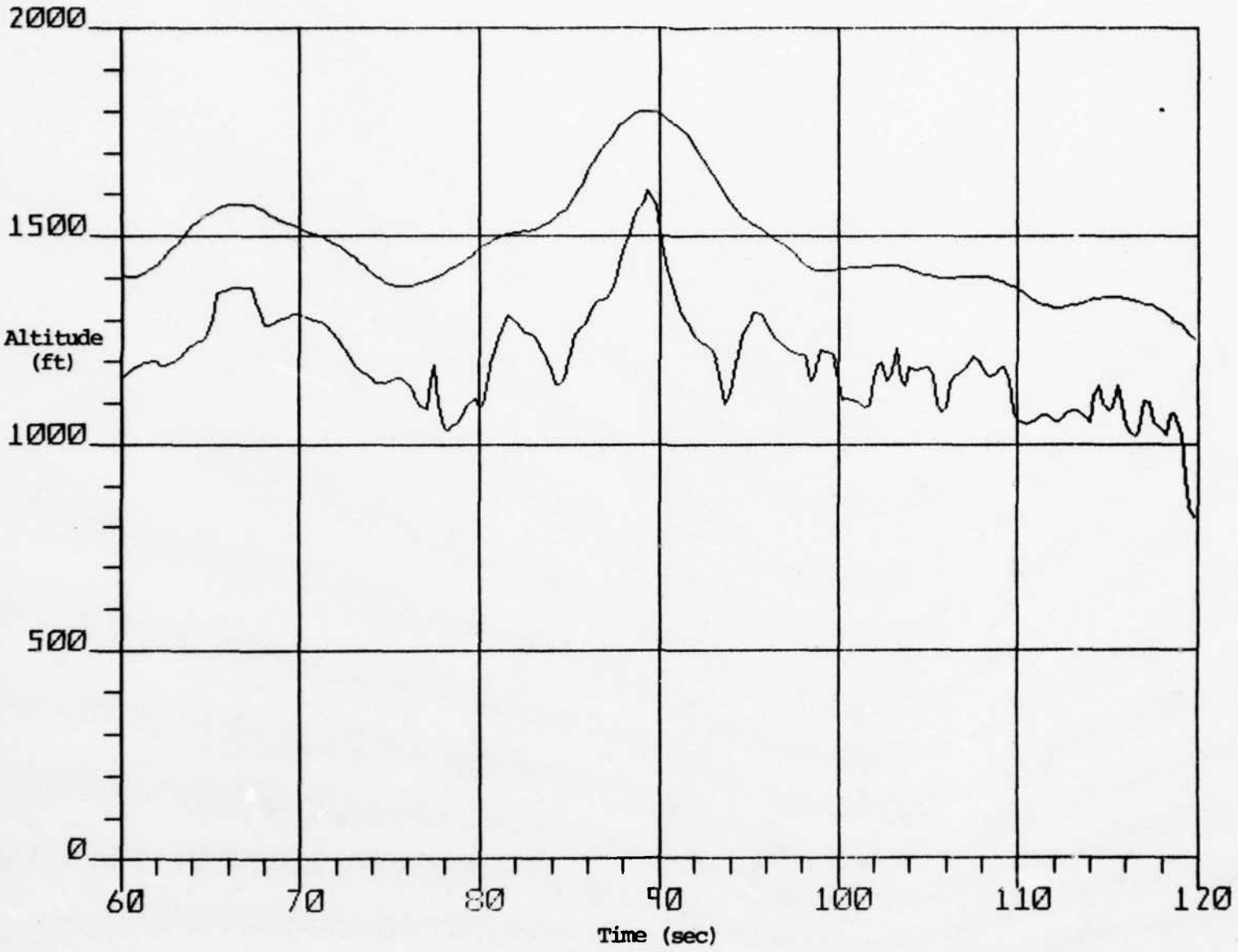
2000
1500
Altitude
(ft)
1000
500
0
60
70
80
90
100
110
120
Time (sec)

Fig 4.7 cont.

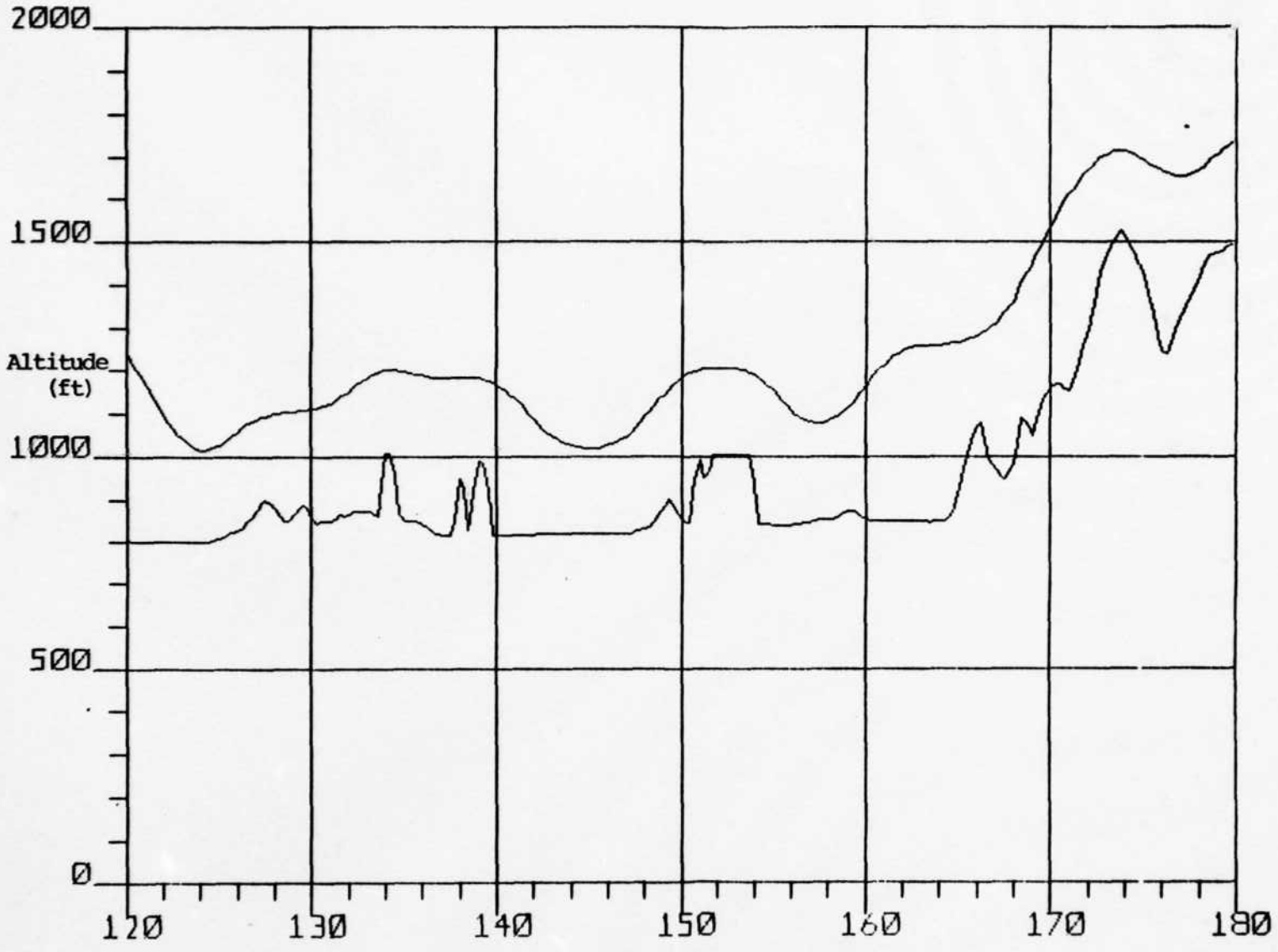
2000
1500
Altitude
(ft)
1000
500
0
120
130
140
150
160
170
180
Time (sec)

Fig. 4.7 cont.

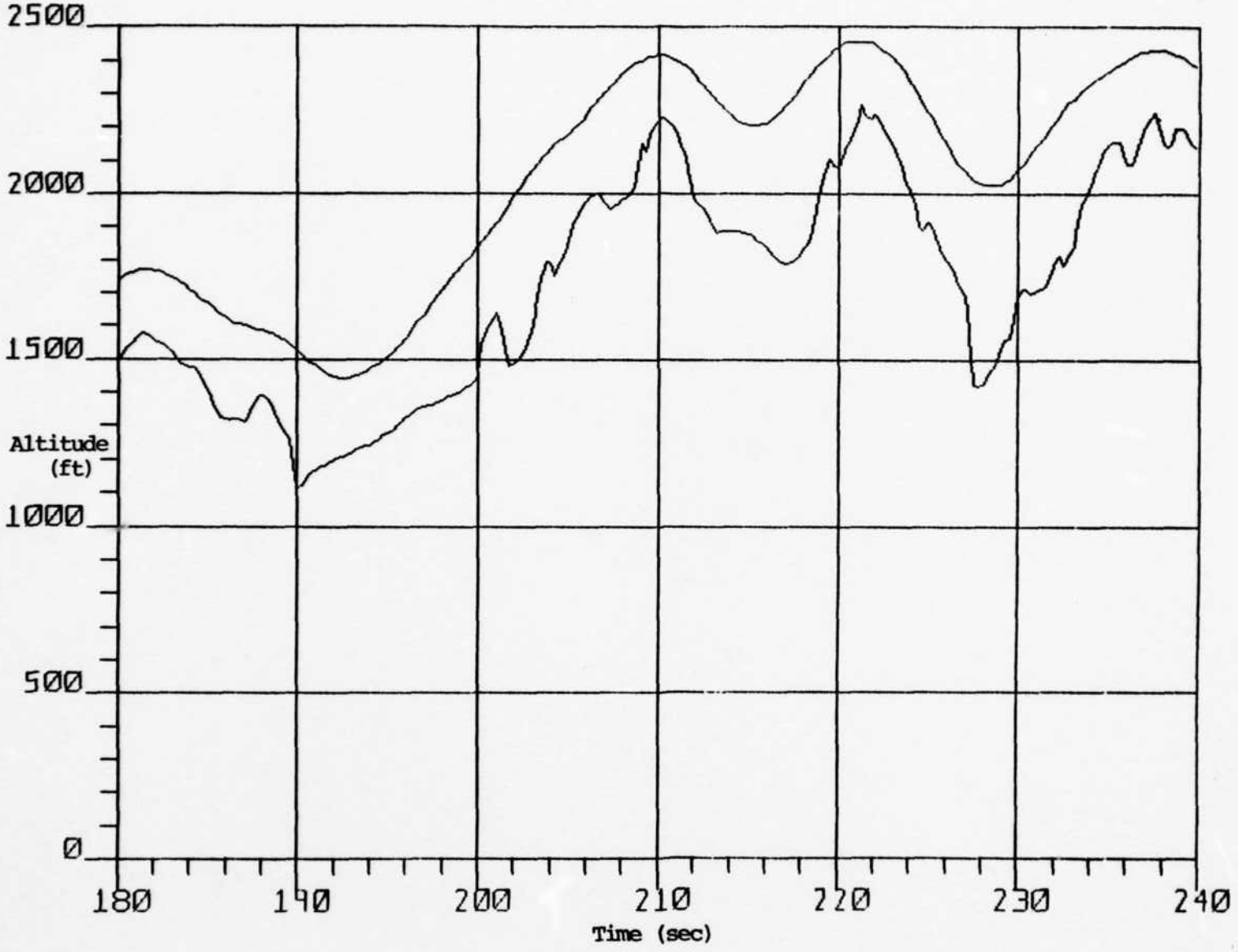
2500
2000
1500
Altitude
(ft)
1000
500
0
180
190
200
210
220
230
240
Time (sec)

Fig. 4.7 cont.

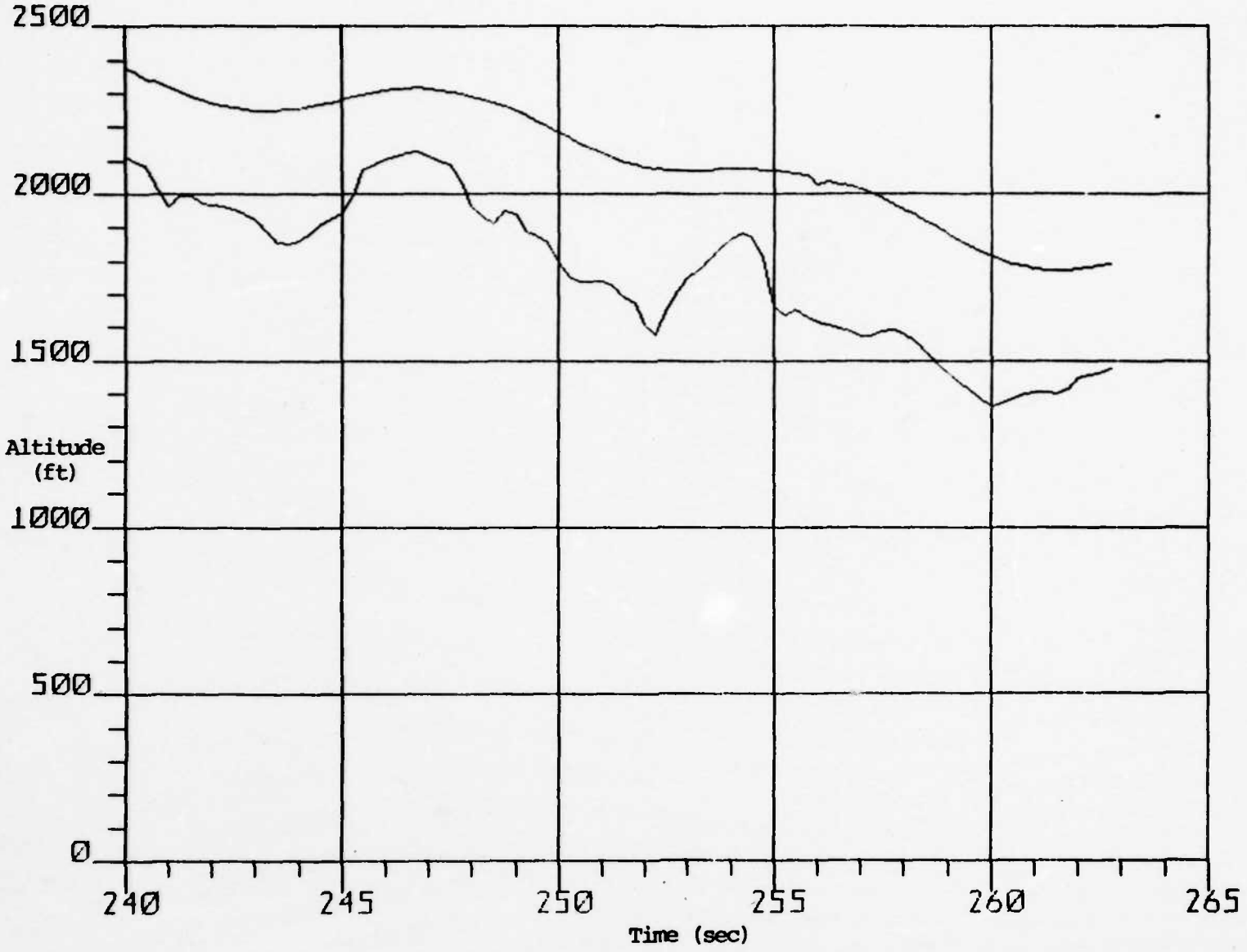

Fig. 4.7 concluded

CHAPTER 5

Flight Control System Design

Introduction

The design of a flight control system (FCS) that will closely follow a terrain profile involves many parameters. The FCS must interpret incoming terrain data, fit a smooth curve through that data, and then follow this generated path as closely as possible. This chapter discusses the off-line calculation by a digital computer program of a generated trajectory to be used by the OPAC controller to fly a specified terrain profile. The use of both elevator and flaps as control inputs should result in excellent tracking of the desired trajectory. This chapter will also look at the relative weighting of both control surface inputs. The state that will be used as feedback is the altitude state but all of the states will be moditored to determine if any state exceeds structural or pilot tolerances. In addition, all of the states will be monitored to try and gain insight into which parameters are important to the trajectory generation problem. These results are discussed in Chapter 6.

Trajectory Controller/Observer Design Aid System (TCODAS)

The Trajectory Controller/Observer Design Aid System (TCODAS) software, Ref. 5.3, is designed as an interactive software package which allows the user to accomplish design and analysis of a modern multivariable estimator/controller system and then accomplish Monte Carlo performance evaluation of the estimator/controller in a simulated closed loop "truth model" situation. TCODAS is split into two primary modes to accomplish this on an interactive basis: the DESIGN MODE and the SIMULATE MODE.

1. Design Mode. The design portion of TCODAS predominantly handles the linear time-invariant ordinary differential equation model in standard state variable format. The software will also find the equilibrium states of a nonlinear system at selected operating points. Once the equilibrium conditions are found, the appropriate linearized state space model is next determined. Such a linearized state model can then be used in the same way as a model that the user might enter in A, B, C, and D matrix form. Once the model has been entered, the TCODAS software next allows the user to analyze and manipulate the model. Time response plots for selected input/output pair combinations may be viewed. Controllability and observability may be analyzed. The model may be discretized at any desired sample time. Different state coordinates may be selected for either the discrete or continuous time models. The model order may be analyzed and reduced to eliminate redundant states. Finally, the process may be repeated to compare a reduced model with the full order matrix. Here the user has a range of different controller techniques as stated above. Next, the resulting closed-loop model may be analyzed. In addition to the direct time and frequency domain analysis of the closed-loop system, the DESIGN MODE also provides a number of performance figures of merit. The control inputs for various closed-loop tasks may be plotted. Finally there is a restricted capability to perform closed-loop simulation analysis under conditions of model mismatch (the robustness issue). Namely, parameter values of the simulation model may be offset from the controller design and the resulting closed-loop performance analyzed.

2. Simulate Mode. The proof of the multivariable controller/estimator is in its closed-loop performance with the actual system in realistic operating conditions. Such assessment is made in TCODAS through the

SIMULATE MODE. By linking the design controller/estimator into a truth model simulation, such closed-loop performance analysis under realistic situations can be made. Furthermore, the user may set up the initial conditions and specifications of the truth model evaluation on an interactive basis. The case runs may be made on a single run or a Monte Carlo basis. If performance results are not satisfactory with the truth model system, the user may return to the DESIGN MODE to reaccomplish analysis and design.

Multivariable Design Procedure

The following design procedures were used to determine the control input to TCODAS to follow the terrain, the weighting on each of the control surfaces, and the spline fit to obtain as smooth a trajectory as possible.

1. The trajectory was plotted as altitude versus time. The plots shown in Figs. 4.6 and 4.7 were calculated with an aircraft velocity of 837 feet per second (fps). A computer program, RDATA, whose listing is shown in Table 5.1, was written that would calculate the path length for any velocity, take the discrete trajectory data points and calculate coefficients to a cubic spline fit, calculate a trajectory through the new data points, then transfer the trajectory to TCODAS which would try to follow the path with the F-111/MAW model. A cubic spline was used due to the fast computation times necessary for a low level penetration mission. The spline routines are part of the IMSL (Ref. 5.2) subroutine library. The routine ICSSCV interpolates the spline coefficients and places a smooth cubic spline along a given set of data points. The routine ICSEVU then evaluates the cubic spline along the above given data points. Since the aircraft model was following a "non-function" path, (i.e. a step, sinusoid, etc.) the data was not continuous which therefore

resulted in some high frequencies in the terrain data. The noise in the terrain combined with very low pitch damping in the model resulted in high frequency oscillations in the control surfaces.

2. The seventh order control model was too large to predict longer than ten seconds into the future. Therefore, the singular values of the Hankel matrix were looked at to see if the order of the control could model be reduced to predict a longer terrain path. Figs. 5.1 through 5.3 show the normalized Hankel matrices. Fig. 5.1 is a plot of the third and fourth singular values. It can be seen that the relative magnitude of each of these singular values are large enough to be included in the control model. Fig. 5.2 is a plot of the fourth and the fifth singular values. The relative magnitude of the fifth singular value is very small when compared to the fourth value. Therefore, the possibility to delete the fifth through the seventh singular values exists because they are very small. Fig. 5.3 shows that a fifth order control model would be excellent because the sixth singular value is too small to be seen. The fourth order control model proved to be unstable when tracking the terrain so the fifth order control model was used. For a fifth order model, the number of future prediction points, L, would be 2n-1 or nine. The number of smoothing points, NSM, for a fifth order control model is n or five. Since five smoothing points did not allow an adequate path length to be calculated, several smoothing points were examined to determine if five were necessary. The terrain to be followed is at a relatively low frequency. The aircraft model's response to a step input at several smoothing points is shown in Fig. 5.4. It can be seen that an NSM of two also provided excellent performance when following the terrain.

3. The singular values of the reduced order Hankel matrix, Fig. 5.3, showed control switch time, TC, of 0.044 to be the optimal value to use.

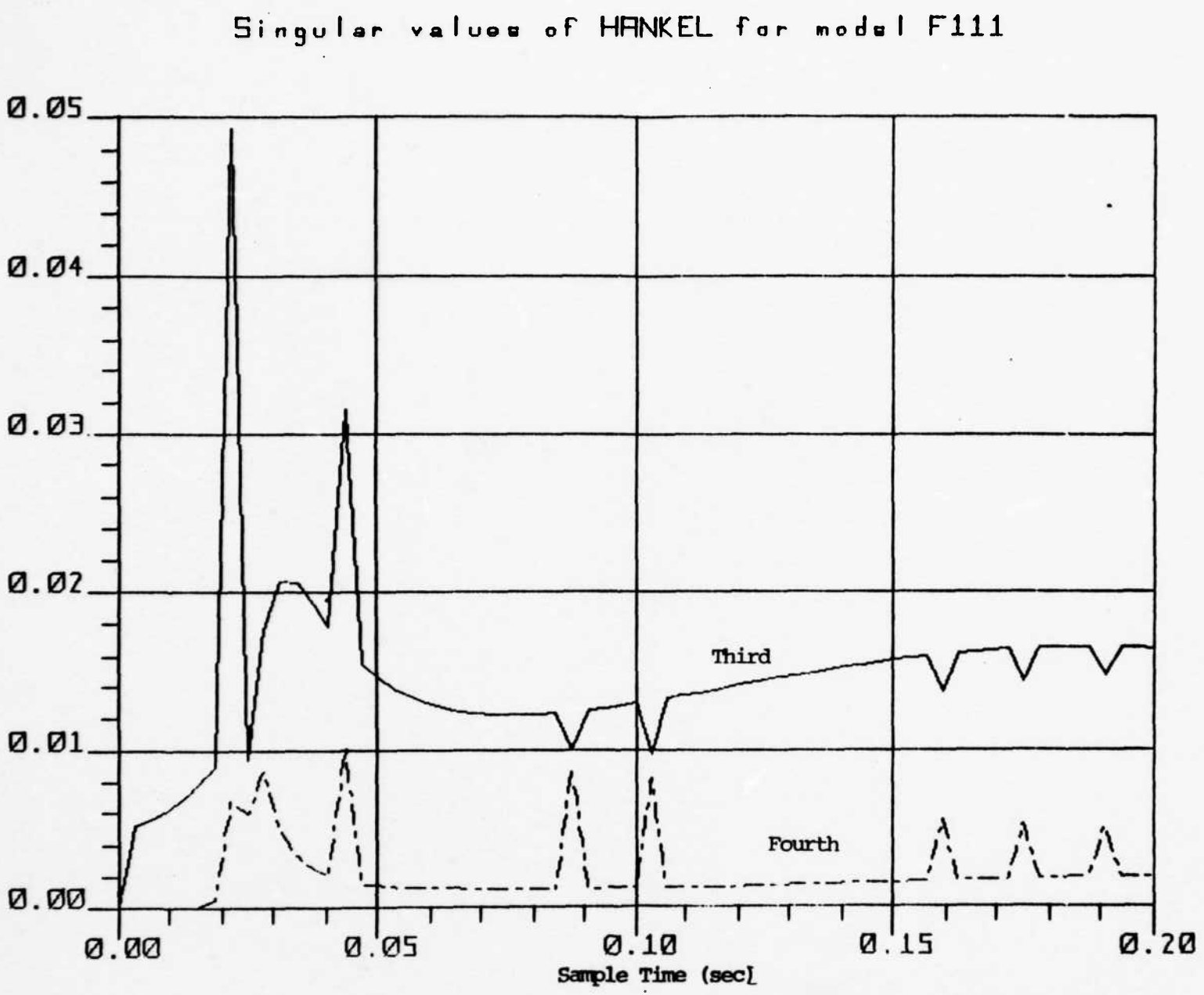

Fig. 5.1 Plot of Third and Fourth Singular Values Normalized

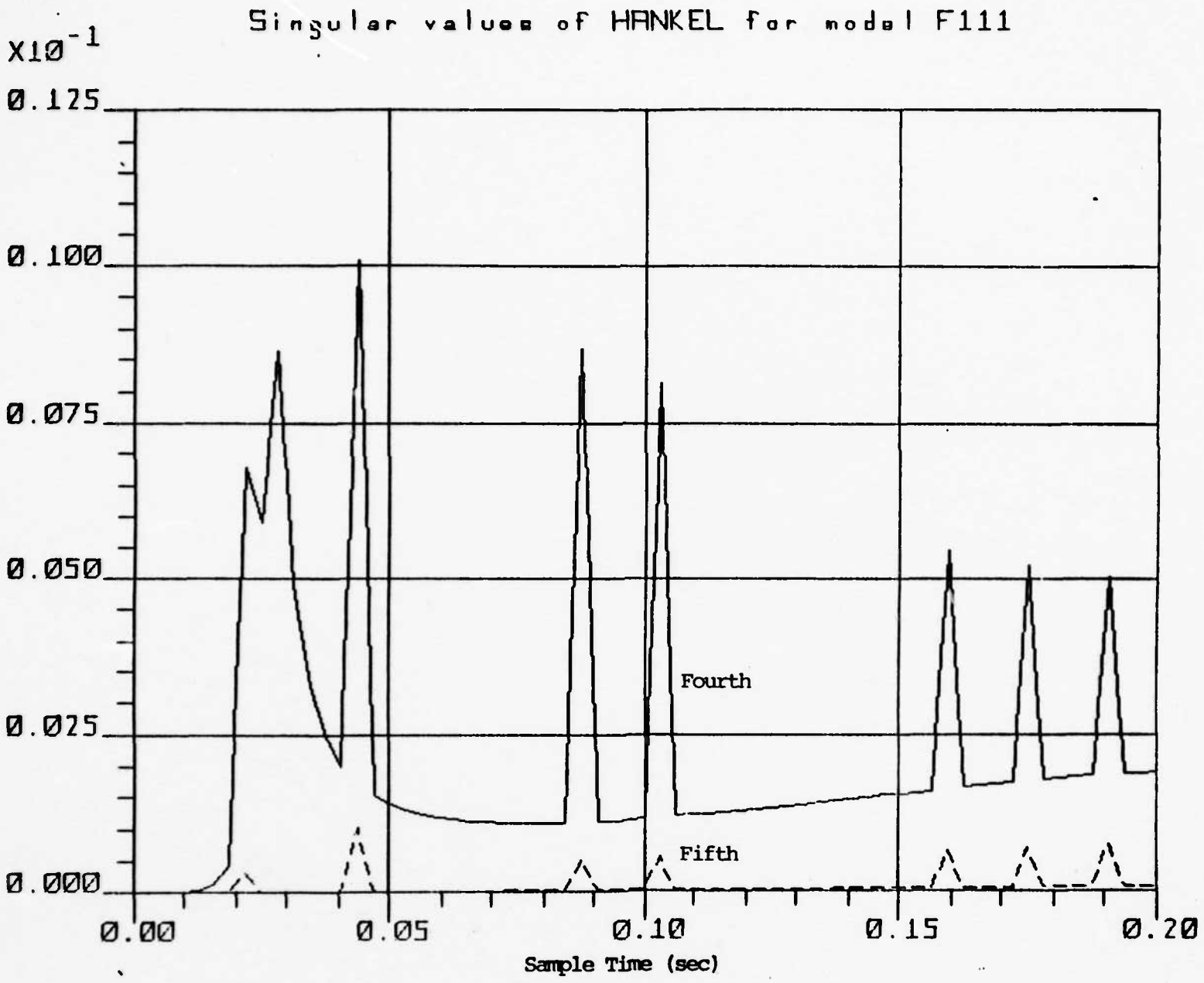

Fig. 5.2 Plot of Fourth and Fifth Singular Values Normalized

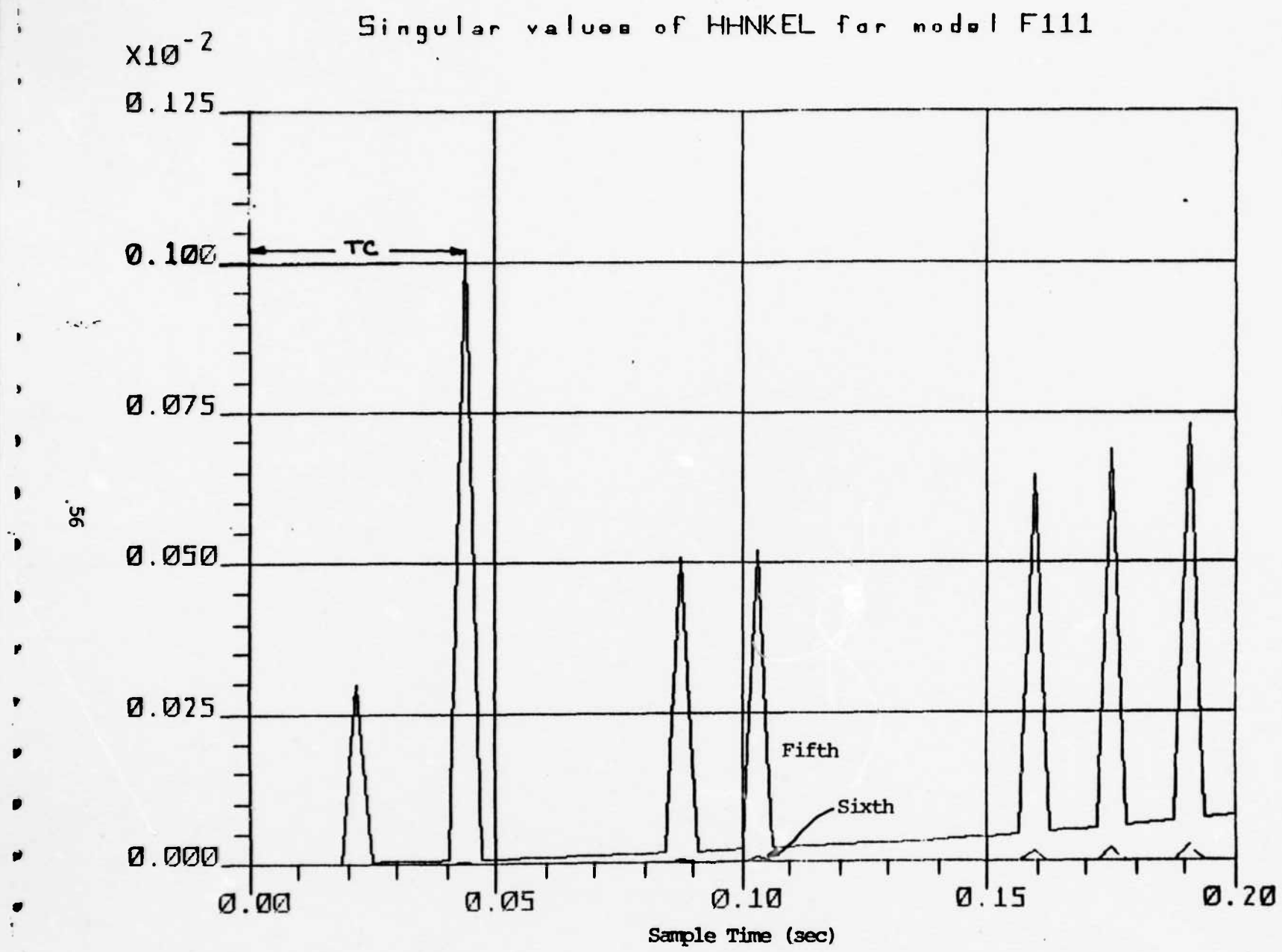

Fig. 5.3 Plot of Fifth and Sixth Singular Values Normalized

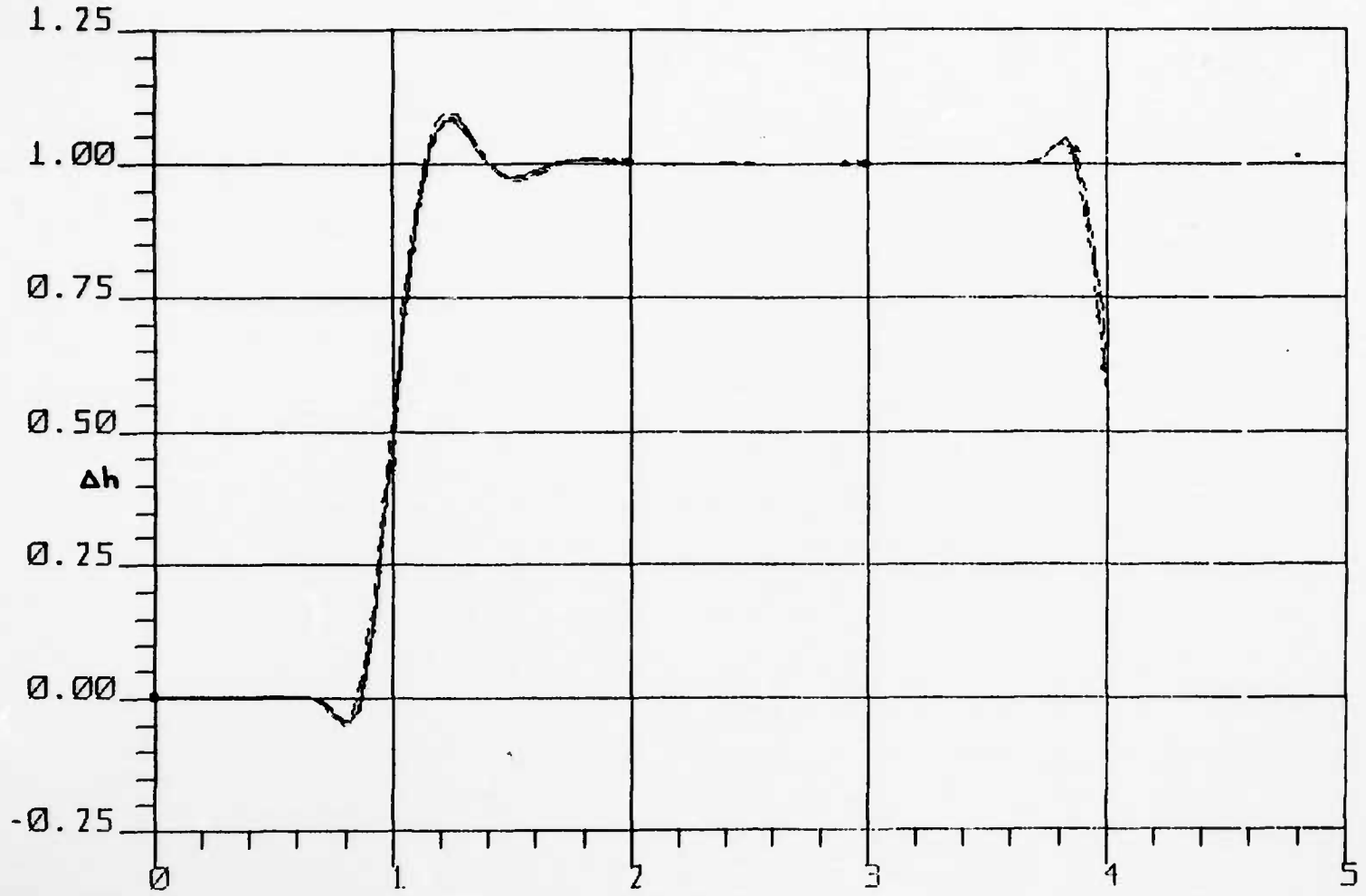

Fig. 5.4 Unit Step Response of F-111/MAW

Legend:

Closed loop resp of F111(1) to STEP(T-1) NSM = 5
Closed loop resp of F111(1) to STEP(T-1) NSM = 4
Closed loop resp of F111(1) to STEP(T-1) NSM = 3
Closed loop resp of F111(1) to STEP(T-1) NSM = 2

A better TC time of 0.05 was used because each sample time matched the terrain update points exactly instead of calculating a new control input on an old terrain data point. The aircraft followed the terrain exactly using TC of 0.05 but the faster control switch time caused the control surfaces to oscillate rapidly. A TC of 0.1 was then used to cause the control surfaces to respond more slowly to the lightly damped pitch of the model and the results (although it did not eliminate the oscillations) showed a more satisfactory response in the control surface deflections.

4. The output weighting matrix was experimented with also to reduce the amount of control surface deflection while at the same time maintaining exact tracking of the terrain. The weighting on the Q (output) matrix is such that the cost to input control deflections into the future are large thus demanding a faster control response in the present. The flap to elevator ratio is twenty to one due to the large control power available to the flaps. The initial conditions on each of the states were not exactly known which would account for the large initial transients seen in the plots in Chapter 6. The control weighting matrices are shown in Fig. 5.5 and are the same for both wing sweeps.

Summary

A large part of the design procedure involved the development of a digital computer program that would take non-function data input and calculate a cubic spline fit to that data anywhere along the trajectory and at any speed. The order of the control model could be reduced from a seventh to a fifth order model thus increasing the length of the future path to be predicted. Weighting both the input and output proved to be more of a trial and error process but the final weighting matrices still allowed exact tracking of the terrain while maintaining small control surface deflections.

```
Control for model F-111/MAW

Control Type: OPAC
NSM = 2
  L = 9


The entries of vector output time weights are as follows:

   1.000     1.000     1.000     1.000     1.000
   1.000     1.000     1.000     1.000    10.000
  10.000    10.000    10.000    10.000    10.000
  10.000    10.000    10.000

The entries of vector output weights are as follows:

   1.000

The entries of vector input weights are as follows:

   1.000    20.000
```

Fig. 5.5 Control Input Weighting Matrices

```
      SUBROUTINE FITDAT
      ENTRY    INIT TRAJ (TSTART,MPLOT,DT,DIM,IER)
C
C     THIS PROGRAM READS THE TERRAIN DATA, CALCULATES THE SPLINE
C     FIT TO THAT DATA, THEN WRITES THE ANSWER TO AN OUTPUT FILE
C
   10 FORMAT(1X,'ENTER START TIME, END TIME, AND VELOCITY (FPS)')
C
      INTEGER NT,IC,NDIM,IER,TEST,N,I,DIM
      DATA    NDIM/200/,NPLOT/2000/,IC/199/,NOUT/-2/
      REAL    T(200),ALT(200),RANGE(200),TD(2000),HD(2000)
      REAL    TVEC(2),INC,C(199,3),RD(2000)
      MPLOT=NPLOT-1
      DIM=2
      WRITE(NOUT,10)
C
C *** READ IN START TIME, END TIME AND AIRCRAFT VELOCITY ***
C
      READ (NOUT,*) TSTART,TEND,VEL
      DT = (TEND-TSTART)/MPLOT
      RATIO=837.75/VEL
      OPEN (UNIT=3,NAME='FIIIMAW.DAT',STATUS='OLD',ERR=200)
  100 READ (3,*) T(I),RANGE(I), ALT(I), IDUMMY
C
C *** CONVERT TIME BY RATIO OF VELOCITIES (837/VEL) ***
C *** SEARCH TERRAIN DATA FOR STARTING POINT ***
C
      IF(T(I).LT.TSTART) GO TO 100
      I=I
C
C *** READ TERRAIN DATA ***
C
      INC=0.25
      DO 105 I=2,NDIM
      READ (3,*) T(I),RANGE(I),ALT(I),IDUMMY
      T(I) = INC*RATIO + T(I-1)
  105 CONTINUE
      CLOSE (UNIT=3,ERR=200)
C
C *** CALCULATE THE SPLINE FIT TO THE TERRAIN DATA ***
C
      CALL SPLINE (T,ALT,NDIM,C,IC,TD,HD,NDIM,NPLOT,TSTART,TEND,IER)
      IF(IER.EQ.0) GO TO 20
   20 WRITE(NOUT,310)
      CALL SPLINE (T,RANGE,NDIM,C,IC,TD,RD,NDIM,NPLOT,TSTART,TEND,IER)
      IF(IER.EQ.0) GO TO 30
   30 WRITE(NOUT,320)
      RETURN
  200 WRITE (NOUT,210)
  210 FORMAT(1X,'FILE ERROR')
  310 FORMAT(1X,'-SPLINE FIT TO ALT "OK"-')
  320 FORMAT(1X,'-SPLINE FIT TO RANGE "OK"-')
      ENTRY TRAJVEC (J,DIM,TVEC)
      TVEC(1) = HD(J+1)
      TVEC(2) = RD(J+1)
      RETURN
      END
```

```
      SUBROUTINE SPLINE(X,Y,NX,C,IC,XPLOT,YPLOT,NDIM,NPLOT,TSTART,
     1                  TEND,IER)
C
C     THIS PROGRAM COMPUTES THE CUBIC SPLINE FIT TO TERRAIN DATA
C     USING THE IMSL LIBRARY ROUTINE "ICSCCU" TO INTERPOLATE THE
C     SPLINE COEFFICIENTS, AND ROUTINE "ICSEVU" TO EVALUATE THE
C     SPLINE AT SELECTED POINTS.
C
      INTEGER   NX,IC,NOUT,NXMI
      DIMENSION X(NDIM),Y(NDIM),C(IC,3),XPLOT(NPLOT)
      DIMENSION YPLOT(NDIM),YK(200),WK(1200)
      DATA NOUT/-2/,IJOB/2/
C
C *** CALL ICSSCV TO INTERPOLATE THE COEFFICIENTS ***
C
      CALL ICSSCV(X,Y,NX,YK,C,IC,IJOB,WK,IER)
C
C *** CHECK FOR SPLINE ERROR IN ICSSCV ***
C
      WRITE(NOUT,20) IER
      IF(IER.NE.0) STOP '-SPLINE ERROR IN ICSSCV-'
C
C *** OUTPUT ORDINATES AND SPLINE COEFFICIENTS TO SCREEN ***
C
      NXMI=NX-1
C
C *** EVALUATE THE SPLINE AT "NPLOT" POINTS ***
C *** NPLOT = 10 * NX, WHERE NX IS THE ORIGINAL DATA LENGTH ***
C
      DO 15 N=1,10*NX+1
      XF=(X(NX)-TSTART)/(10*NX)
      XPLOT(N)=XF*(N-1) + TSTART
   15 CONTINUE
C
C *** CALL ICSEVU TO EVALUATE THE SPLINE AT NPLOT POINTS ***
C
      CALL ICSEVU(X,Y,NX,C,IC,XPLOT,YPLOT,NPLOT,IER)
C
C *** CHECK FOR ICSEVU SPLINE ERROR ***
C
      WRITE (NOUT,20) IER
      IF(IER.NE.0) STOP '-SPLINE ERROR IN ICSEVU-'
C
   20 FORMAT(1X,'SPLINE IER=',I3)
   25 FORMAT(1X,'I',4X,'Y(I)',2X,'C(I,1)',2X,'C(I,2)',2X,'C(I,3)')
   30 FORMAT(1X,I1,4F8.4/)
      END
```

Table 5.1 Listing of Computer Program RDATA

CHAPTER 6

Results and Discussion

Introduction

The linearized math model of the F-111/MAW with its multiple input control surfaces proved to be an excellent aircraft to fly the low altitude penetration mission. The model used is the bare airframe version which is stable but lightly damped in pitch. The following sections will discuss and compare the aircraft's performance at both wing sweeps plus show the effect on the control surface deflections when the pitch damping is increased.

Simulation Results

As shown in Fig. 6.1 the aircraft model (at both wing sweeps) followed the desired trajectory exactly. The portion of terrain shown in Fig. 6.1 is the highest frequency encountered along the entire forty-two mile stretch of land, yet it is still at a relatively low frequency. This low frequency path can be attributed to structural and ride quality constraints, and control surface rate limits all incorporated into the path generator. These constraints helped to smooth the generated path over any type of terrain encountered, which then allows the controller to easily track the desired path. As shown in Fig. 6.1, the OPAC controller easily followed the desired trajectory. An interesting part of the simulation, however, was the effect that each wing sweep had on the aircraft's states. The 35 degree wing sweep model had over twice the flap authority (direct lift) than the 58 degree sweep model which smoothed the ride of the aircraft. Each wing sweep will be discussed seperately and then compared.

Figs. 6.2 through 6.12 are the outputs of each of the aircraft's states along the desired trajectory. The first thing that can immediately be seen in these figures is the oscillations in each of the outputs. These oscillations are more dramatic in pitch rate and both control surface deflections. This oscillatory motion can be attributed to the low damping in pitch of the bare airframe math model of the F-111/MAW and is evident in both wing sweeps. Therefore, there are two plots associated with each of the output states. The second plot is at a shorter time interval to give more detail and less high frequency oscillation. Fig. 6.2 shows a maximum forward velocity loss of twenty-four feet per second (fps) which is less than one half of one percent of the overall velocity of the aircraft. This shows that velocity need not be used as feedback to control speed because the variation in speed is not significant. The variation in angle of attack (Figs. 6.4 and 6.5) ranged between 4.8 degrees and -4.3 degrees. This small variation is well within acceptable performance limits and is due to the smoothing of the desired path by the trajectory generator. The variation in pitch rate (Figs. 6.6 and 6.7) show an initial maximum rate of 15 deg/sec which may be due to errors in initializing the states. The maximum variations after this initial peak are from 10.3 deg/sec to -9.2 deg/sec. While these rates are not large, they occur frequently resulting in a rough ride for the pilot. The plots of altitude rate (Figs. 6.8 and 6.9) show how fast the aircraft reacts vertically to changes in the terrain profile. This fast vertical velocity change allows close tracking of the terrain as seen in Fig. 6.1. The elevator and flap responses are shown in Figs. 6.10 through 6.12. Fig. 6.10 shows the control surface motions over forty seconds or approximately 7.6 miles of flight. Therefore, Figs. 6.11 and 6.12 are included to more easily observe the control surface motions. While the

control surfaces are oscillatory, the maximum elevator deflections range from 2.9 degrees to -2.9 degrees and the flap deflections range from 1 degree to -1.5 degrees.

The 35 degree wing sweep plots (Figs. 6.13 through 6.23) show basically the same results as the 58 degree sweep plots with one difference. With the addition of the inboard flaps, and thus the increased direct lift capability, the elevators were not used as extensively. This decreased use of the elevators caused the pitch rate response to decrease, resulting in an overall decrease in the magnitudes of the oscillations of the output states. Fig. 6.15 shows the variation in angle of attack to range from 2.2 degrees to -2.3 degrees. Fig. 6.17 shows pitch rate to vary between 6.9 deg/sec to -6.9 deg/sec and Fig. 6.19 shows identical vertical velocity changes as seen in the 58 degree sweep plot (Fig. 6.8). Fig. 6.21 shows an elevator variation between 2.8 degrees and -2.6 degrees with the flaps varying between 1 degree and -4.8 degrees.

Figs. 6.24 through 6.32 show a comparison of the output states of both the 35 and 58 degree sweep models over a designated portion of the terrain. These plots clearly show the effect of the addition of the inboard flap on each of the output states. Again, while the oscillations do remain, the addition of the inboard flap reduces the amount of control necessary to follow the terrain. The magnitude of the various changes in output rates and angles are smaller, thus providing less fatigue to the pilot and less stress on the aircraft itself. For an extended low altitude penetration mission this could be important for survival.

In order to try to eliminate the problem of the model being lightly damped in pitch, the pitch damping coefficient was doubled to simulate pitch rate feedback. This change was made to the 35 degree sweep model

only because it was the least oscillatory of the two models. As shown in Figs. 6.33 and 6.34, the oscillations remained although the magnitudes did decrease. This response may have been further improved by trying to optimize the control weighting matrices. A second doubling of the pitch damping coefficient resulted in the disappearance of the short period and phugoid modes. These were replaced by two exponentially decaying real roots and the appearance of a third oscillatory mode. The oscillations were of low frequency now but the magnitudes of the control surface deflections increased (Figs. 6.35 and 6.36). The eigenvalues of the two plants are shown below.

	Case 1 ($2*M_q$)	Case 2 ($4*M_q$)
EV(1)=	(-0.01144) + j(0.037037)	(-0.011401) + j(0.032151)
EV(2)=	(-0.01144) + j(-0.037037)	(-0.011401) + j(-0.032151)
EV(3)=	(-3.0517) + j(3.3916)	(-3.4333) + j(0.0)
EV(4)=	(-3.0517) + j(-3.3916)	(-7.6702) + j(0.0)
EV(5)=	(0.0) + j(0.0)	(0.0) + j(0.0)
EV(6)=	(-0.628) + j(0.0)	(-0.628) + j(0.0)
EV(7)=	(-0.698) + j(0.0)	(-0.698) + j(0.0)

Summary

Both aircraft models followed the desired trajectory exactly. The output states never reached large amplitudes; however, there were oscillations in all of the output states. These oscillations could be attributed to the bare airframe model being lightly damped in pitch. The addition of the inboard flaps on the 35 degree wing sweep model allowed exact tracking of the desired trajectory while at the same time allowing the aircraft to use less elevator. The decrease in elevator inputs decreased the pitch rate of the aircraft. Addition of "pitch rate feedback" by doubling and quadrupling the pitch damping coefficient in the plant matrix showed some improvement. The amplitudes were smaller in pitch rate and control surface deflection, and an optimized control

weighting matrix could improve the aircraft's performance. By changing the plant matrix, however, the model is no longer an F-111/MAW.

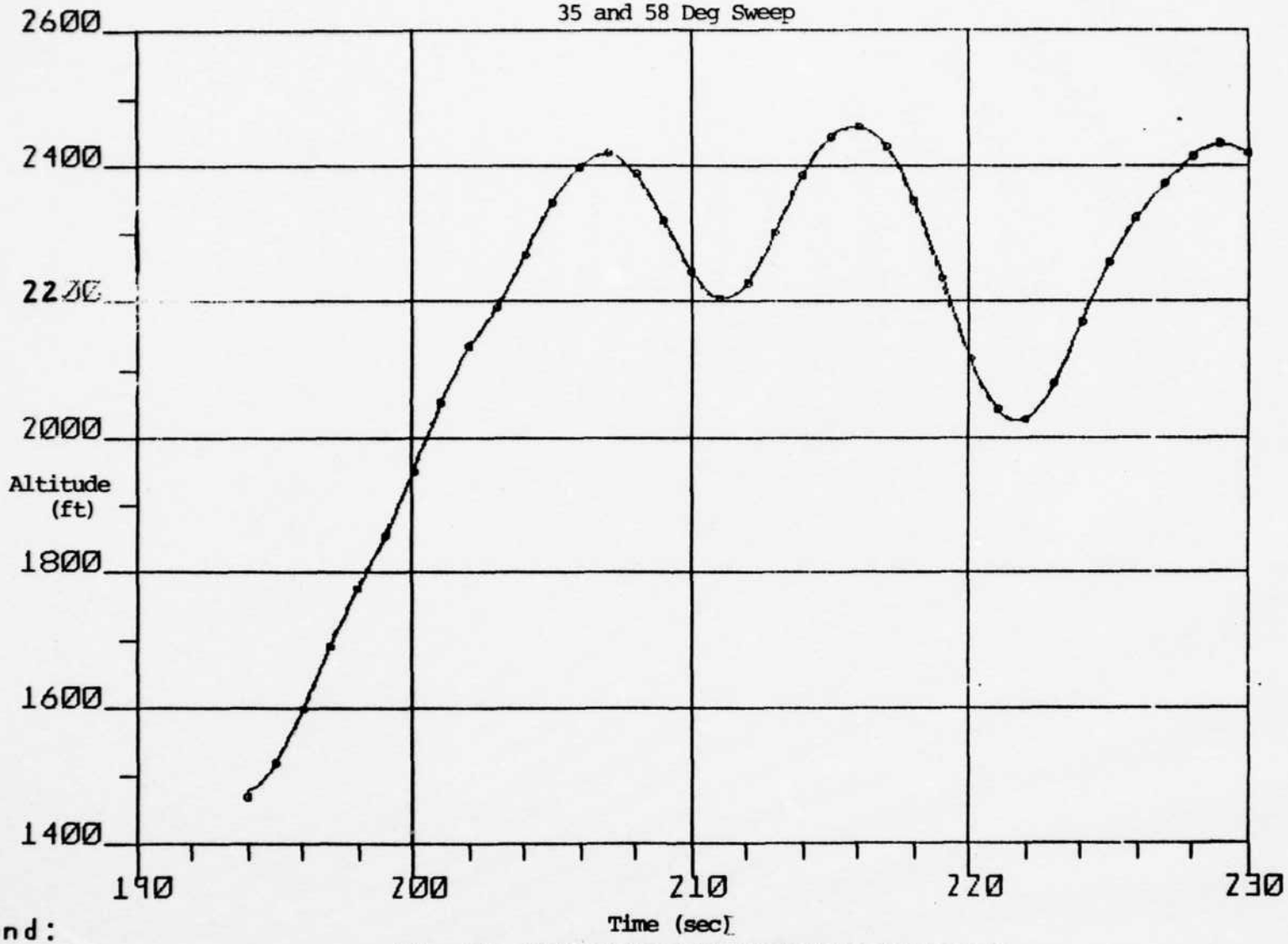

Fig. 6.1 Plot of Aircraft Trajectory and Terrain

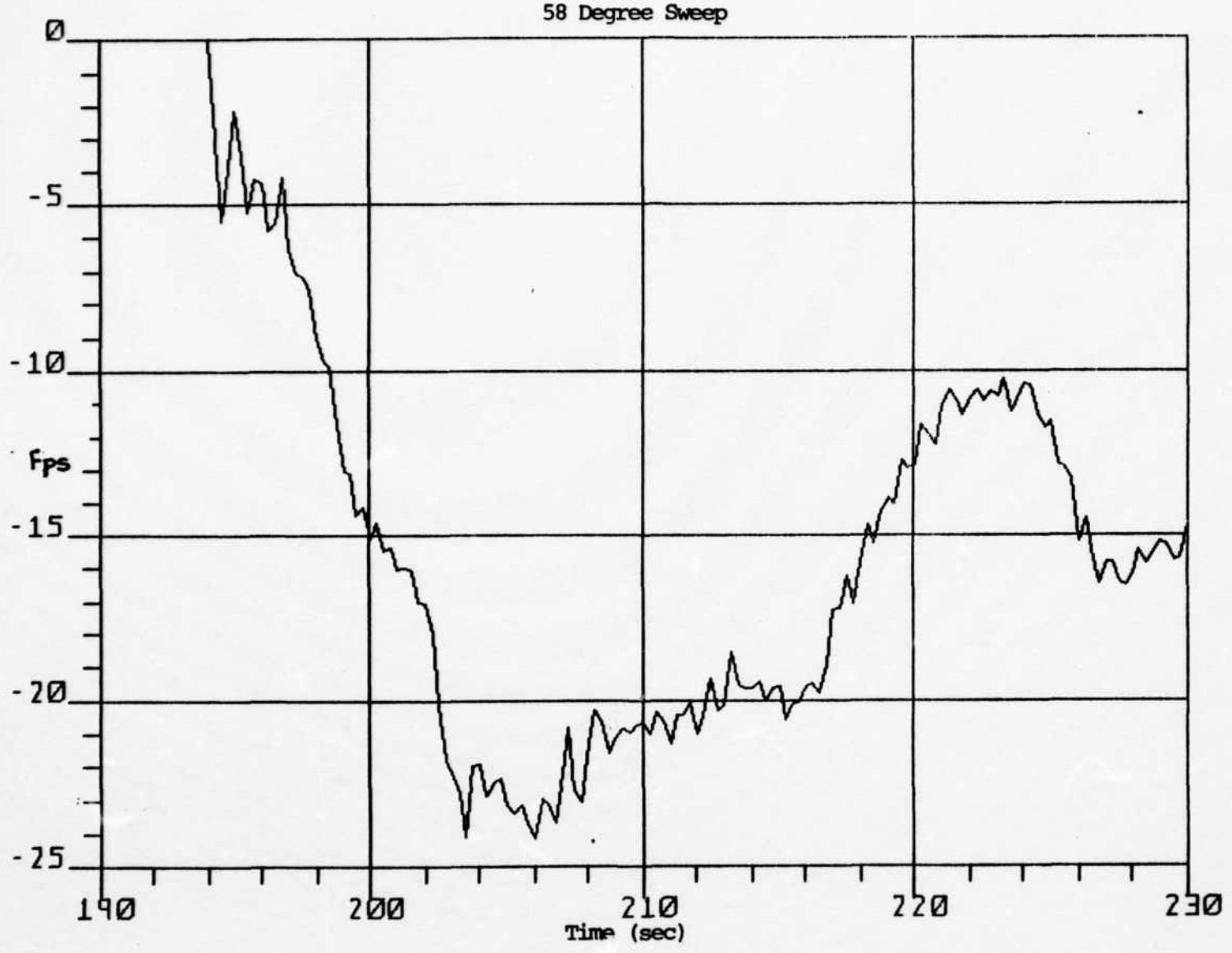

Fig. 6.2 Plot of Forward Velocity State (fps)

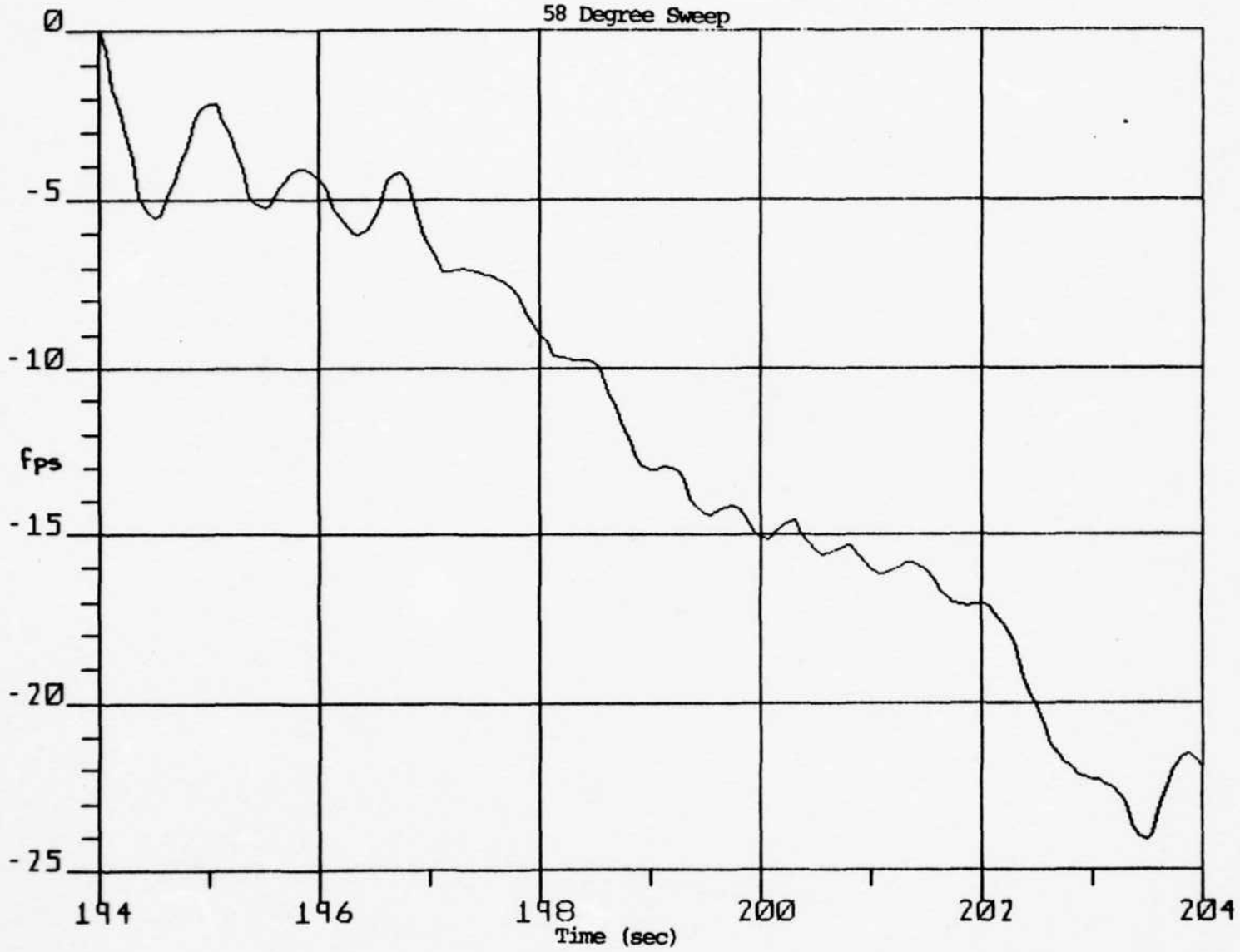

Fig. 6.3 Plot of Forward Velocity State - First 10 sec.

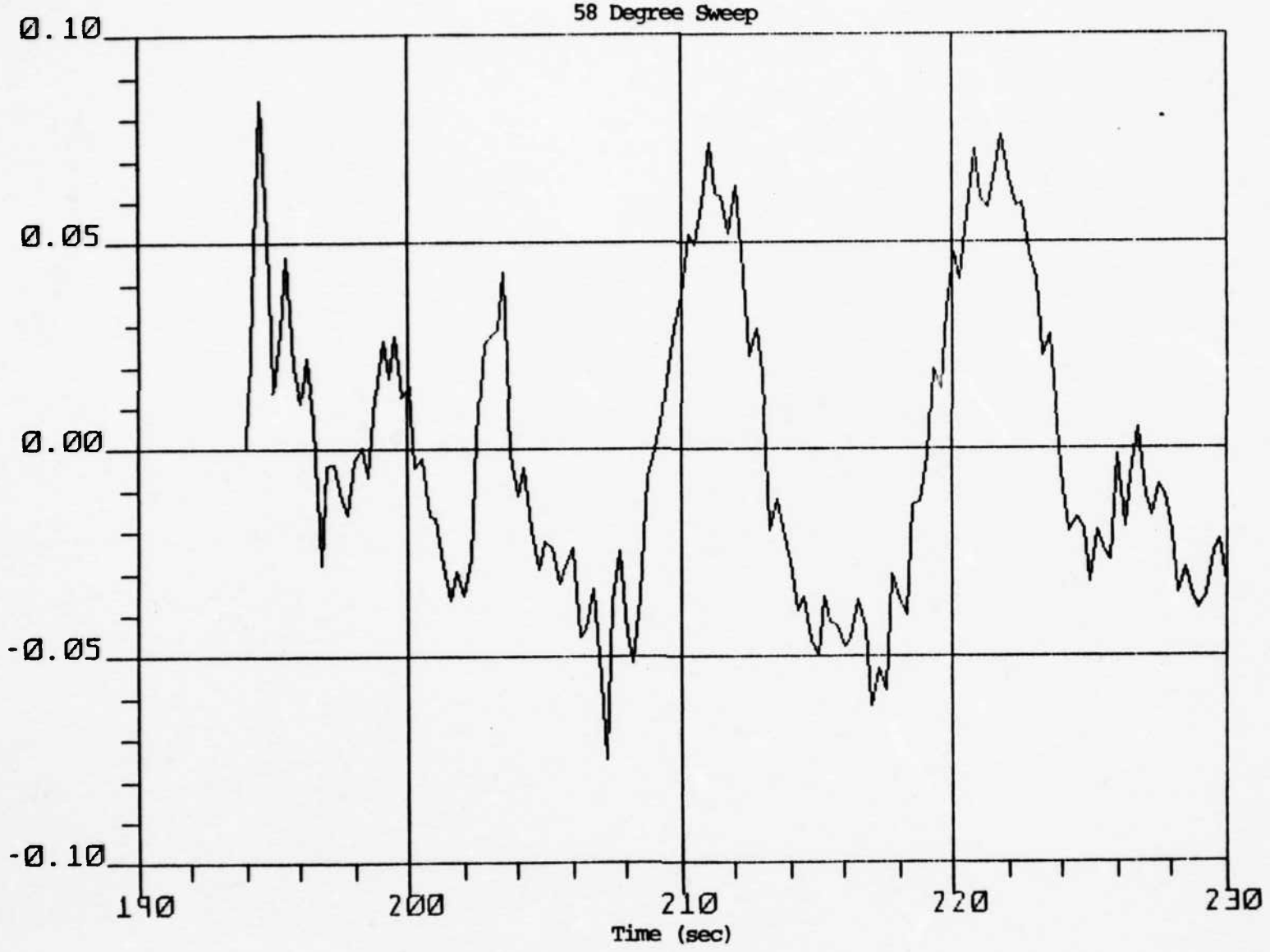

Fig. 6.4 Plot of Angle of Attack State (rad)

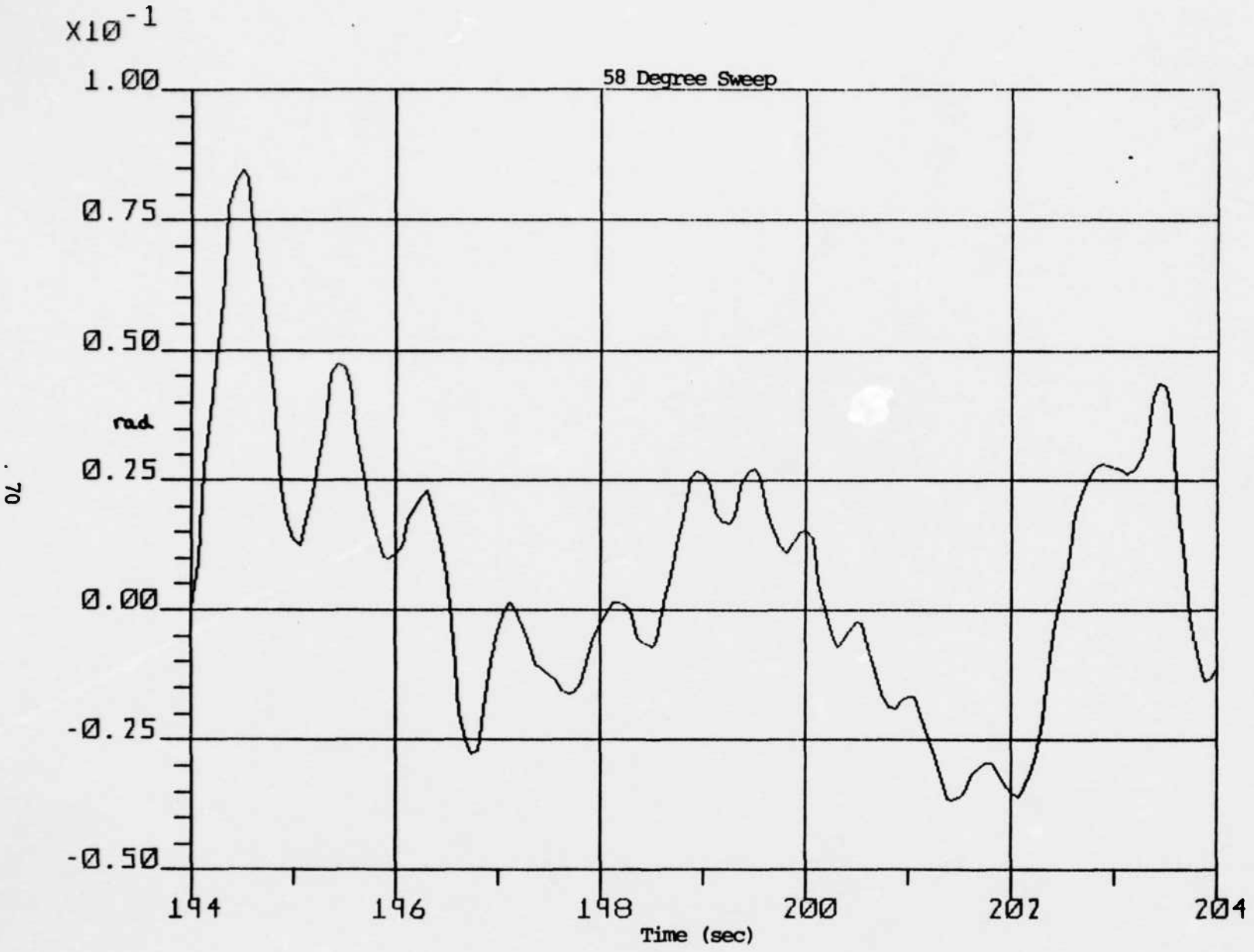

Fig. 6.5 Plot of Angle of Attack State - First 10 sec.

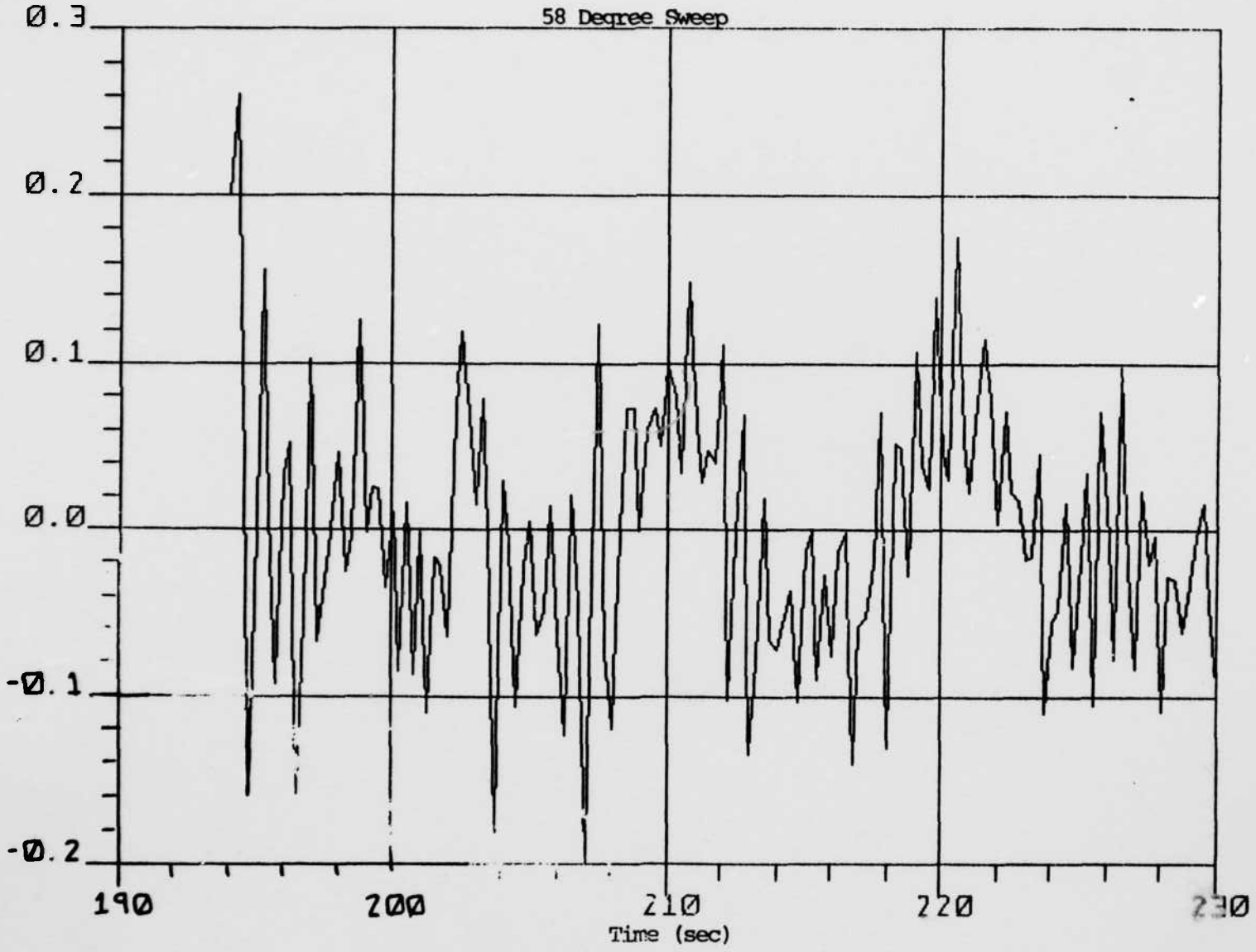

Fig. 6.6 Plot of Pitch Rate State (rad/sec)

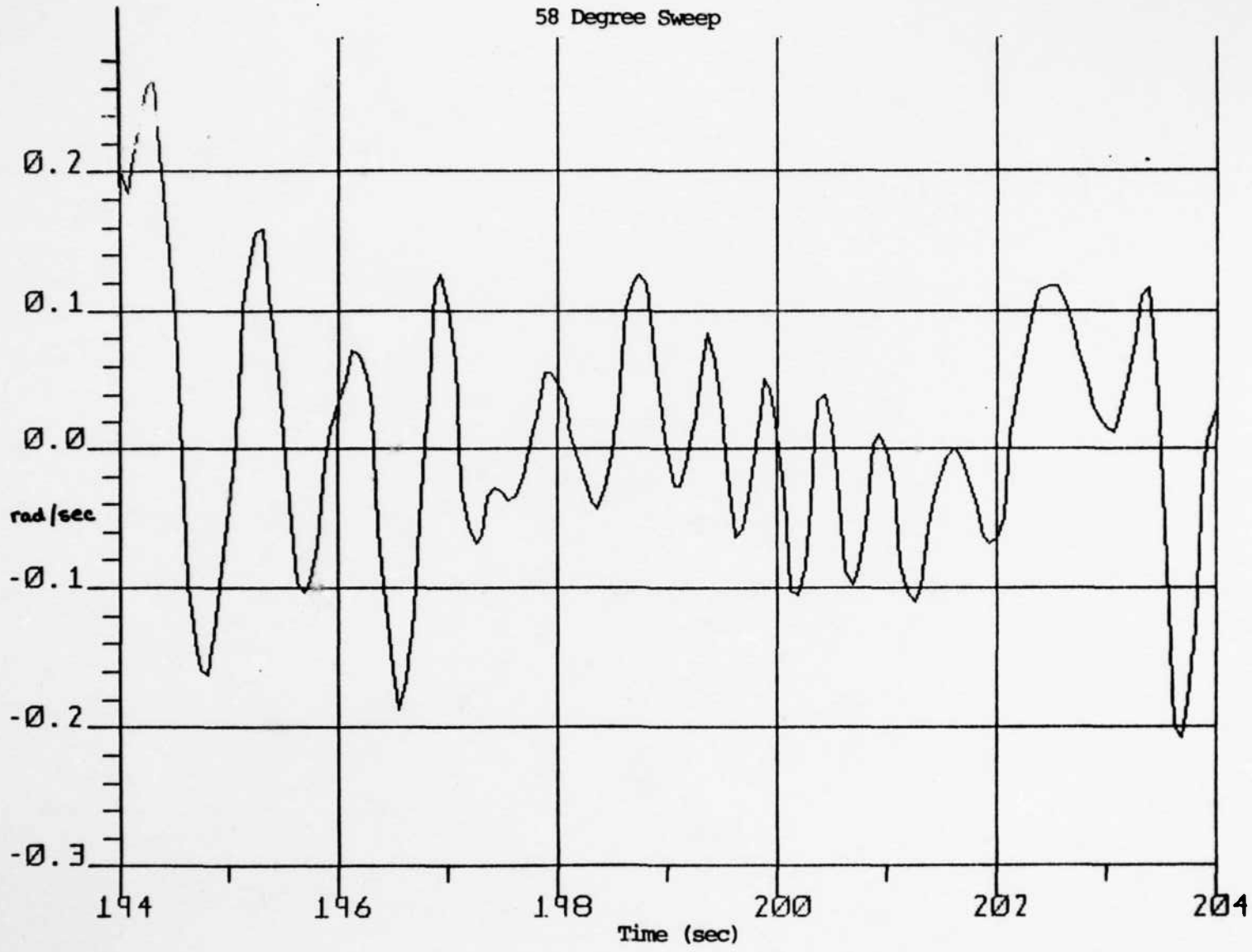

Fig. 6.7 Plot of Pitch Rate State - First 10 sec.

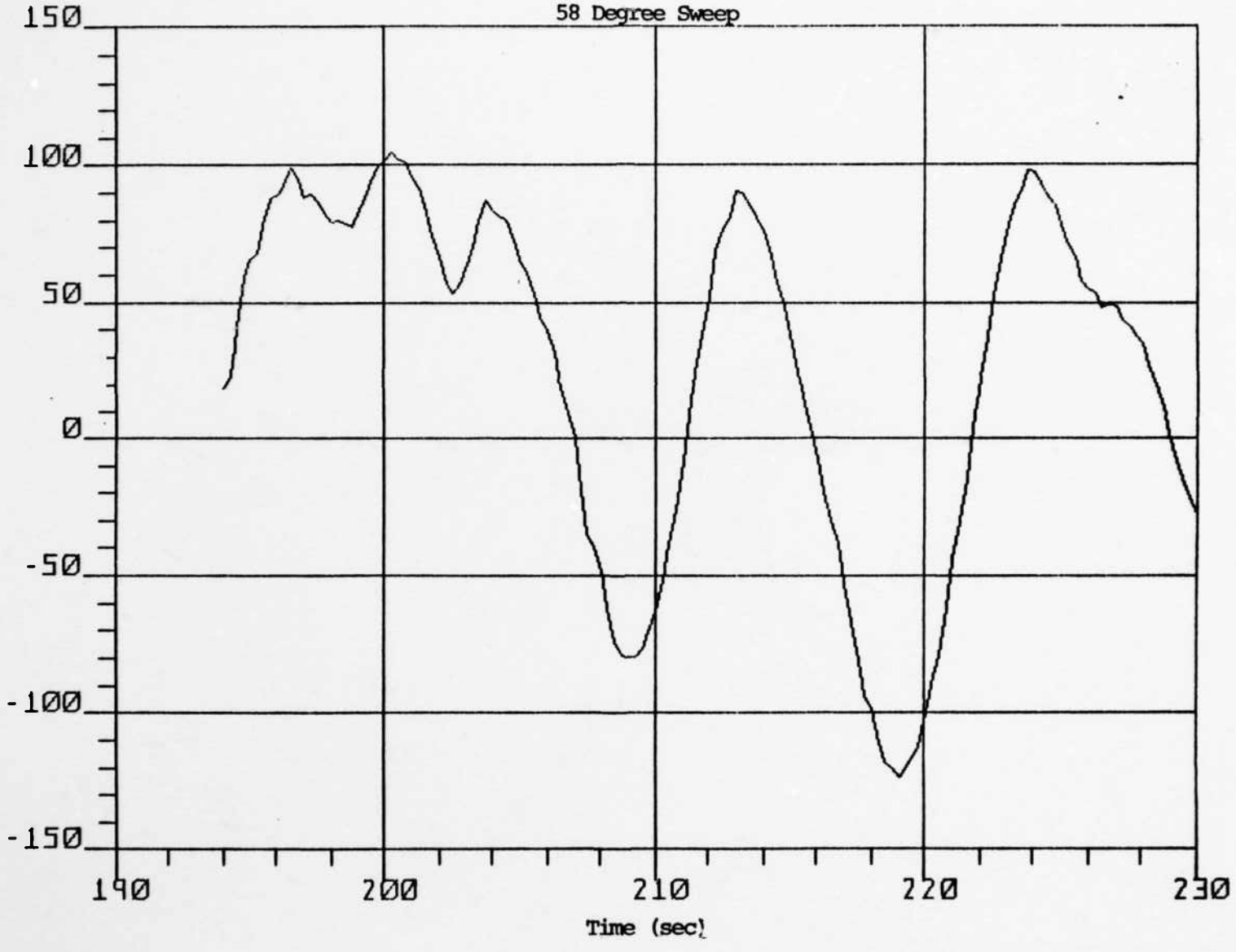

Fig. 6.8 Plot of Altitude Rate State (fps)

Fig. 6.9 Plot of altitude Rate State - First 10 sec.

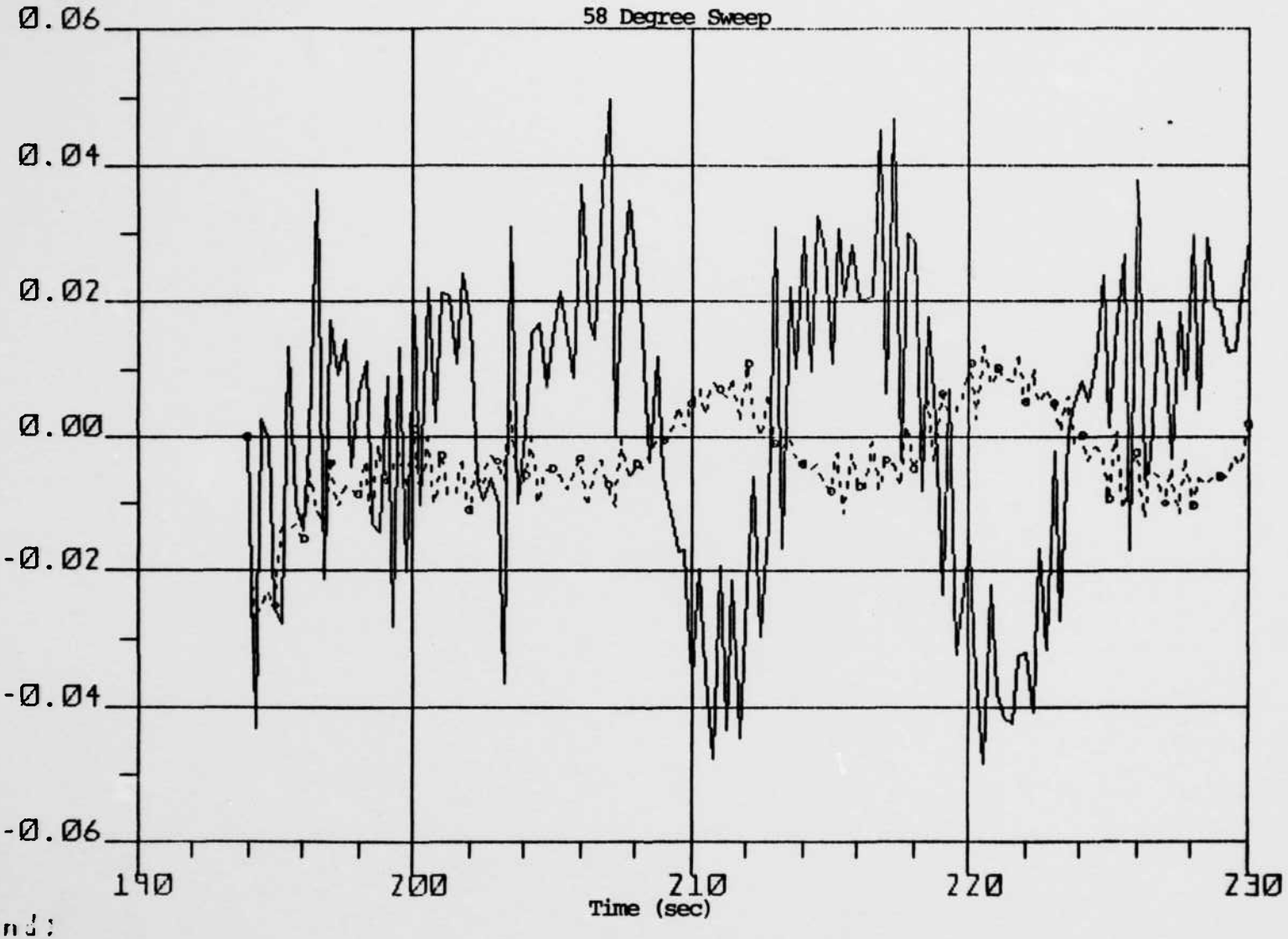

Fig. 6.10 Plot of Control Surface States (rad)

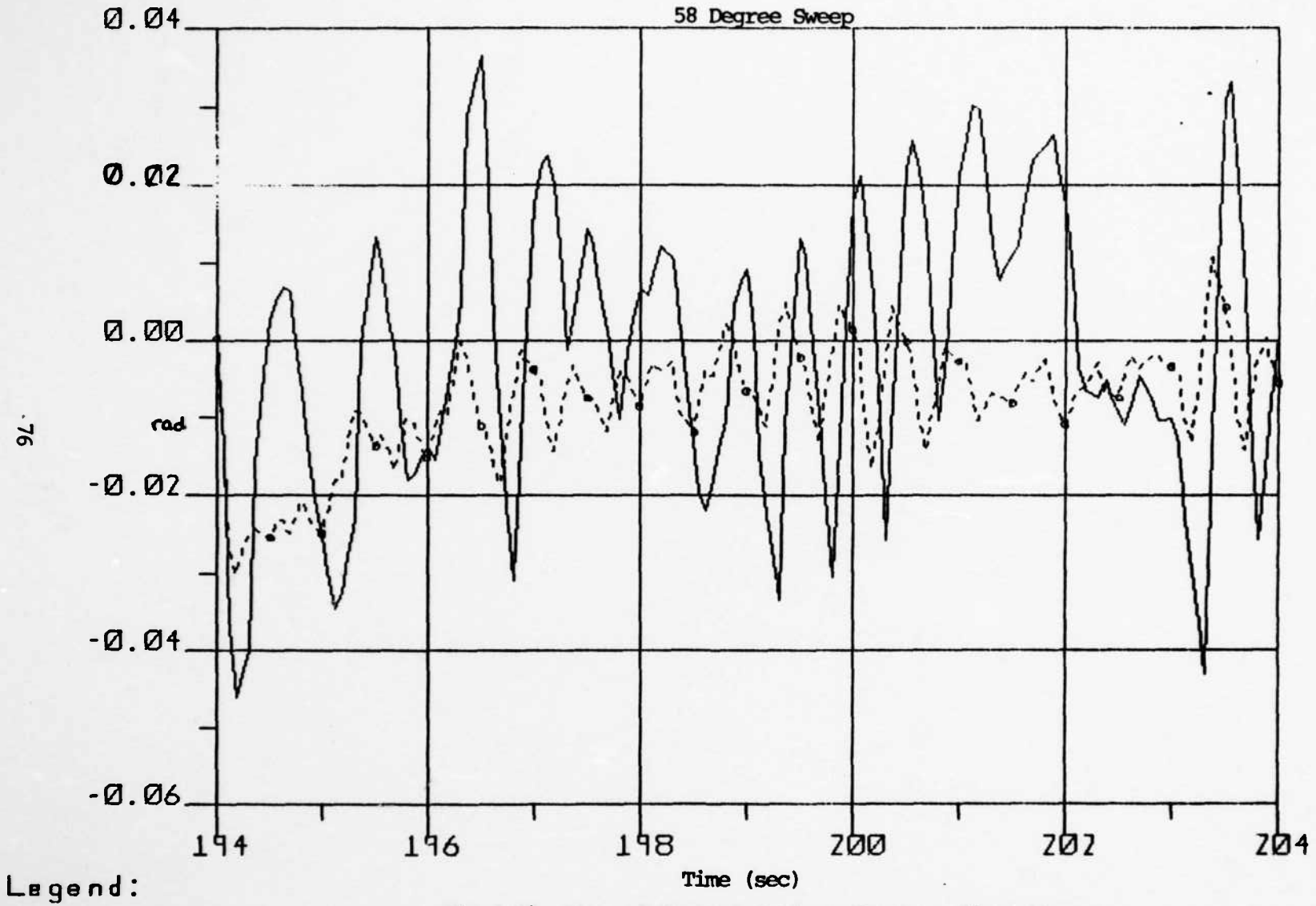

Fig 6.11 Plot of Control Surface States - First 10 sec.

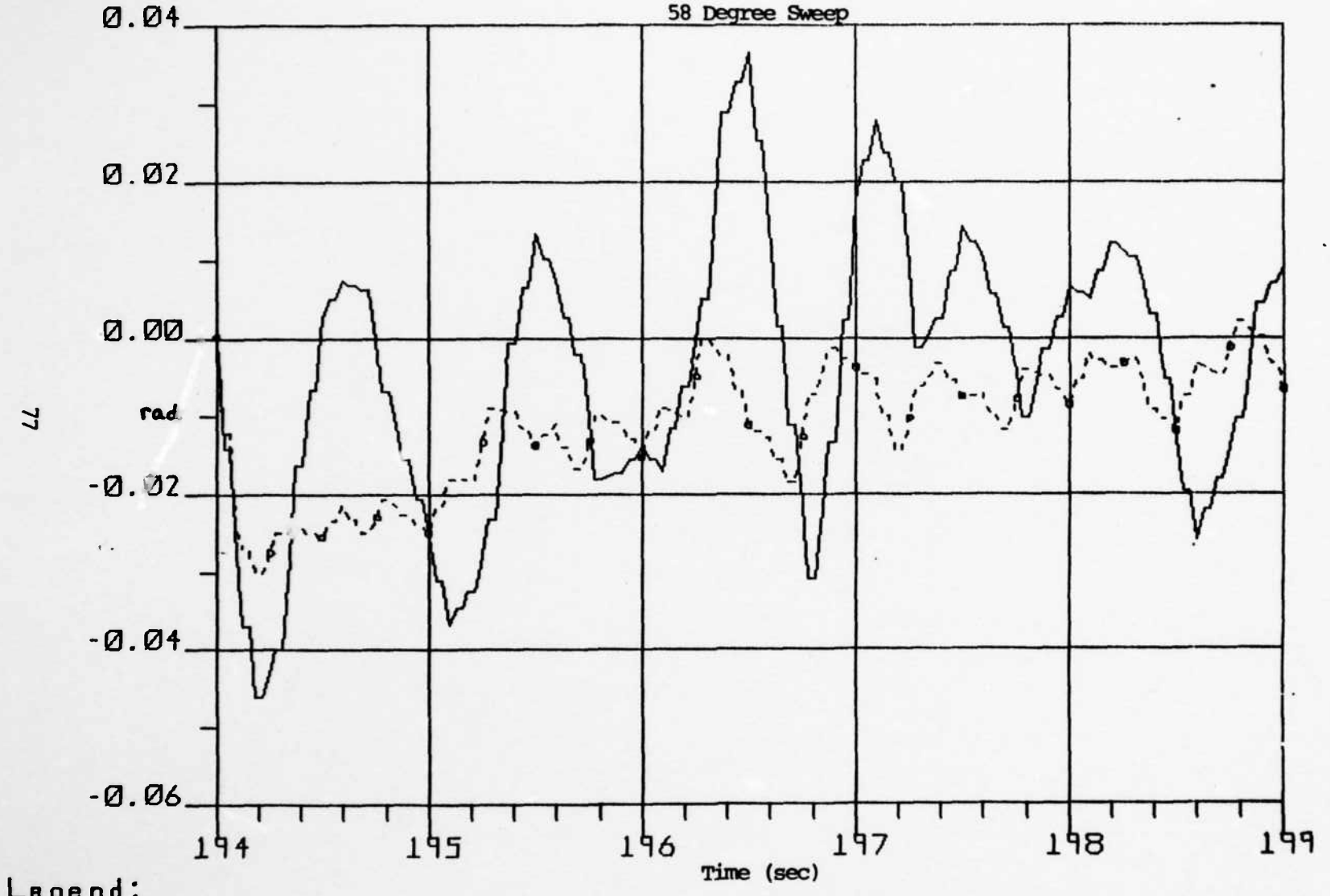

Fig. 6.12 Plot of Control Surface States - First 5 sec.

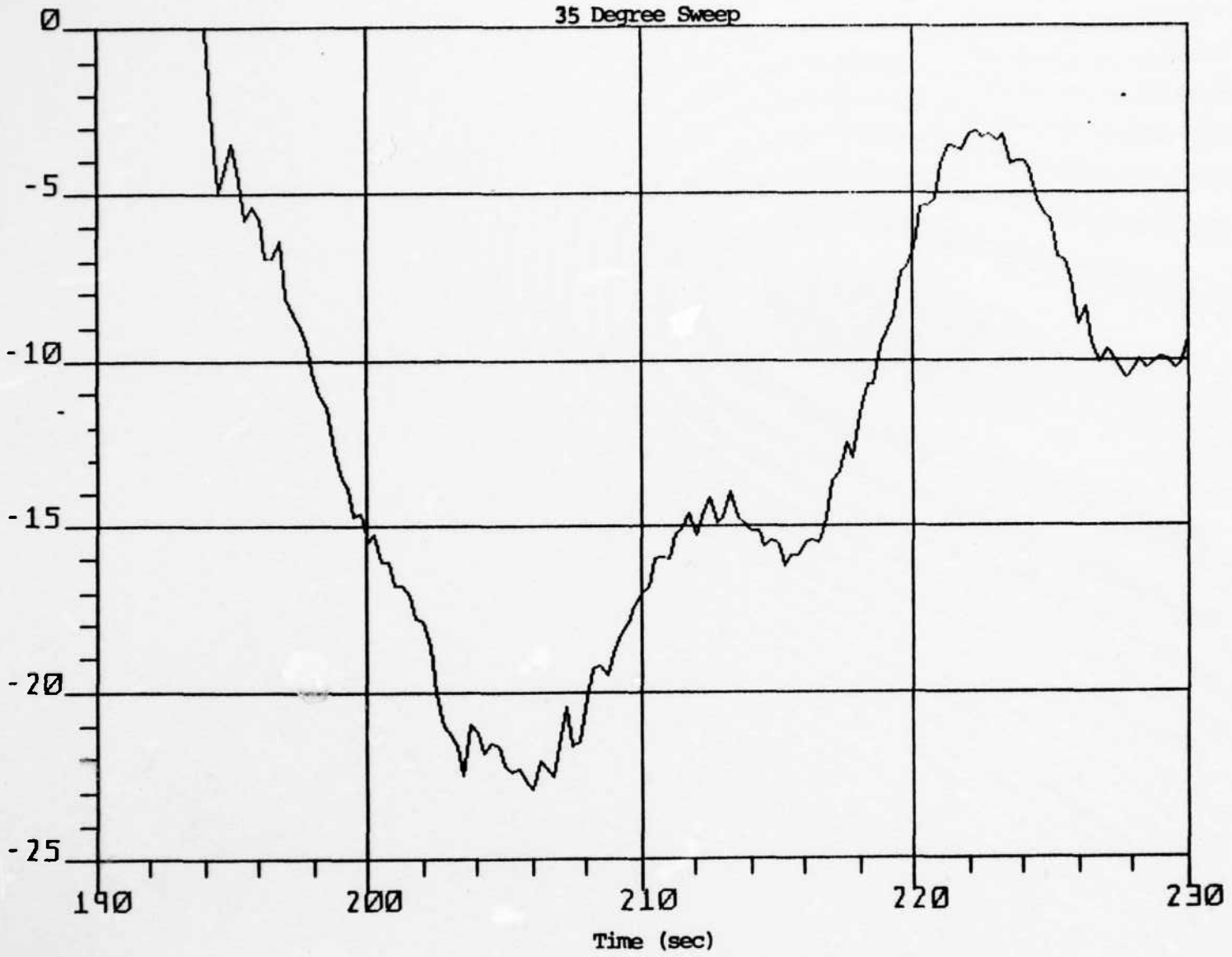

Fig. 6.13 Plot of Forward Velocity State (fps)

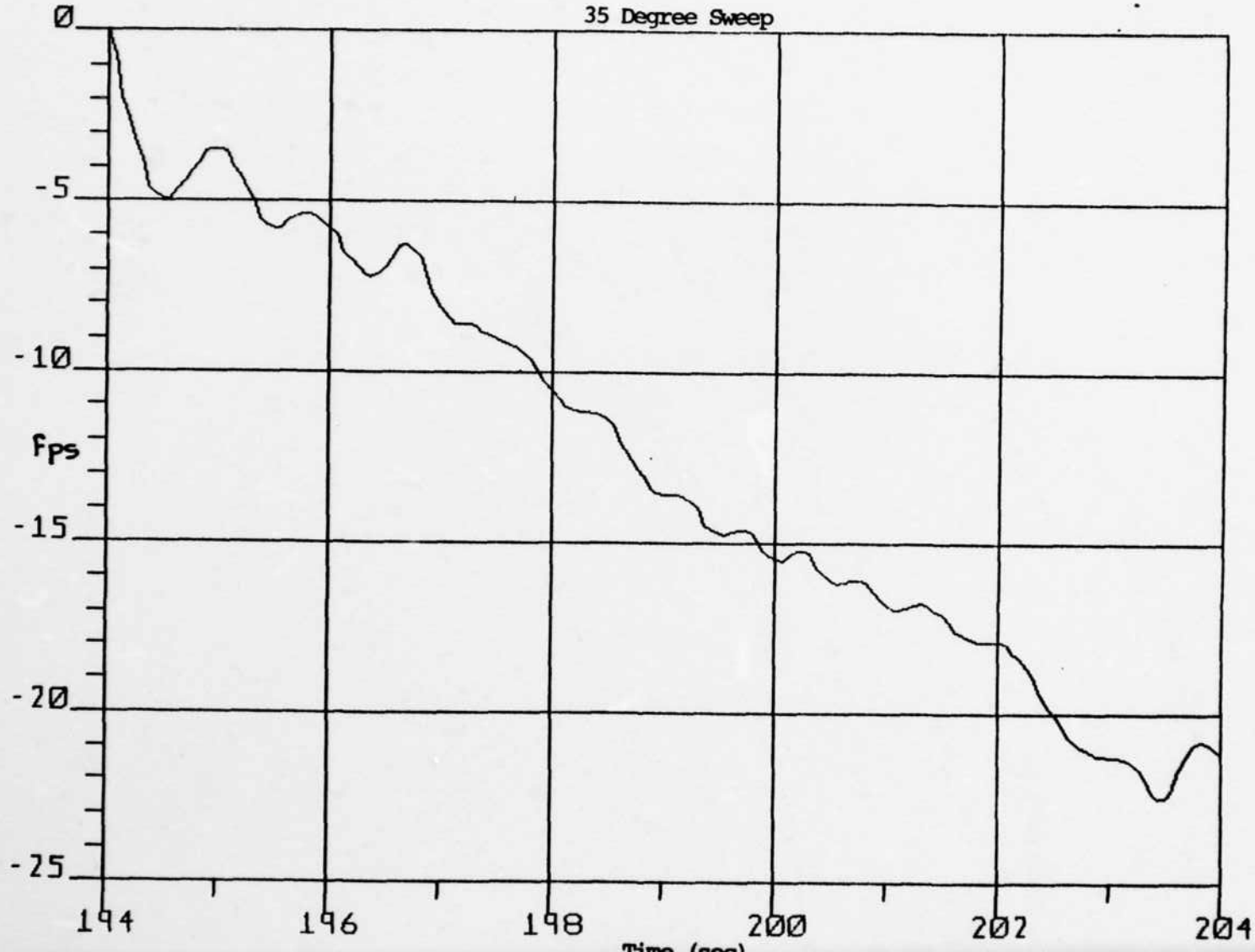

Fig. 6.14 Plot of Forward Velocity Step

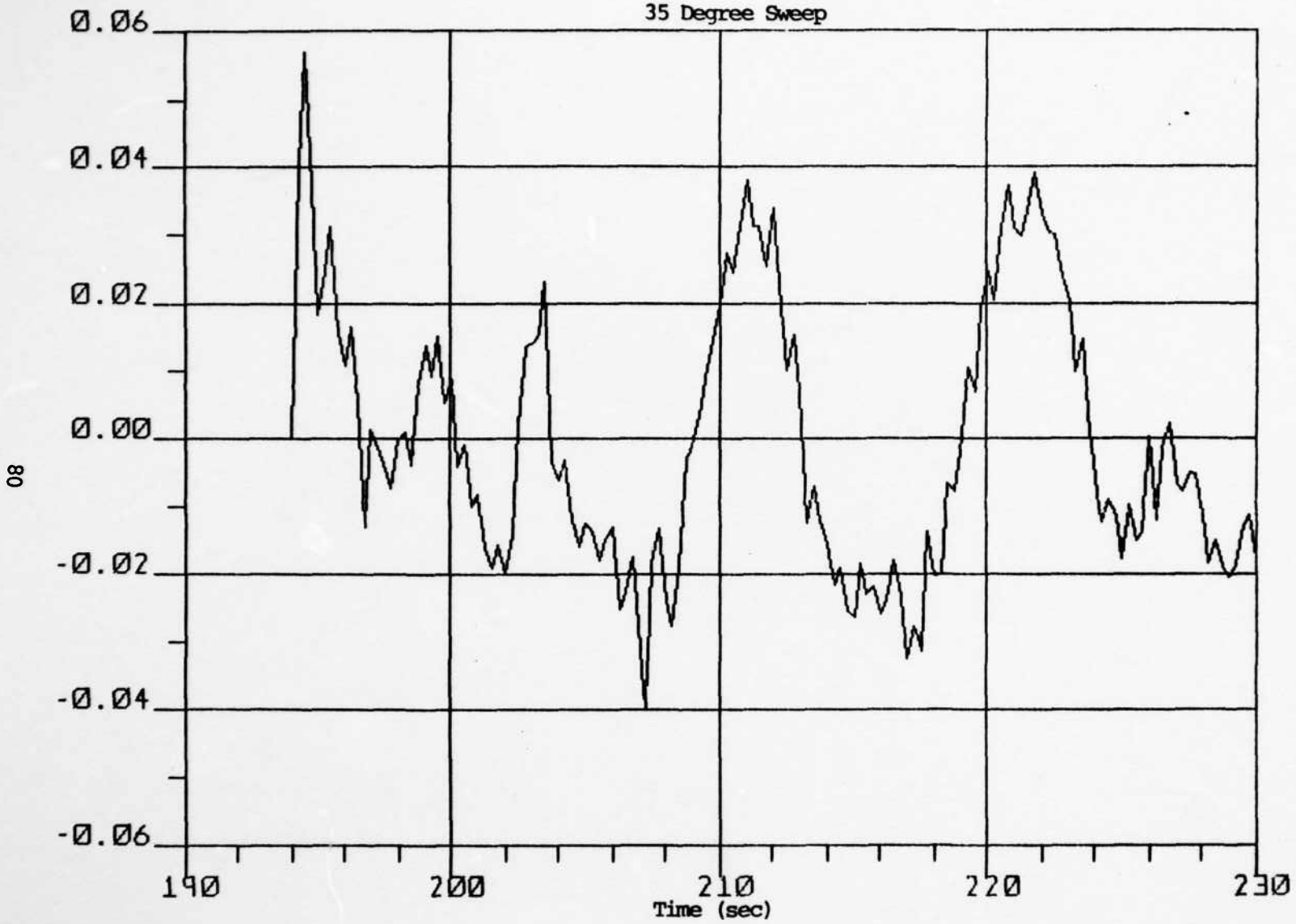

Fig. 6.15 Plot of Angle of Attack State (rad)

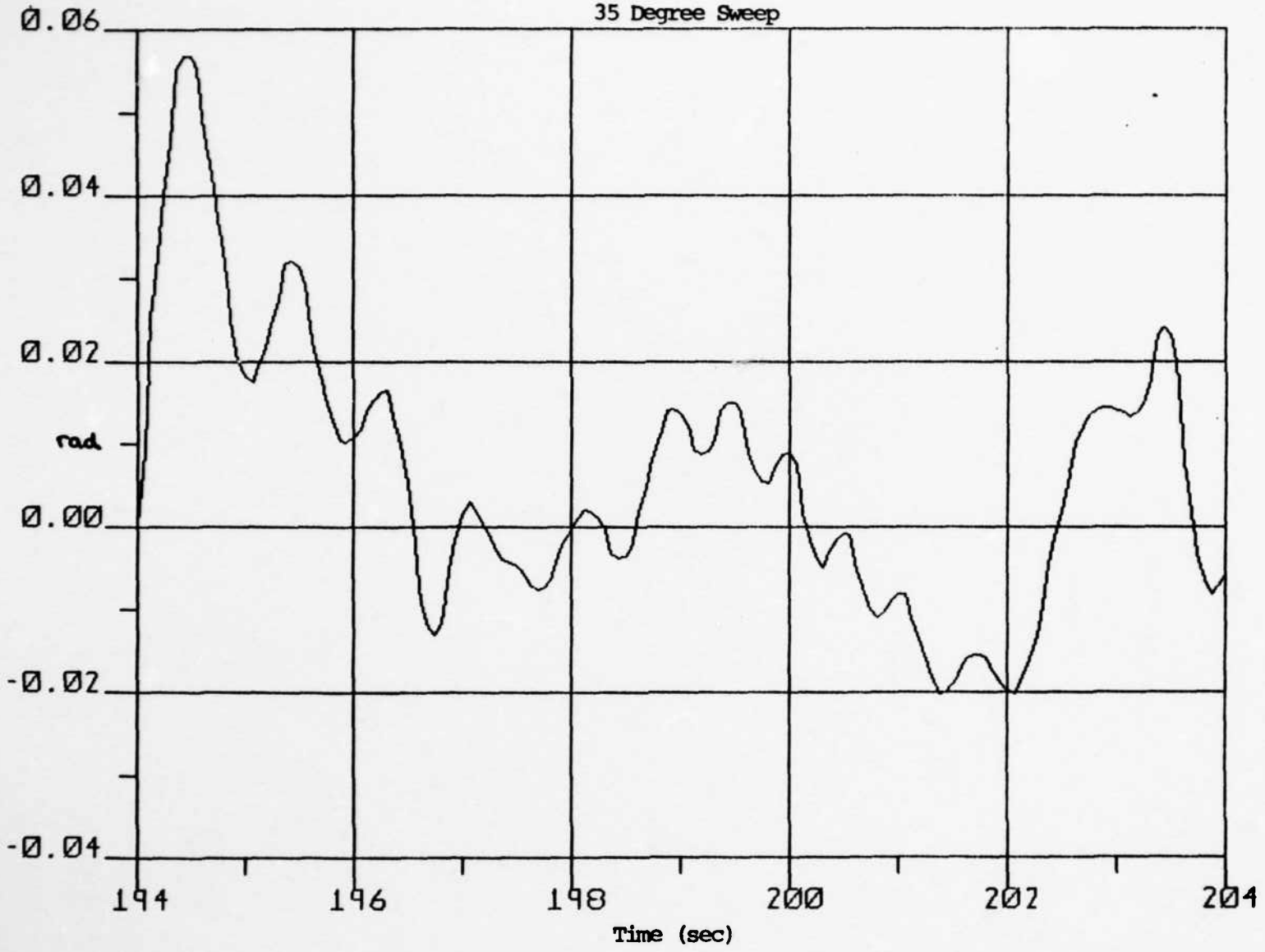

Fig. 6.16 Plot of Angle of Attack State - First 10 sec.

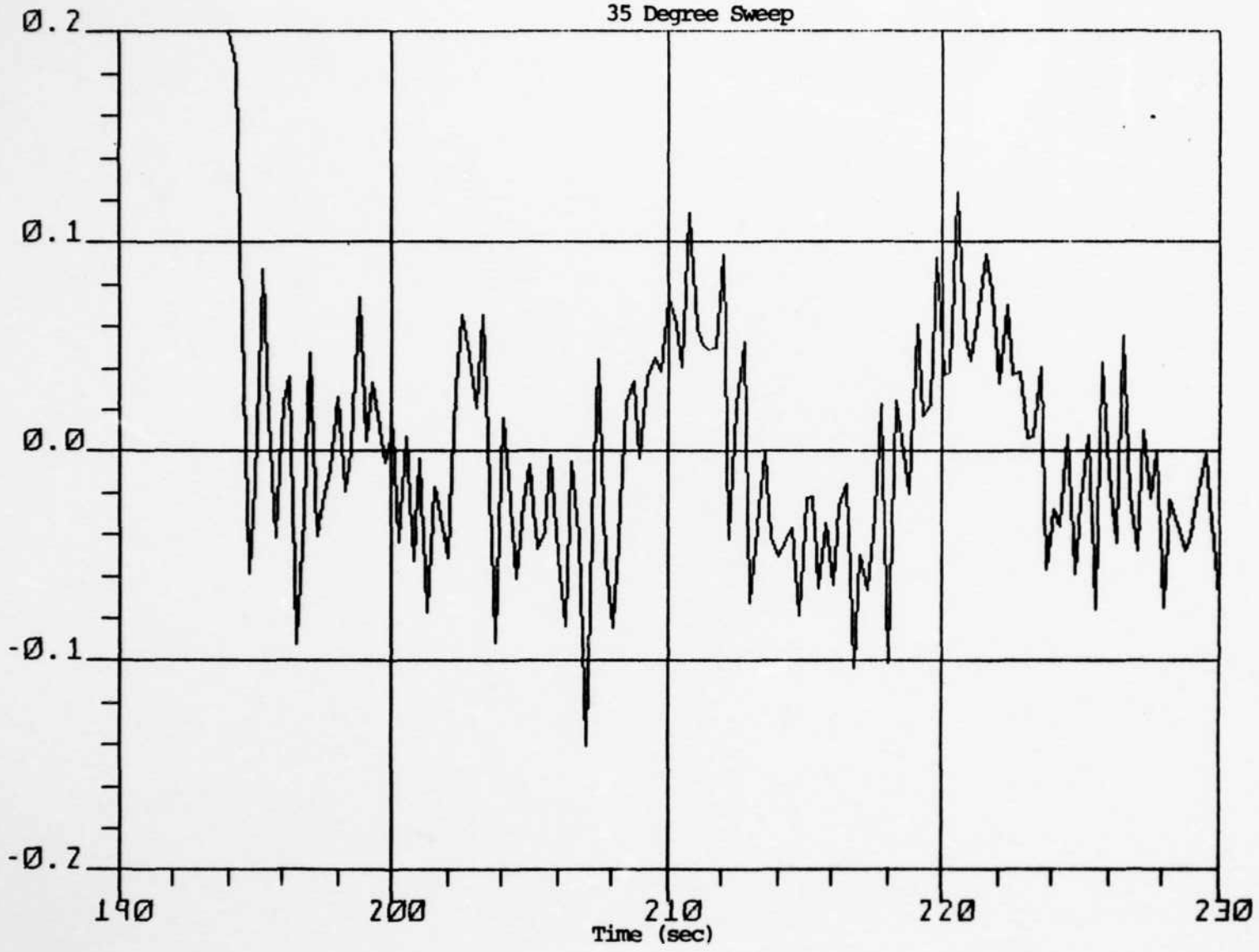

Fig. 6.17 Plot of Pitch Rate State (rad/sec)

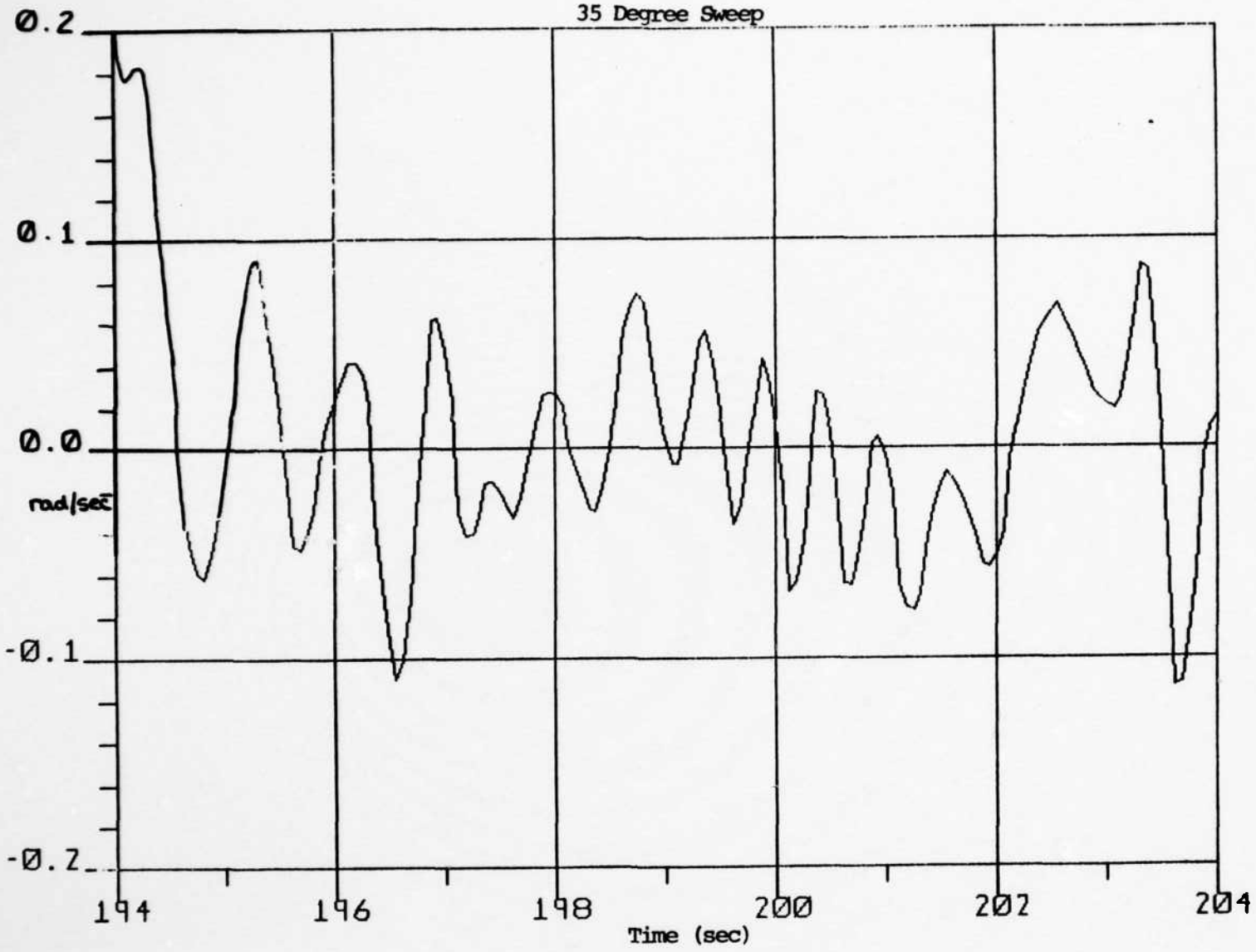

Fig. 6.18 Plot of Pitch Rate State - First 10 sec.

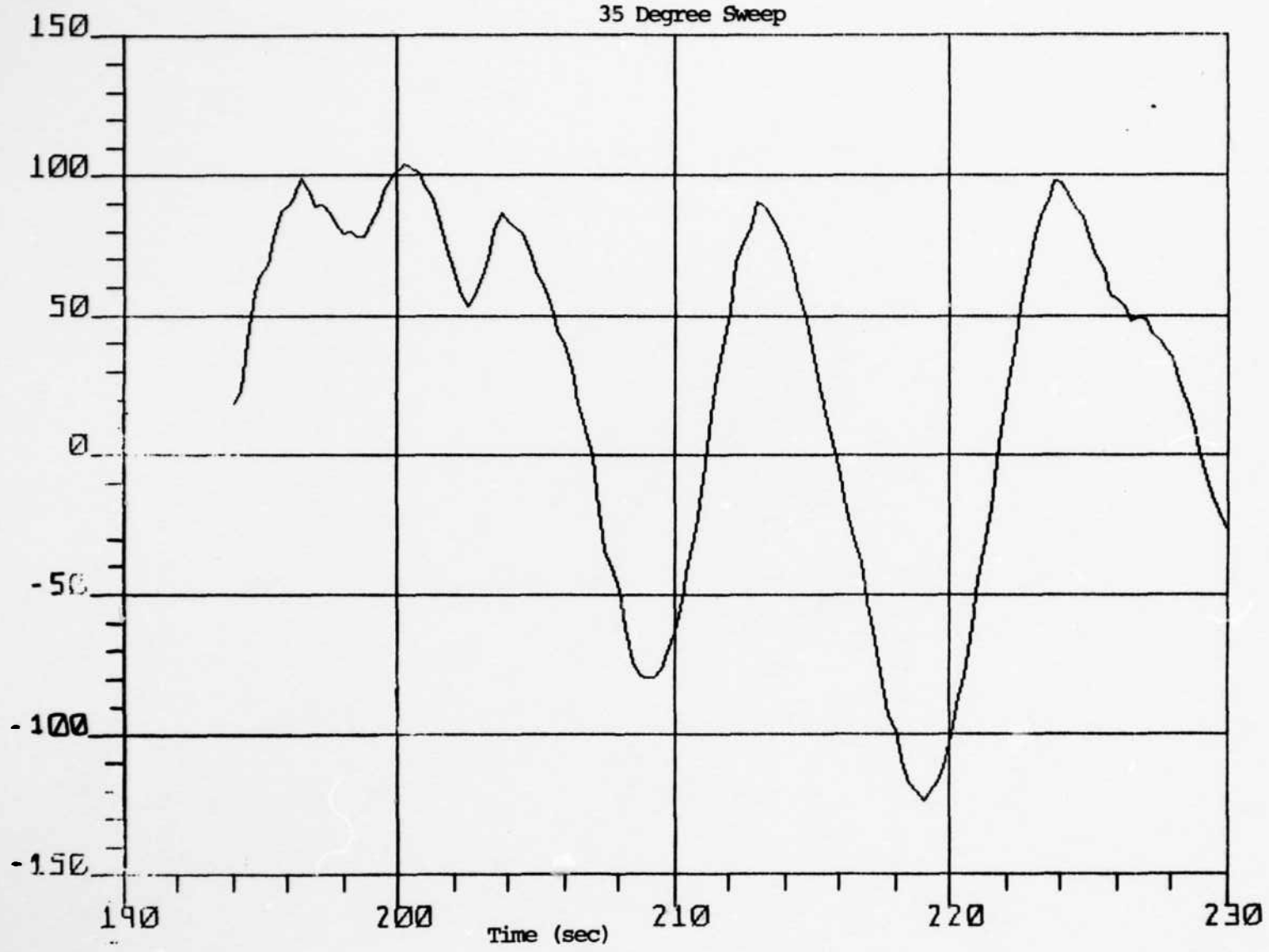

Fig. 6.19 Plot of Altitude Rate State (fps)

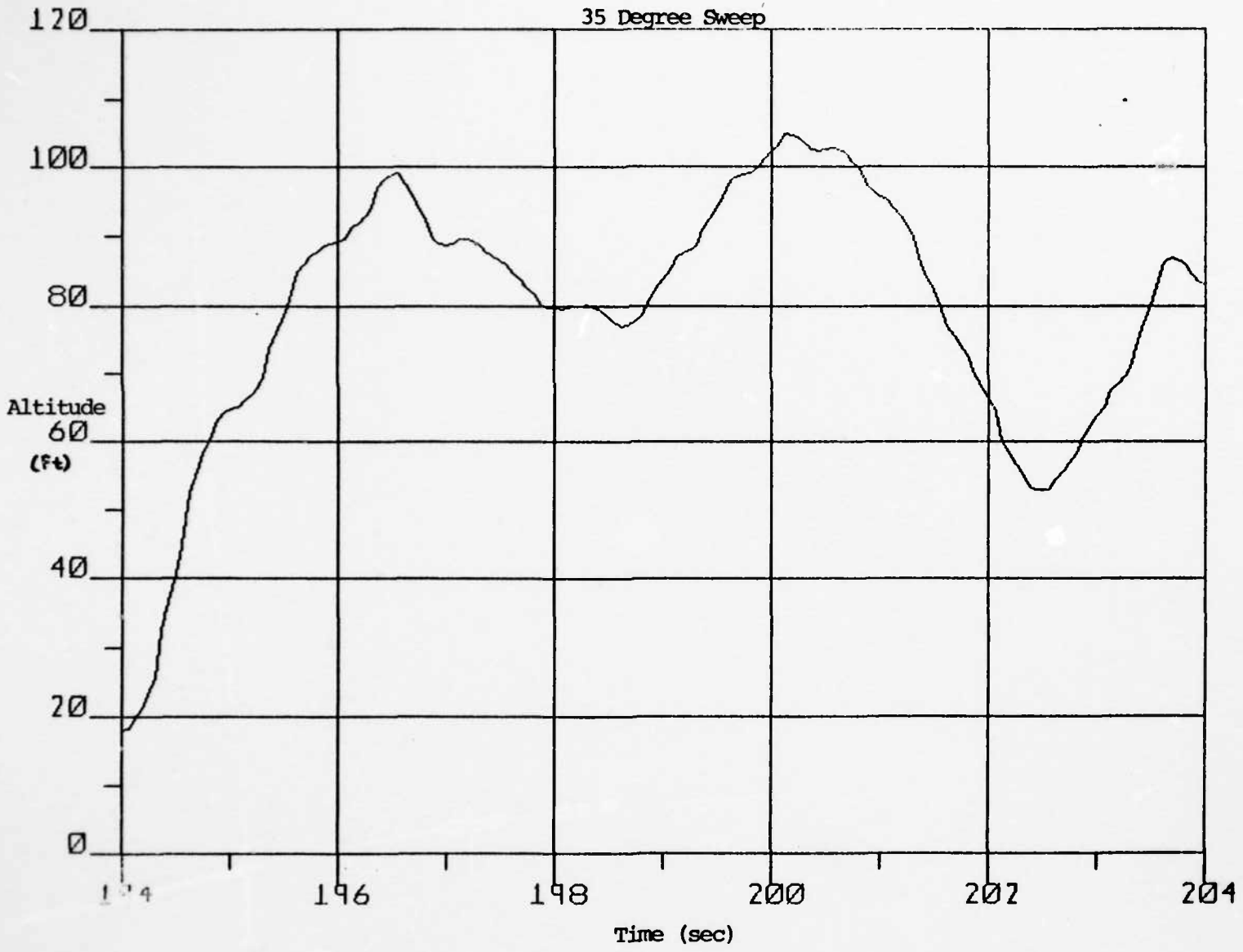

Fig. 6.20 Plot of Altitude Rate State - First 10 sec.

AD-A118 038 AIR FORCE INST OF TECH WRIGHT-PATTERSON AFB OH SCHOO--ETC F/G 17/7
APPLICATION OF OUTPUT PREDICTIVE ALGORITHMIC CONTROL TO A TERRA--ETC(U)
MAR 82 M E BISE

UNCLASSIFIED AFIT/GE/EE/82M-1 NL

2 OF 2
AD A118038

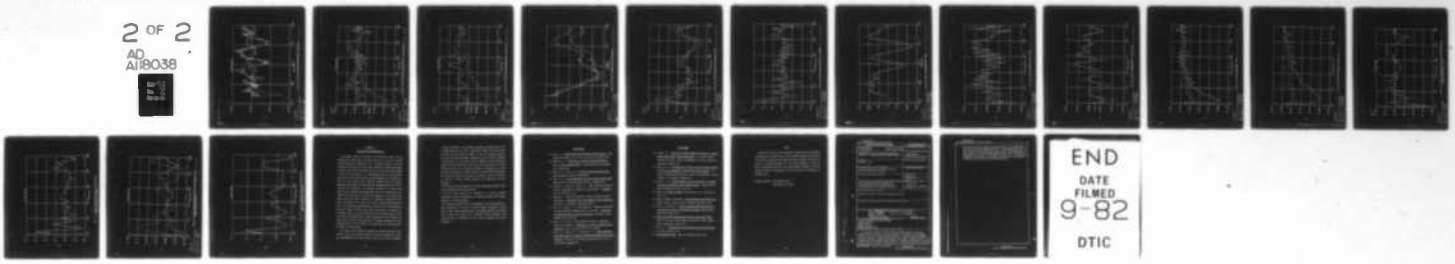

END
DATE FILMED
9-82
DTIC

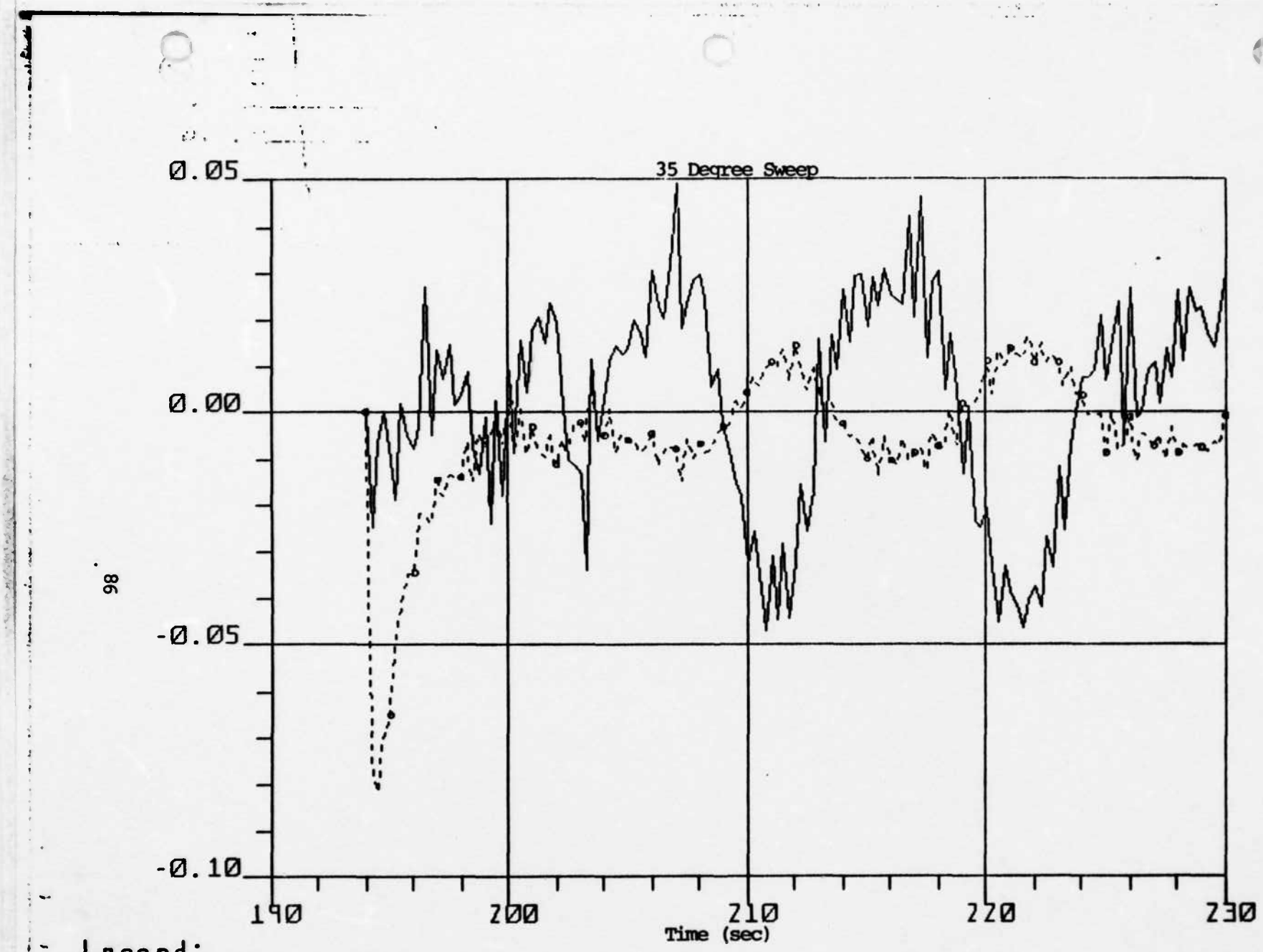

Fig. 6.21 Plot of Control Surface States (rad/sec)

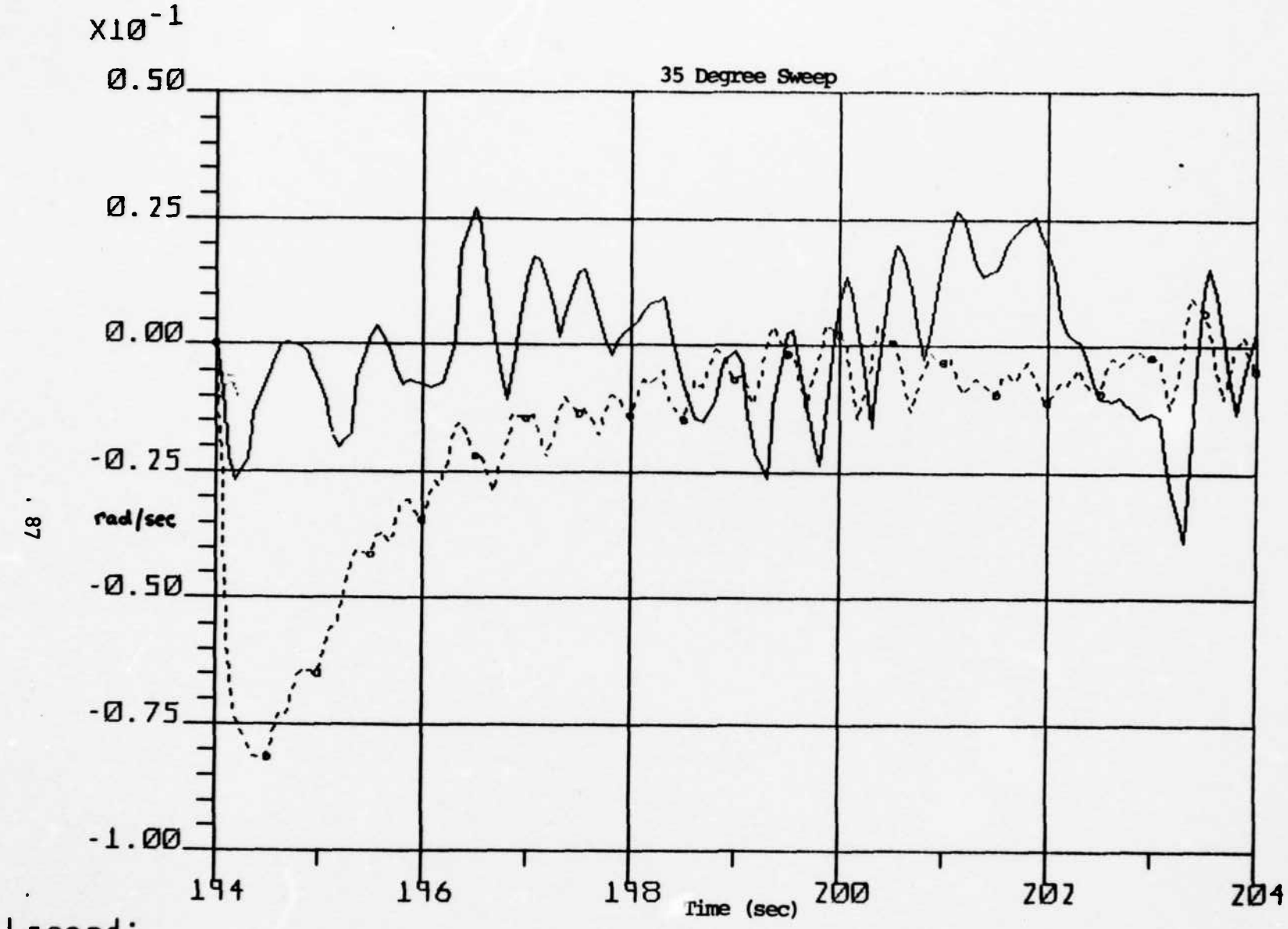

Fig. 6.22 Plot of Control Surface States - First 10 sec.

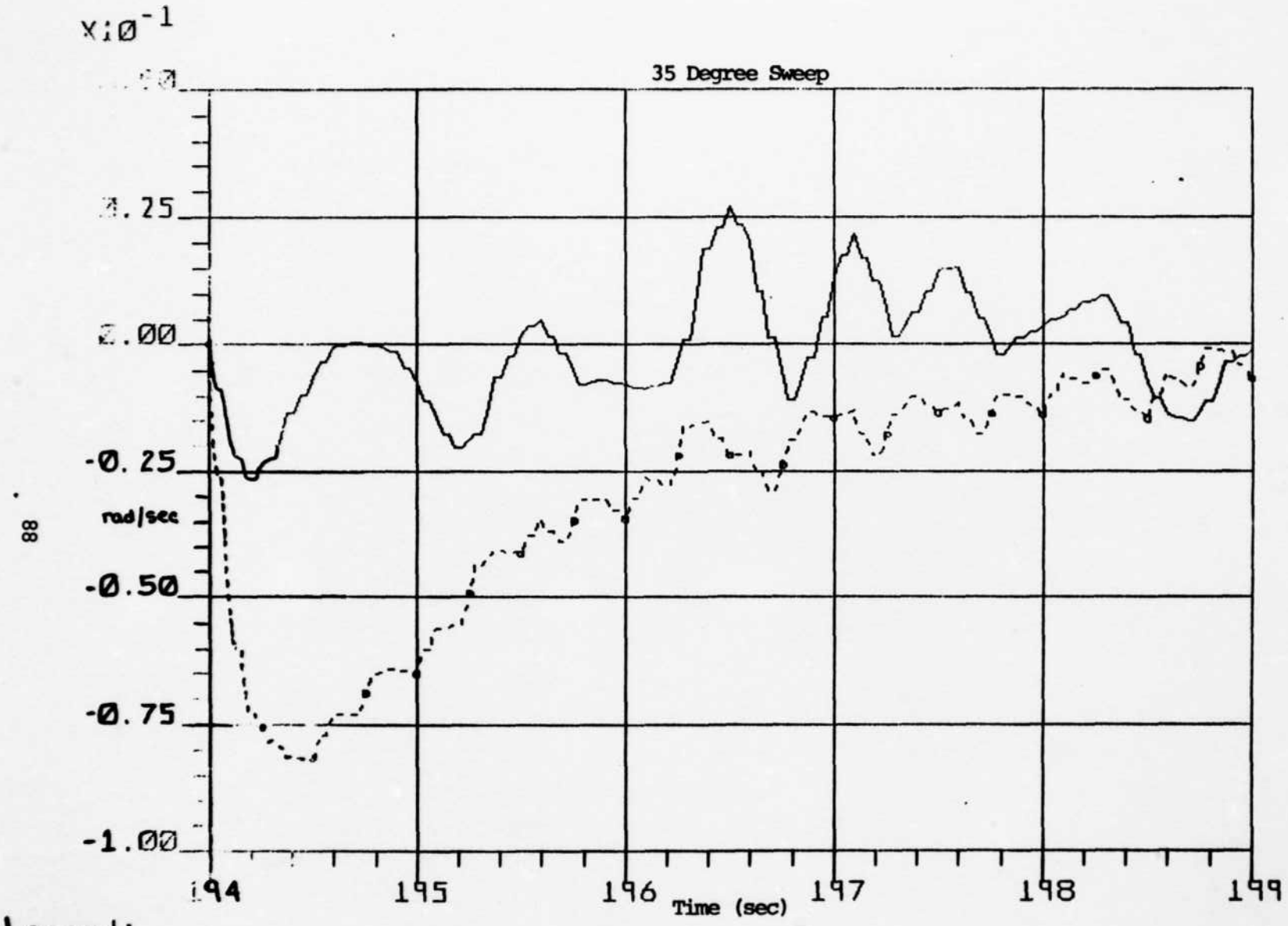

Fig. 6.23 Plot of Control Surface States - First 5 sec.

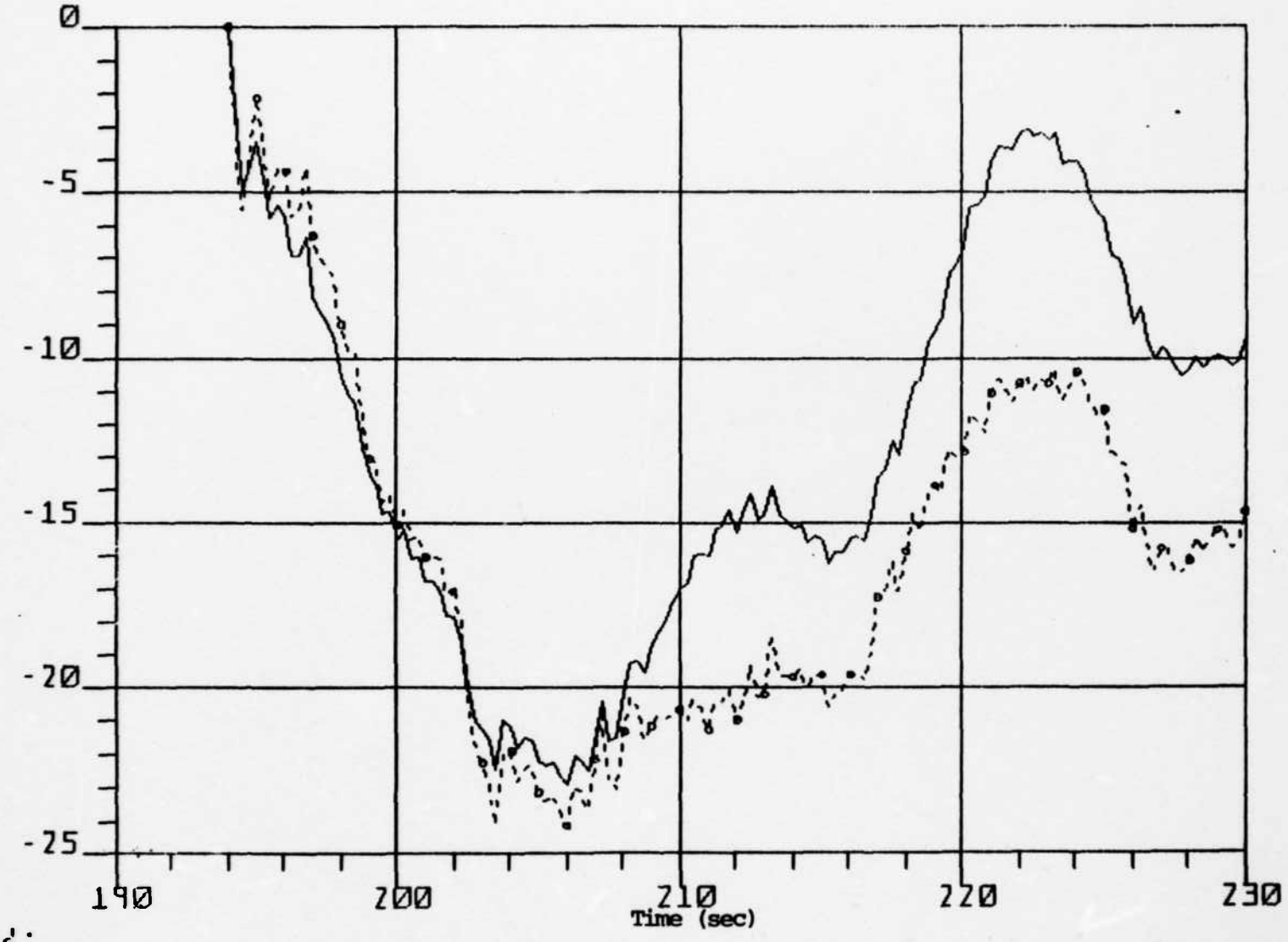

Legend:

Fig. 6.24 Plot of Forward Velocity State (fps)

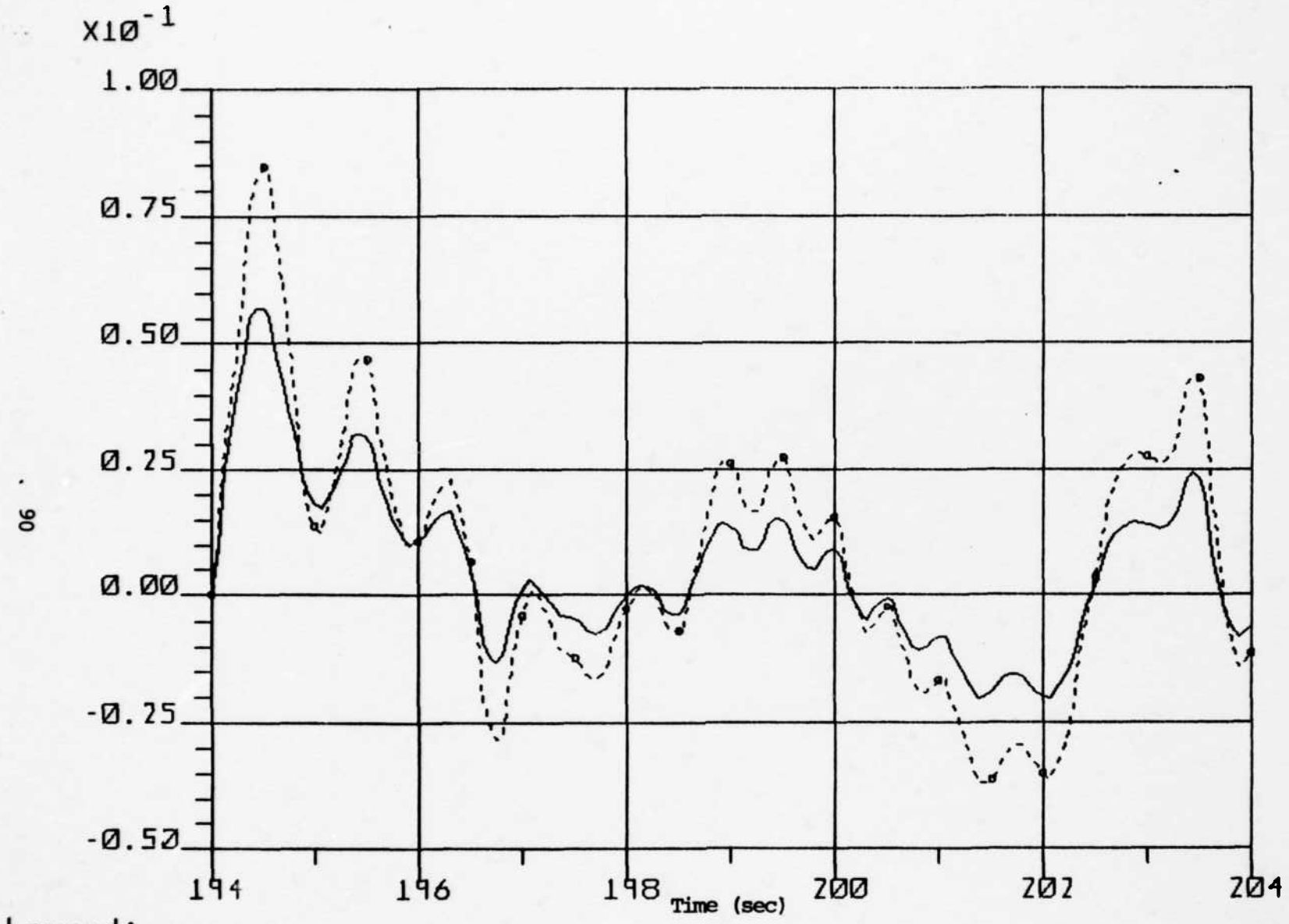

Fig. 6.25 Plot of Angle of Attack State (rad)

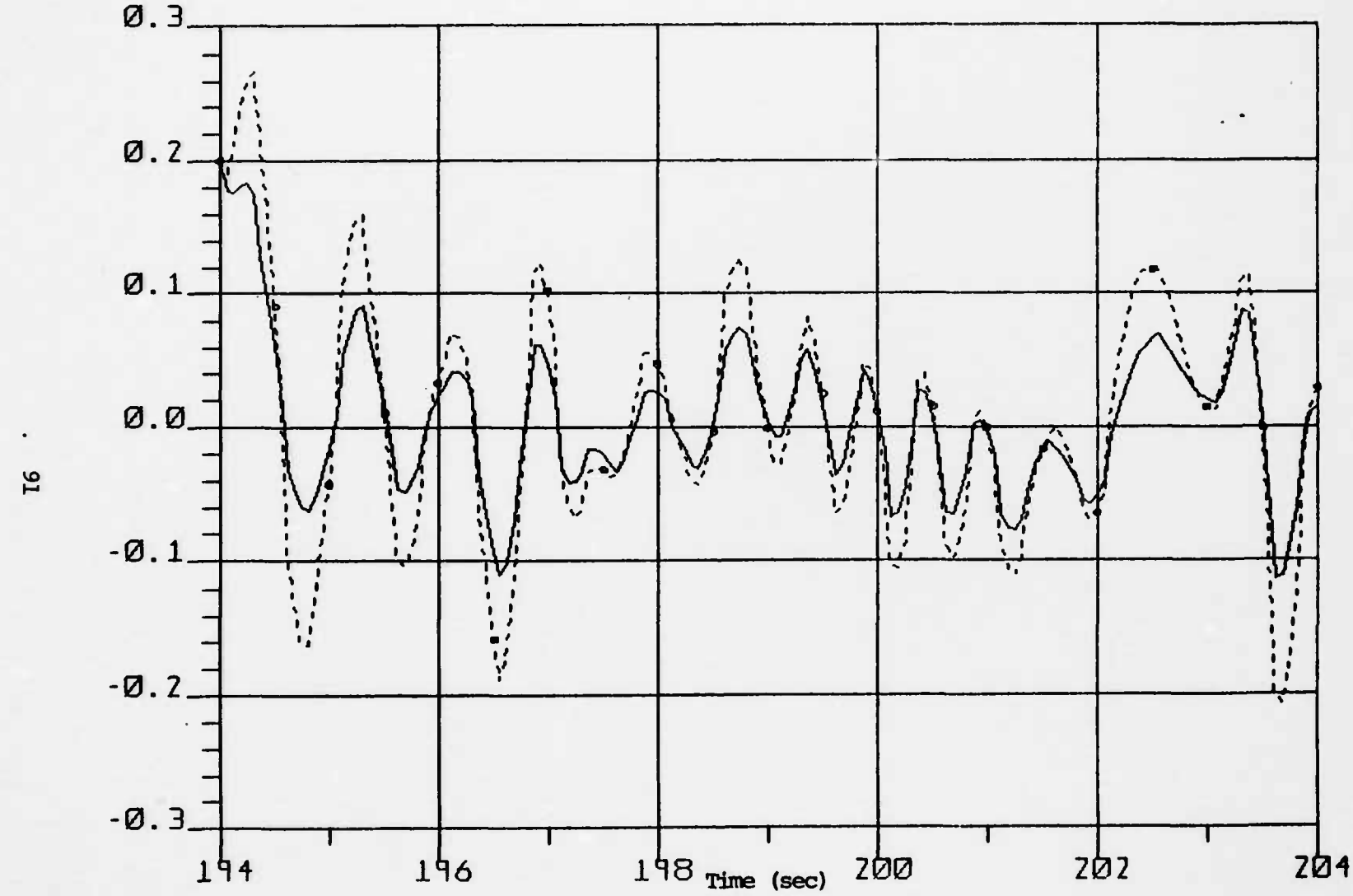

Legend:

Fig. 6.27 Plot of Pitch Rate State (rad/sec)

35 Deg Sweep

58 Deg Sweep

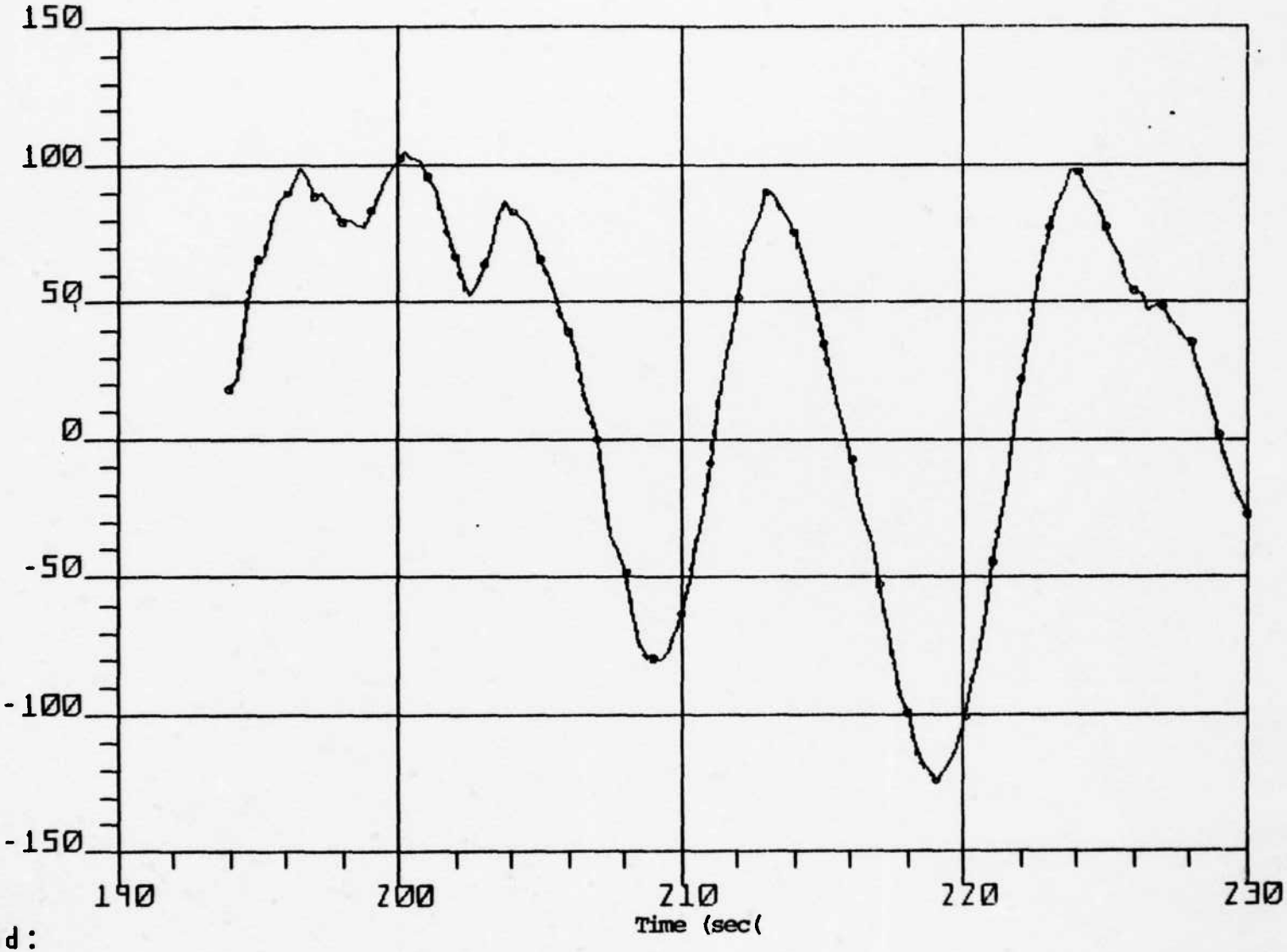

Legend:

Fig. 6.28 Plot of Altitude Rate (fps)

35 Deg Sweep

58 Deg Sweep

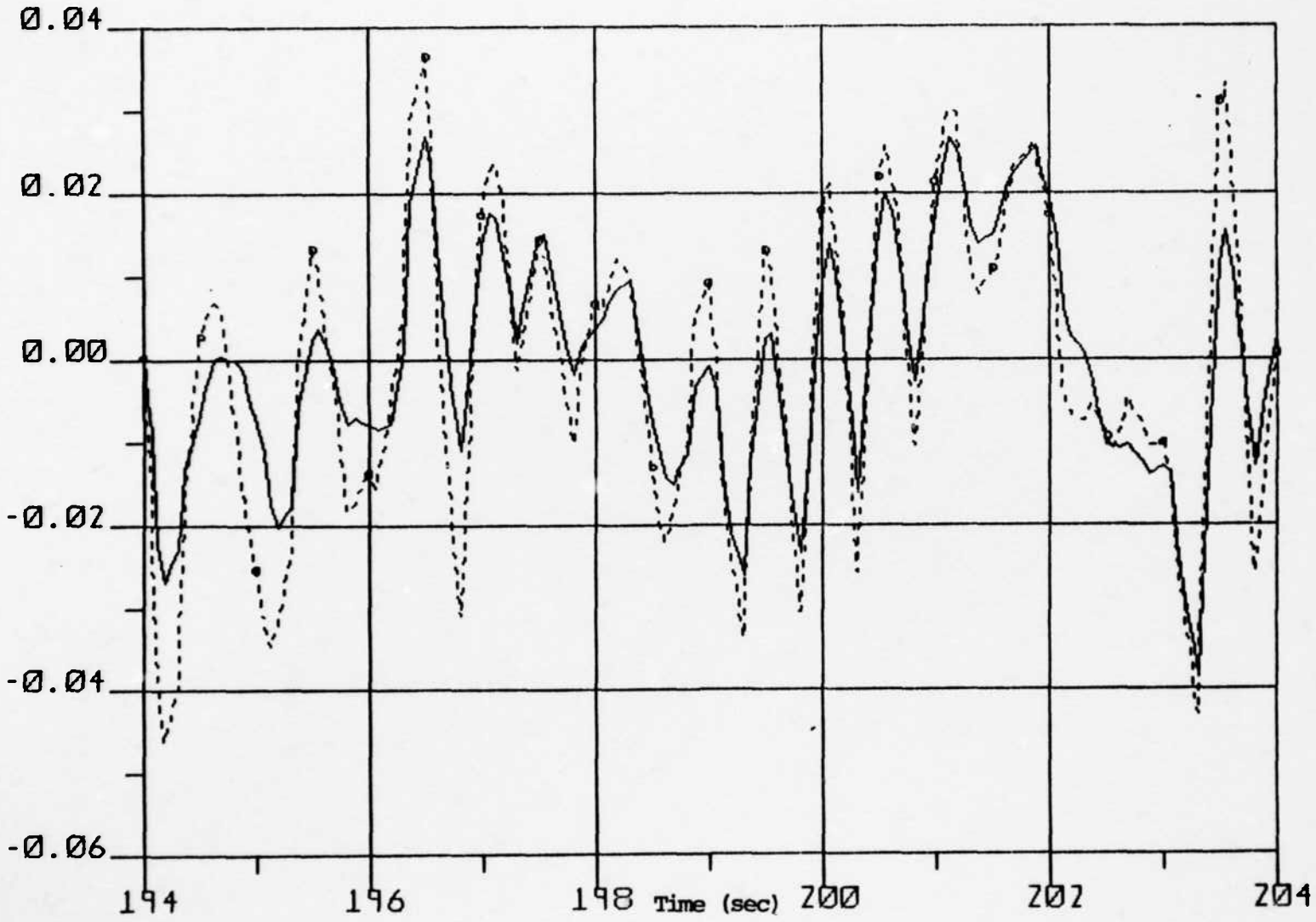

Legend:

Fig. 6.29 Plot of Elevator State (rad)

35 Deg Sweep

58 Deg Sweep

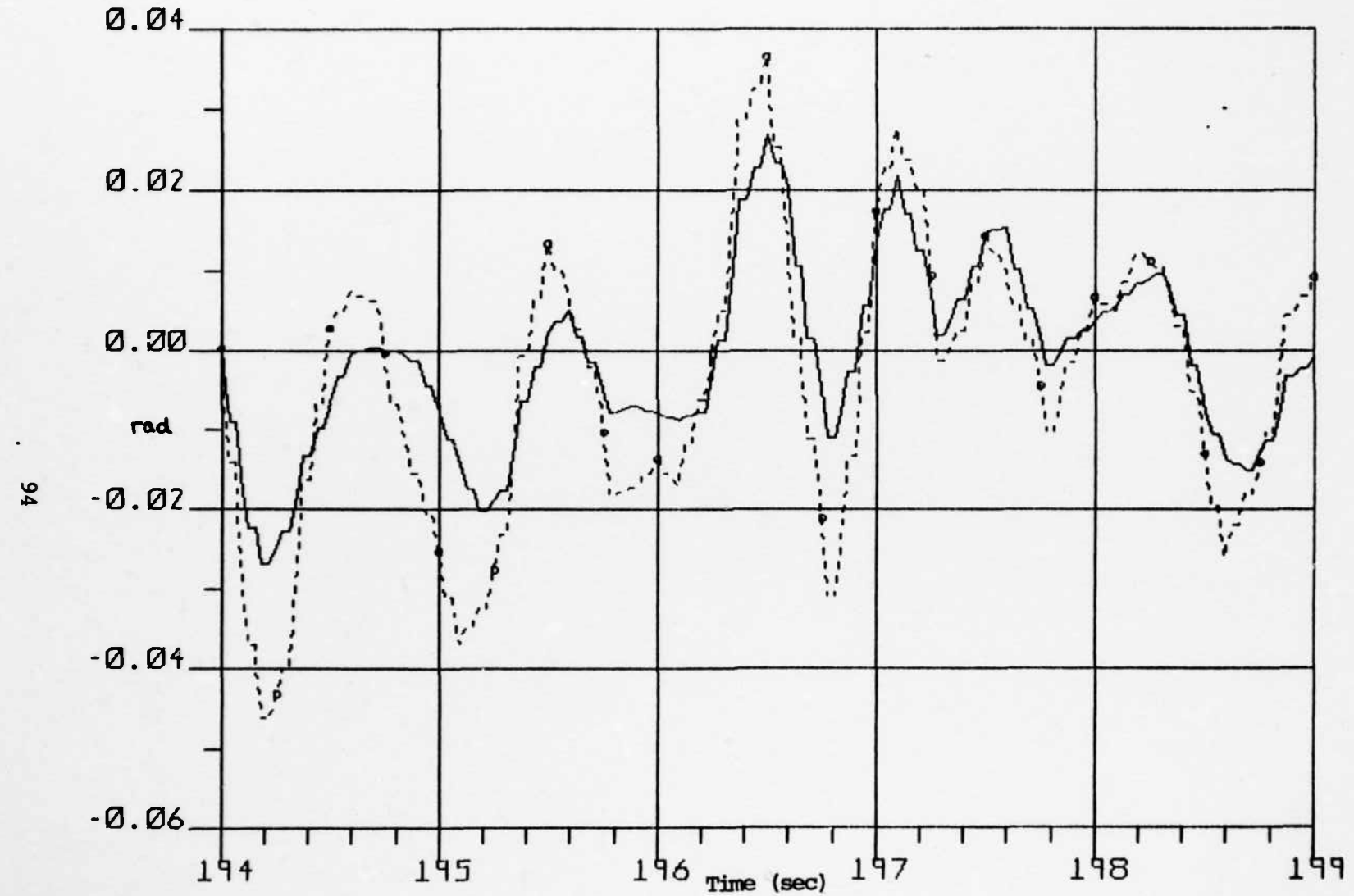

Legend:

35 Deg Sweep

58 Deg Sweep

Fig. 6.30 Plot of Elevator State - First 5 sec.

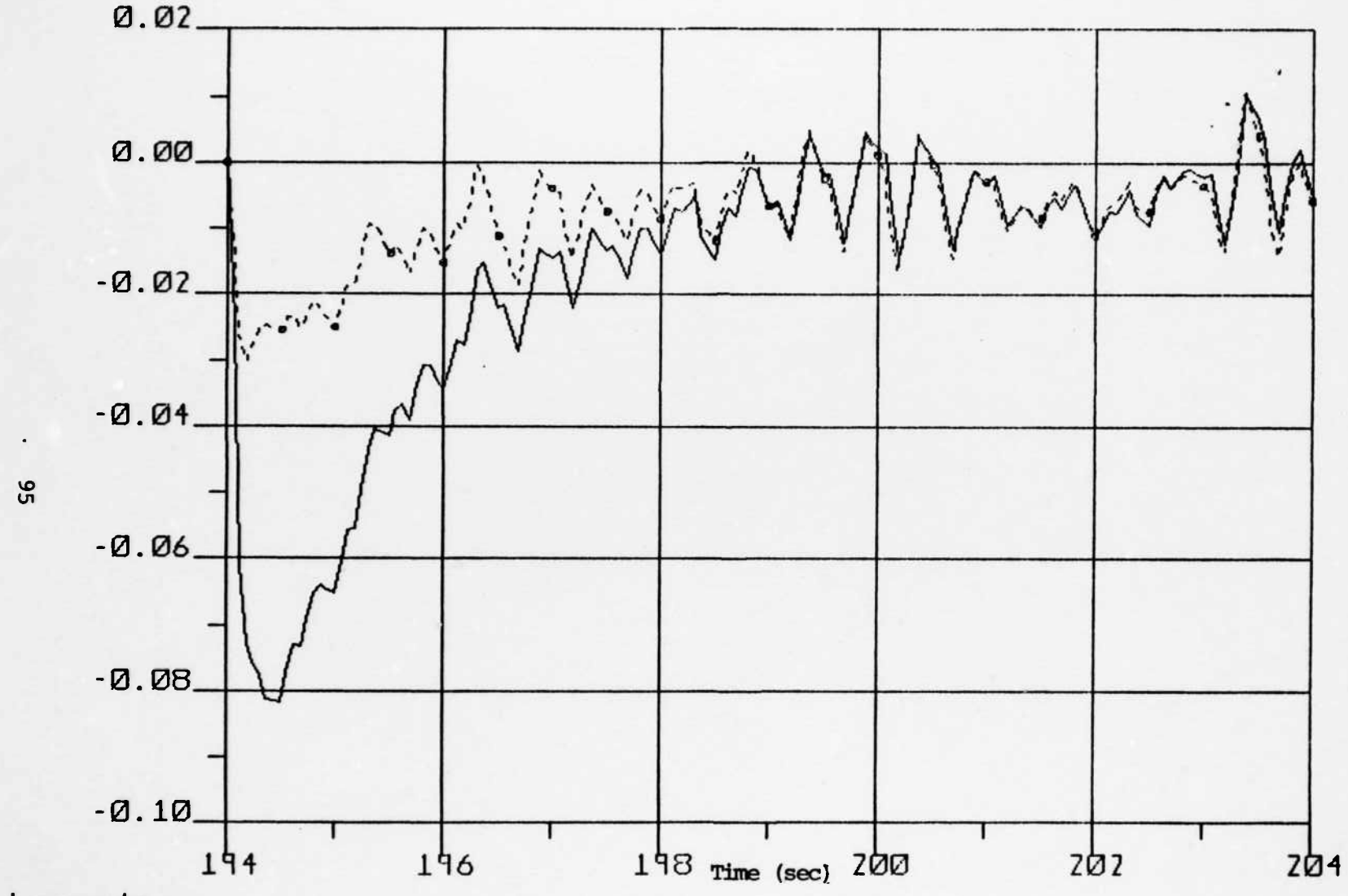

Fig. 6.31 Plot of Flap State (rad)

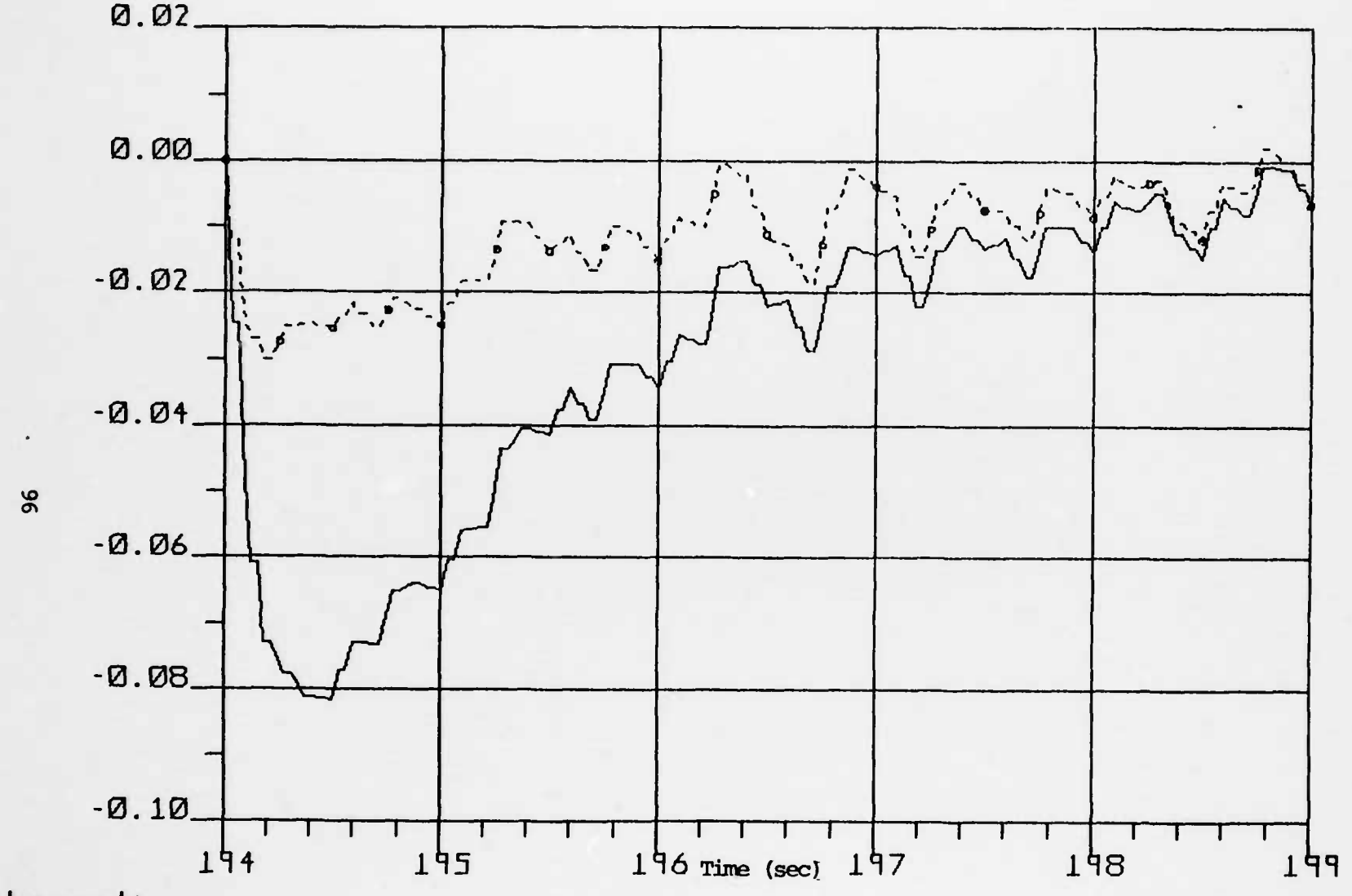

Legend:

Fig. 6.32 Plot of Flap State - First 5 sec.

35 Deg Sweep

58 Deg Sweep

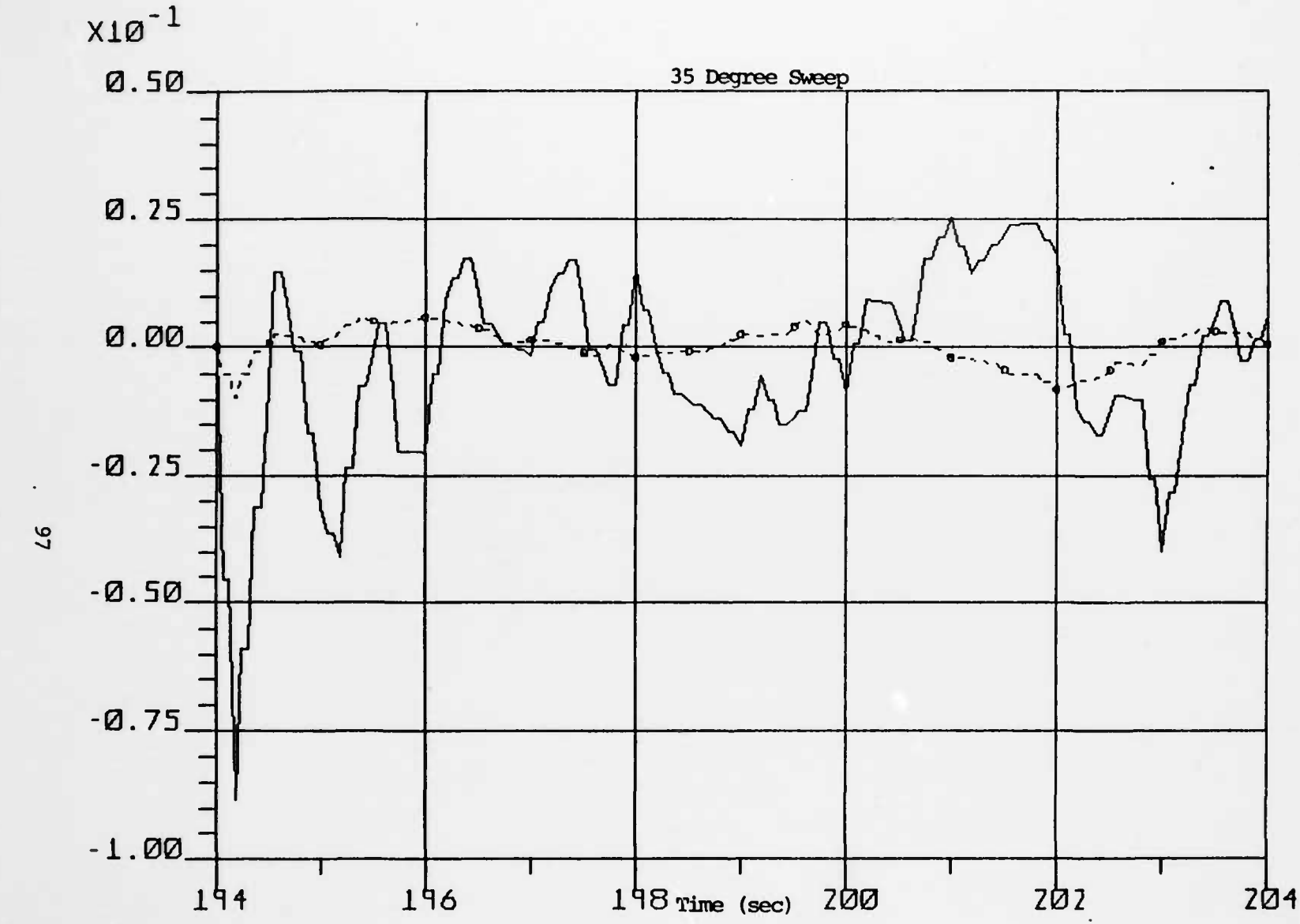

Fig. 6.33 Plot of Control Surface States for Doubled Pitch Damping Coefficient (rad)

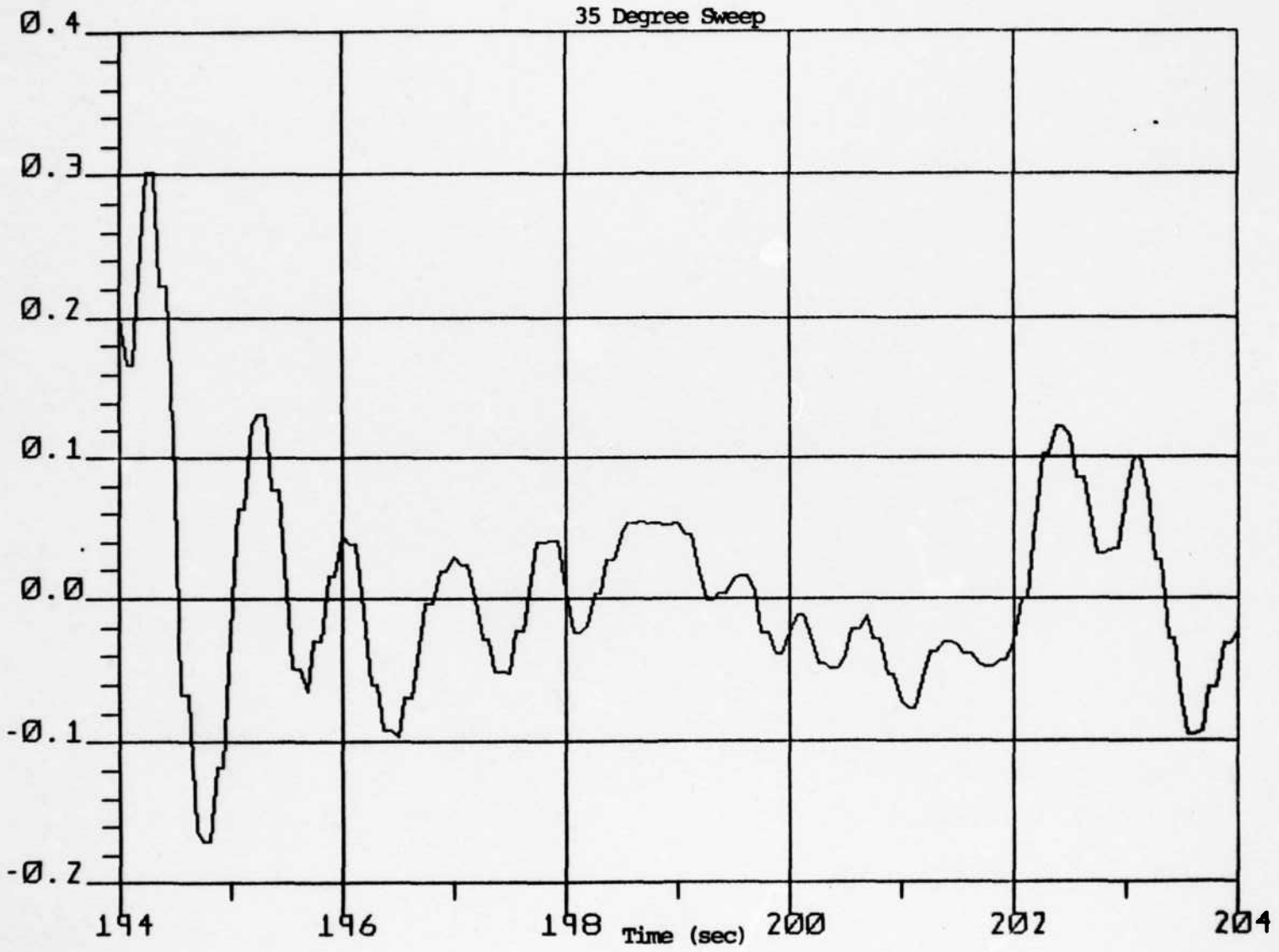

Fig. 6.34 Plot of Pitch Rate State for Doubled Pitch Damping Coefficient (rad/sec)

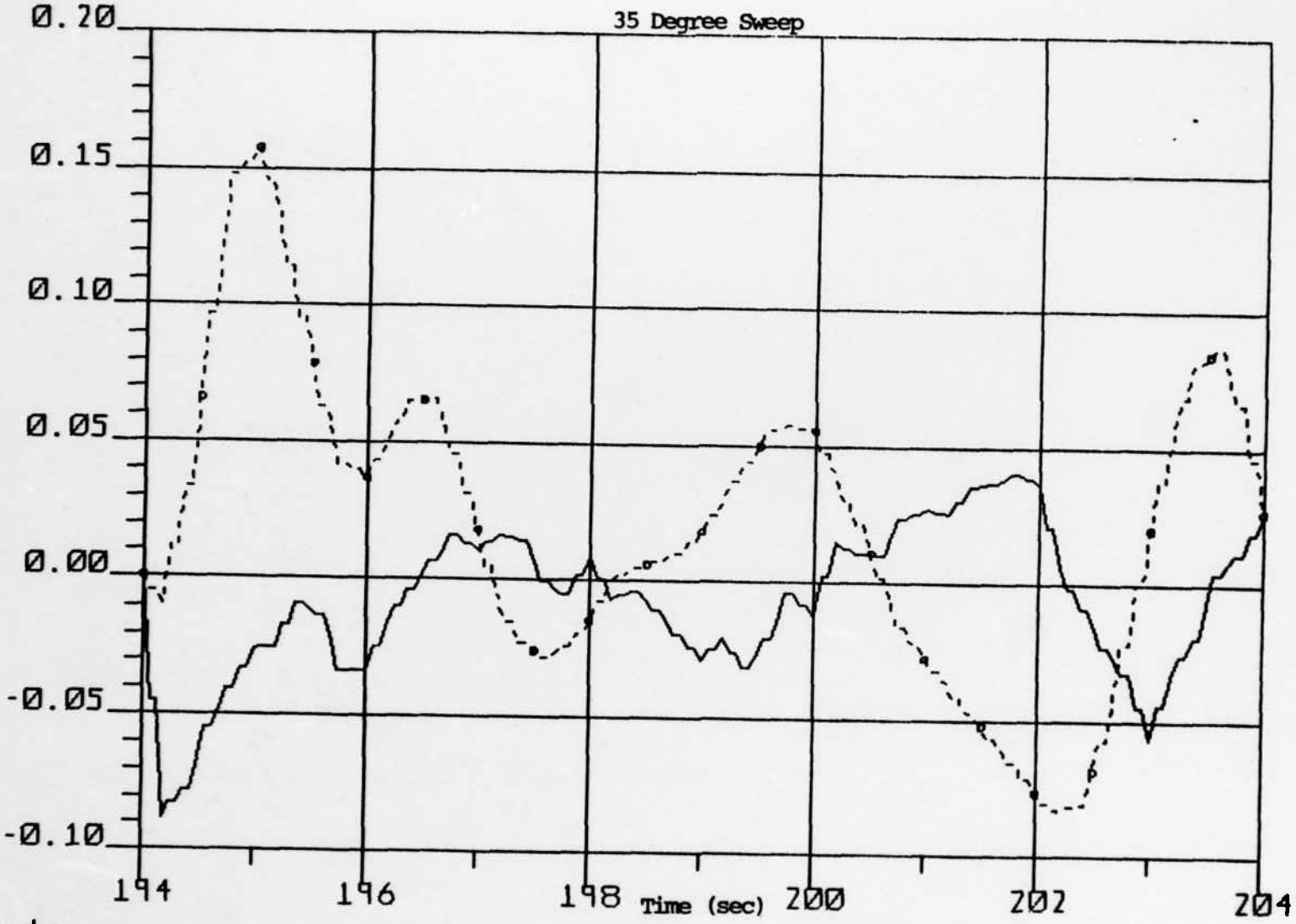

Fig. 6.35 Plot of Control Surface States for Quadrupled Pitch Damping Coefficient (rad)

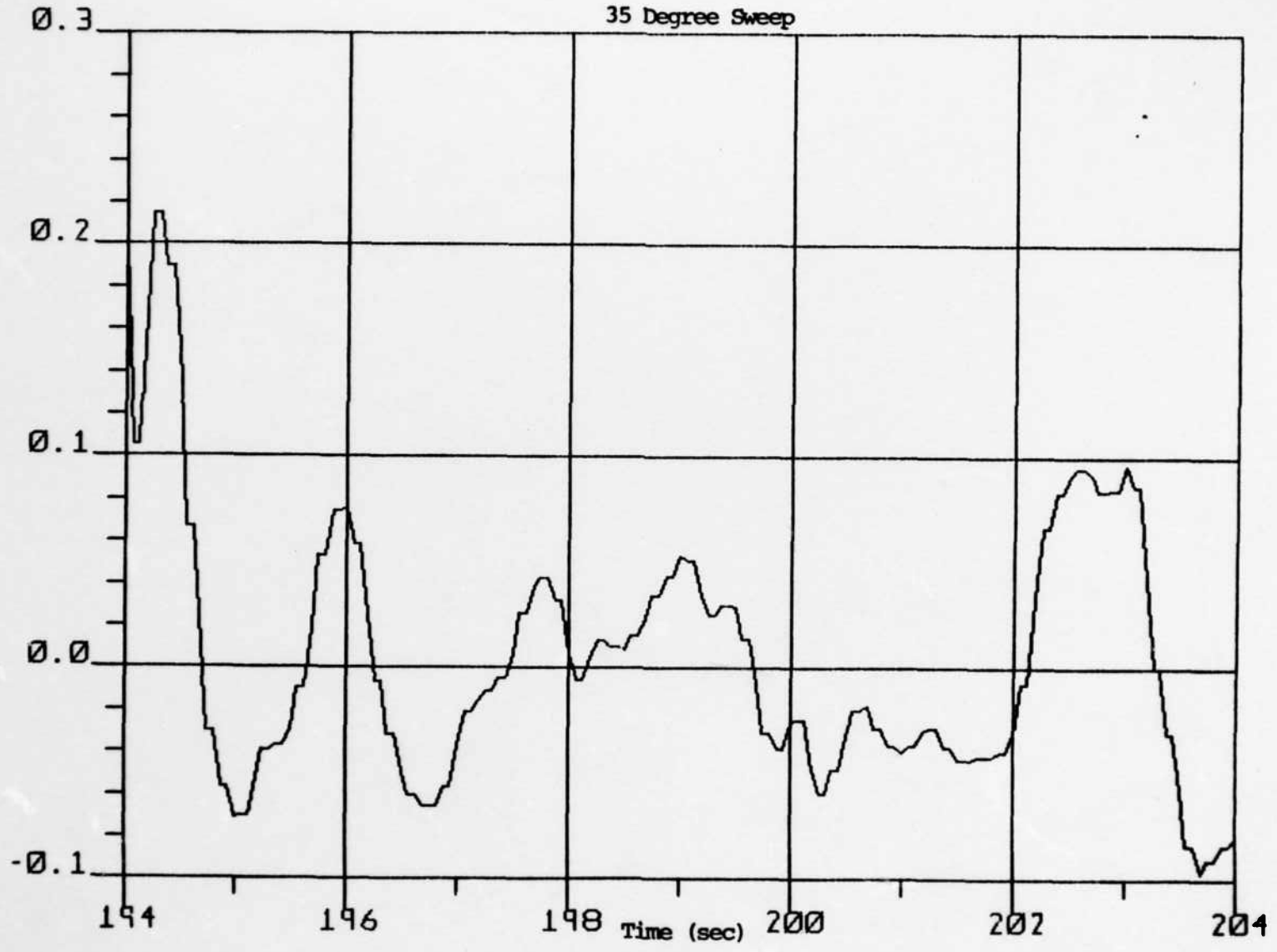

Fig. 6.36 Plot of Pitch Rate State for Quadrupled Pitch Damping Coefficient (rad/sec)

CHAPTER 7

Conclusions and Recommendations

The primary result of this effort is to show that given a set of "non-function" data points, the OPAC controller can control an actual aircraft system and accurately track a desired trajectory. The OPAC controller interpreted the terrain data, calculated a smooth path through the data points, and then followed the path. The model was lightly damped in pitch which would result in an uncomfortable ride for the pilot and, although the pitch rate and control surface deflections were oscillatory, they were well within their respective maximum rates and angles. Additional pitch damping did show show some improvement but still did not eliminate the oscillations. The comparison between the 35 degree wing sweep and the 58 degree wing sweep showed that with the added use of the inboard flaps and, thus, more direct lift capability, the 35 degree wing sweep used less elevator resulting in a decrease in magnitude of the pitch oscillations. The flaps also allowed increased maneuverability while at the same time using less angle of attack. Since this decrease in drag due to angle of attack is less than the drag due to the addition of the inboard flaps, the overall maneuverability is enhanced. Figs. 6.4 and 6.15 show the increased angle of attack excursions of the 58 degree wing sweep model, and Fig. 6.24 reflects the increased maneuverability (and decreased drag) of the 35 degree wing sweep model by showing smaller variations in forward speed.

The results of the simulation proved that the OPAC controller could follow a terrain path exactly using actual aircraft dynamics, but there are recommendations for further study in the area of terrain following.

1. With the addition of the stability augmentation system (SAS) in the F-111/MAW would the two control loops tend to fight or help each other? The OPAC controller would be trying to track the desired trajectory exactly but the SAS would tend to dampen any large or fast input changes.

2. The addition of a gust model into the simulation would provide more insight into what effect direct lift has on gust alleviation in a terrain following mission. Can the actuator dynamics be optimized for better control? This question is closely related to the gust model development. As aircraft are forced to fly closer to the ground, this gust alleviation (a function of control surface dynamics) will become more and more important.

3. How does ride quality affect the tracking performance and how is ride control integrated into the controller?

4. Can the OPAC controller be optimized in a terrain avoidance environment? The task now becomes a six degree-of-freedom (DOF) problem instead of a three DOF problem.

5. The biggest problem would be the development of a trajectory generator that incorporates ride control, aircraft dynamic constraints, varying flight control system characteristics, and command generation techniques into a single, fast update, well integrated control algorithm. This algorithm must be optimized to both terrain following and terrain avoidance.

Bibliography

2.1 Funk, J. E. Optimal-Path Precision Terrain Following System. AIAA Journal of Aircraft, Vol. 14, No. 2 (pp 128-134), February 1977.

2.2 Schwartz, E. C. ADLAT Terrain Avoidance Techniques Evaluation, Vol. I: Control System Studies. Cornell Aeronautical Laboratory, Inc., October 1965.

2.3 Gerson, M. S., Scott, J. H. The ADLAT Terrain Following System. Boeing Document D6-19544, September 1967.

2.4 Gerson, S. M. Direct Comparison of Terrain Following Control Laws. AFFDL-TR-78-142, Wright-Patterson AFB, Ohio, November 1978.

3.1 Richalet, J., Rault, A., Testud, J. L. "Model Predictive Heuristic Control: Application to Industrial Process Control". Automatica, Vol. 14, pp 413-419, 1976.

3.2 Richalet, J. General "Principles of Scenerio Predictive Control Techniques." Proceedings, 1980 Joint Automatic Control Conference, San Francisco, California, August 1980, FA9-A.

3.3 Reid, J. G., Mehra, R. K., and Kirkwood, W. "Robustness Properties of Output Predictive Deadbeat Control: SISO Case". Proceedings, 1979 IEEE Conference on Decision and Control, Clearwater, Florida, December 1979, pp 307-314.

3.4 Mehra, R. K., et al. "Model Algorithmic Control: Theoretical Results on Robustness". Proceedings, 1979 Joint Automatic Control Conference, Denver, Colorado, June 1979, pp 387-392.

3.5 Reid, J. G., Chaffin, D. E., Silverthorn J. T. Output Predictive Algorithmic Control: Precision Tracking With Application to Terrain Following. AIAA Journal of Guidance and Control, Vol. 4, No. 5 (pp 502-509), September 1981.

Bibliography

3.6 Colson, H. J. Application of Model Algorithmic Control to a Lightly Damped Single Input, Single Output System. M.S. Thesis, Wright-Patterson AFB, Ohio: School of Engineering, Air Force Institute of Technology, December 1979.

3.7 Chaffin, D. E. The Application of Output Predictive Digital Control to Wing Flutter Suppression and Terrain Following Problems. M.S. Thesis, Wright-Patterson AFB, Ohio: School of Engineering, Air Force Institute of Technology, December 1979.

4.1 Griffin, J. M. Digital Computer Solution of Aircraft Longitudinal and Lateral-Directional Dynamic Characteristics. AFFDL-TR-78-203, Wright-Patterson AFB, Ohio, July 1979.

4.2 Etkin B. Dynamics of Flight, Wiley and Sons, Inc., New York, New York, 1959.

4.3 McRuer, Ashkenas, and Graham. Aircraft Dynamics and Automatic Control, Princeton University Press, Princeton, New Jersey, 1973.

4.4 Sim, A., and Currey, R. Flight Determined Stability and Control Derivatives for the F-111 TACT Research Aircraft, NASA Technical Paper 1350, October 1978.

4.5 AFTI/F-111 Mission Adaptive Wing Wind Tunnel Force Data Report, Test No. 449-1-11T, Boeing Document D365-10070-1, Boeing Company, Seattle, Washington, August 1981.

5.1 Reid, J. G. Proceedings, Fourth AIAA Avionics Systems Conference. St. Louis, Missouri, 1981.

5.2 IMSL Reference Manual. IMSL Inc., Houston, Texas, 1979.

Vita

Michael E. Bise was born 13 June 1953 in Dayton, Ohio. He graduated from high school in Dayton, Ohio in 1971 and then attended the University of Cincinnati, Cincinnati, Ohio where he earned the degree of Bachelor of Science in Aerospace Engineering in 1976. Upon graduation, he went to work at Wright-Patterson AFB in the Flight Dynamics Laboratory. He then entered the School of Engineering, Air Force Institute of Technology, in September 1980.

Permanent Address: 2513 Marscott Drive
Centerville, Ohio 45440

UNCLASSIFIED

SECURITY CLASSIFICATION OF THIS PAGE (When Data Entered)

REPORT DOCUMENTATION PAGE	READ INSTRUCTIONS BEFORE COMPLETING FORM
1. REPORT NUMBER: AFIT/GE/EE/82M-1	2. GOVT ACCESSION NO.: AD-A118038 / 3. RECIPIENT'S CATALOG NUMBER:
4. TITLE (and Subtitle): APPLICATION OF OUTPUT PREDICTIVE ALGORITHMIC CONTROL TO A TERRAIN FOLLOWING AIRCRAFT SYSTEM	5. TYPE OF REPORT & PERIOD COVERED: MASTERS THESIS
	6. PERFORMING ORG. REPORT NUMBER:
7. AUTHOR(s): MICHAEL E. BISE	8. CONTRACT OR GRANT NUMBER(s):
9. PERFORMING ORGANIZATION NAME AND ADDRESS: Air Force Institute of Technology (AFIT/EN) Wright-Patterson AFB, OH 45433	10. PROGRAM ELEMENT, PROJECT, TASK AREA & WORK UNIT NUMBERS:
11. CONTROLLING OFFICE NAME AND ADDRESS:	12. REPORT DATE: March 1982
	13. NUMBER OF PAGES: 116
14. MONITORING AGENCY NAME & ADDRESS(if different from Controlling Office): Flight Dynamics Laboratory (AFWAL/FIGC) AF Wright Aeronautical Laboratories, AFSC Wright-Patterson Air Force Base, Ohio 45433	15. SECURITY CLASS. (of this report): Unclassified
	15a. DECLASSIFICATION/DOWNGRADING SCHEDULE:

16. DISTRIBUTION STATEMENT (of this Report)

Approved for public release; distribution unlimited

17. DISTRIBUTION STATEMENT (of the abstract entered in Block 20, if different from Report)

18. SUPPLEMENTARY NOTES

APPROVED FOR PUBLIC RELEASE: IAW AFR 190-17

LYNN E. WOLAVER
Dean for Research and Professional Development

AIR FORCE INSTITUTE OF TECHNOLOGY (ATC)
WRIGHT-PATTERSON AFB, OH 45433

23 JUL 1982

19. KEY WORDS (Continue on reverse side if necessary and identify by block number)

OUTPUT PREDICTIVE ALGORITHMIC CONTROL
TERRAIN FOLLOWING
HANKEL MATRIX
SINGULAR VALUES
MISSION ADAPTIVE WING

20. ABSTRACT (Continue on reverse side if necessary and identify by block number)

An effective automatic terrain following command generation system is required to safely maintain a desired clearance altitude above the terrain. For survivability, the aircraft must penetrate at transonic or high subsonic speeds at very low altitudes above ground level. This introduces new problems such as wind gusts, a faster radar update of the terrain, faster aircraft response time, and increased pilot workload. To insure survivability, a control algorithm must be capable of interpreting all of the above input data and per-

DD FORM 1 JAN 73 1473 EDITION OF 1 NOV 65 IS OBSOLETE

UNCLASSIFIED

SECURITY CLASSIFICATION OF THIS PAGE (When Data Entered)

form flawlessly during a terrain following mission. This report uses the terrain following scenario to evaluate a new digital controller, the Output Predictive Algorithmic Controller. This controller was able to track, during low level penetration, actual terrain data using as an aircraft model the F-111/MAW (Mission Adaptive Wing). The F-111/MAW was chosen for this study due to its direct lift capability. Two wing sweeps (35 degrees and 58 degrees) were chosen to evaluate the effectiveness of direct lift during terrain following missions.


ATE
LMEI
8